

Analysis of Lipid Droplet Proteins and their Contribution to Phospholipid Homeostasis during Lipid Droplet Expansion

Dissertation der Fakultät für Biologie der
Ludwig-Maximilian-Universität München

vorgelegt von
Natalie Krahmer
Juni 2011

Ehrenwörtliche Erklärung

Hiermit erkläre ich, dass ich die vorliegende Dissertation selbstständig und ohne unerlaubte Hilfe angefertigt habe. Ich habe weder anderweitig versucht, eine Dissertation einzureichen oder eine Doktorprüfung durchzuführen, noch habe ich diese Dissertation oder Teile derselben einer anderen Prüfungskommission vorgelegt

München, den 22. Juni 2011

Promotionsgesuch eingereicht am: 22.Juni 2011

Datum der mündlichen Prüfung: 26.Juli 2011

Erster Gutachter: Prof. Dr. Stefan Jentsch

Zweiter Gutachter: Prof. Dr. Charles David

Diese Dissertation wurde von Prof. Dr. Stefan Jentsch betreut.

Die vorliegende Arbeit wurde zwischen März 2008 und Juni 2011 am Max-Planck-Institut für Biochemie in Martinsried in der Arbeitsgruppe von Prof. Dr. Tobias Walther durchgeführt.

Wesentliche Teile dieser Arbeit sind in den folgenden Publikationen veröffentlicht:

Natalie Krahmer, Yi Guo, Florian Wilfling, Maximiliane Hilger, Susanne Lingrell, Klaus Heger, Heather W. Newman, Marc Schmid-Supprian, Dennis E. Vance, Matthias Mann, Robert V. Farese, Jr. and Tobias C. Walther. **Localized Activation of CTP:phosphocholine cytidyltransferase (CCT) is required for Phosphatidylcholine Synthesis during Lipid Droplet Expansion** (Cell Metabolism, in press, 2011).

Natalie Krahmer, Yi Guo, Robert V. Farese, Jr. and Tobias C. Walther (2009). **SnapShot: Lipid Droplets**. Cell 139, 1024-1024 e1021.

TABLE OF CONTENTS

1	SUMMARY	1
2	INTRODUCTION	3
2.1	Cellular functions of LDs	3
2.2	LD formation and breakdown	5
2.2.1	LD formation	5
2.2.2	LD breakdown.....	7
2.3	Protein targeting to LDs	10
2.4	Lipid synthesis for LD formation and growth	13
2.4.1	LD growth and neutral lipid synthesis	13
2.4.2	Phospholipid synthesis for LDs	15
3	AIMS OF THE THESIS	20
4	RESULTS	22
4.1	High confident LD proteome by protein correlation profiling.....	22
4.1.1	Quantitative analysis of a PCP for LD proteins by SILAC labeling	22
4.1.2	Identification of proteins specifically localizing to LDs by hierarchical clustering	25
4.1.3	Correlation of protein correlation profiling with fluorescence microscopy..	28
4.1.4	Comparison of proteomic data with genome-wide RNAi screens	32
4.2	CCT binding to LDs activates synthesis of PC for their expansion	35
4.2.1	CCT is a principal enzyme regulating phospholipid homeostasis during LD formation	35
4.2.2	PC serves as surfactant stabilizing LDs and preventing LD coalescence	41
4.2.3	Among PC synthesis enzymes, only CCT localizes to LDs	42
4.2.4	CCT directly binds to LDs by an amphipathic alpha helix	45
4.2.5	CCT is targeted to LDs when the PC to TG ratio decreases.....	47
4.2.6	CCT1 is highly mobile and shuttles between nucleus and cytosol before oleate loading.....	52
4.2.7	CCT binds stably to LDs during their expansion	55
4.2.8	CCT is activated by LD targeting	58
4.2.9	LD binding is essential for CCT1 function in LD biogenesis.....	61
4.2.10	CCT regulates LD size <i>in vivo</i>	62
4.2.11	CCT targeting and function in LD stabilization is conserved in mammalian cells	63

5	DISCUSSION	68
5.1	Protein correlation profiling identifies LD proteins with high confidence.....	68
5.2	Identification of key players for LD phospholipid homeostasis by comparing proteomic data with genome-wide screens	70
5.3	PC is a crucial surfactant stabilizing LDs and preventing their coalescence ..	71
5.4	CCT adjusts PC synthesis during LD expansion by a homeostatic feedback loop	74
5.5	CCT surveys PC levels on the LD surface and binds to PC deficient LDs	77
5.6	PC must be transported from its site of de novo synthesis in the ER to the LD surface	79
5.7	Regulating PC synthesis by CCT relocalization might be a general mechanism to maintain cellular PC levels	80
5.8	The regulation of PC synthesis by CCT relocalization during LD formation may be conserved in mammalian cells	81
6	EXPERIMENTAL PROCEDURES	83
6.1	Cell culture	83
6.2	Transgenic flies.....	86
6.3	Microscopy	86
6.4	Lipid biochemical methods.....	86
6.5	Protein biochemical methods	87
6.6	Mass spectrometry–based proteomics.....	90
7	REFERENCES	93
8	SUPPLEMENTAL TABLES	103
9	ABBREVIATIONS	110
10	ACKNOWLEDGEMENT	115
11	CURRICULUM VITAE	116

1 SUMMARY

Lipid droplets (LDs) are storage organelles for neutral lipids. Recently, these organelles have been more and more recognized as dynamic structures with a complex and interesting biology. They store energy for later use and protect cells from lipotoxicity caused by excess free fatty acids and cholesterol. Dysregulation of fat storage and mobilization, as well as excessive accumulation of LDs in tissues are key factors in pathogenesis of common diseases including obesity, insulin resistance, or hepatic steatosis. LDs have a unique physical structure. They are consisted of a neutral lipid core composed mainly of triglycerides (TG) and sterol esters (SE) that is surrounded by a phospholipid monolayer. Many proteins act on the LD surface to regulate LD functions. Despite considerable effort in determining the protein set of LDs, a reliable inventory of the LD proteome was so far missing. This thesis contains a first high confident LD proteome of *Drosophila* S2 cells that allows distinguishing between *bona fide* LD proteins and contaminants from other cellular organelles. Using a method called protein correlation profiling, I identified 106 proteins as candidates for LD proteins. Localization of a subset of these proteins by fluorescent microscopy confirmed LD targeting for more than 90% of the candidates. A comparison of proteomics data with genome-wide RNAi screens for genes whose knockdown alters LD morphology in S2 cells, revealed several LD proteins crucial for LD biology. One of them is CTP:phosphocholine cytidyltransferase (CCT), the rate-limiting enzyme for phosphatidylcholine (PC) synthesis. Studying CCT targeting and function on the LD surface led me to the discovery of an elegant paradigm for the activation of PC synthesis by enzyme relocalization to maintain organelle phospholipid homeostasis. During conditions that promote lipid storage, LDs rapidly increase their core volume and surface area, and yet it was unknown how the need for surface phospholipids is sensed and balanced during this process. Here, I show that LDs require sufficient amount of PC, which acts as surfactant to prevent

coalescence during their growth. PC synthesis for LD expansion is regulated by the activation of CCT, which binds to the surface of growing LDs. Activation of CCT by LD targeting is reversible and correlates with the need for PC at LDs, and thus may be part of a homeostatic feedback loop regulating PC synthesis. The localization and requirements for CCT were similar in *Drosophila* and murine cell lines, indicating evolutionary conservation.

2 INTRODUCTION

2.1 *Cellular functions of LDs*

The cytoplasm of eukaryotic cells is compartmentalized into distinct organelles providing functionally specialized spaces for different biochemical reactions (Rafelski and Marshall, 2008). Most organelles are surrounded by a lipid bilayer that is impermeable to most hydrophilic molecules. Consequently, import and export of specific metabolites can be controlled by specialized membrane transporters.

Important exceptions of this biological principle are LDs. LDs store lipids for metabolic energy and membrane precursors. They have a unique structure, as they are surrounded by a single phospholipid monolayer that shields the hydrophobic core consisting of neutral lipids, mainly TG and SE, from the aqueous environment in the cell (Bartz et al., 2007; Tauchi-Sato et al., 2002).

For a long time LDs were considered as inert fat particles serving no other function than a storage depot. This made them the most understudied cellular organelle and consequently to date little is known about LD cell biology. However, recently LDs are more and more recognized as highly dynamic organelles that play crucial roles in energy homeostasis and lipid metabolism. Recent functional analyses show that LDs are involved in cellular lipid and protein trafficking (Murphy et al., 2009). Moreover, they maintain tight interactions with several other organelles (Beller et al., 2010). Another interesting feature of LDs is that their size and abundance are highly regulated according to cellular needs. In response to changes in cellular conditions LD number and size can increase by several orders of magnitude within minutes (Walther and Farese, 2009). Excessive accumulation of TG droplets is observed in obesity that is further associated with increasing prevalence of pathologies, such as steatosis or type 2 diabetes, whereas storage of SEs in macrophages leads to intima thickening and is involved in the development of atherosclerosis (Brown et al., 1979).

LDs are found in all eukaryotic cells from yeast to humans and also in some prokaryotes (Figure 1) (Alvarez et al., 1996). They vary strongly in size (1-200 μm) depending on cellular conditions and cell types. Adipocytes, the most specialized cells for lipid storage form one large LD that can occupy up to 90% of the total cell volume (Fruhbeck et al., 2001).

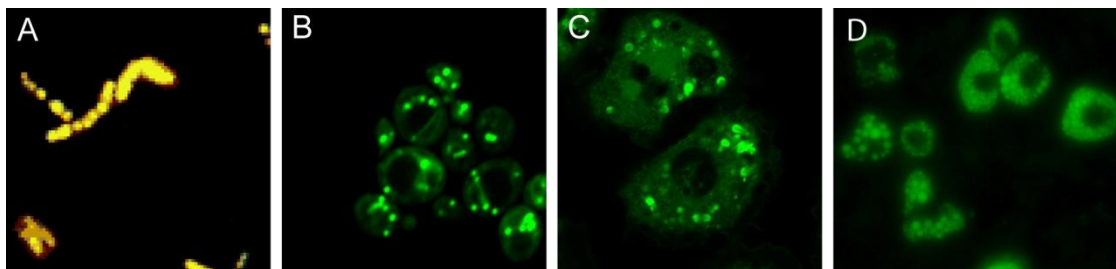


Figure 1. Examples of LDs in cells.

LDs stained with BODIPY (yellow or green) in (A) *Rhodococcus opacus* (picture from Waltermann et al., 2005). (B) *Saccharomyces cerevisiae*, (C) *Drosophila* S2 cells, (D) murine adipocytes.

LDs may provide an important evolutionary advantage, as they help the cell to tolerate environmental fluctuations between surplus of energy and starvation. In times of excessive energy availability, the cell can store energy and precursors for membranes or hormones in form of lipids in LDs, at the same time sequestering free fatty acids and cholesterol in an inert form. The accumulation of free fatty acids and cholesterol would otherwise be toxic for cells and can even lead to cell death. However, the molecular mechanisms underlying lipotoxicity still remain poorly understood (Listenberger et al., 2003). At times of increased energy needs, the cell mobilizes stored lipids and uses them to produce energy (Brasaemle, 2007; Ducharme and Bickel, 2008; Zechner et al., 2005).

In addition to their crucial role for cellular energy homeostasis, LDs were found to be important for other cellular functions. For example, studies found large amounts of histones localizing to LDs in *Drosophila* embryos, implicating LDs to be a protein storage depot during embryogenesis (Cermelli et al., 2006). Moreover, α -synuclein was found on LDs, suggesting that unfolded toxic proteins may be sequestered there

until they are degraded (Cole and Murphy, 2002). However, the mechanisms behind histone and α -synuclein targeting to LDs, as well as the regulation of their release or degradation are not known.

Besides their functions in lipid metabolism and protein storage, LDs also have an important function for the reproduction of certain pathogens. Recently, it was discovered that in hepatocytes the hepatitis C virus core protein binds to LDs and that this is an important step during the viral life cycle (Miyanari et al., 2007). The specific role of LDs in the viral replication stills needs to be fully understood but these findings suggest that therapy impairing LD formation and/or function could restrict hepatitis C virus reproduction.

2.2 *LD formation and breakdown*

2.2.1 LD formation

The current model of LD formation suggests that LDs are derived from the endoplasmic reticulum (ER) in eukaryotes. This hypothesis is supported by evidence that in some organisms, for example yeast, LDs are observed exclusively in close proximity to ER membranes (Szymanski et al., 2007). Moreover, all enzymes involved in the synthesis of TG or cholesterol ester (CE), the main components of the LD core, are localized to the ER membrane. Thus, it is thought that neutral lipids accumulate between the two leaflets of the ER membrane, forming a lipid lens that buds off the ER. In this model, the phospholipid monolayer delimiting LDs is derived exclusively from the outer leaflet of the ER membrane (Figure 2) (Fujimoto et al., 2008). Besides, alternative models, such as excision of LDs from both leaflets of the ER membrane, were also discussed. However, this model may be inconsistent with ER integrity (Figure 2) (Ploegh, 2007).

Furthermore, it is still unknown which proteins are involved in the budding process and the regulation of LD formation. So far, several proteins were found to be important for LD formation, such as seipin, a protein involved in congenital generalized lipodystrophy type 2 (Boutet et al., 2009) or the PAT-protein TIP47 (47-kDa tail interacting protein) (Bulankina et al., 2009). The PAT-proteins (originally named for perilipin, ADRP and TIP47) were among the first discovered LD proteins. However, genome-wide screens in *Drosophila* or yeast could not identify a single protein whose knockdown is sufficient to completely abolish LD formation (Guo et al., 2008; Szymanski et al., 2007).

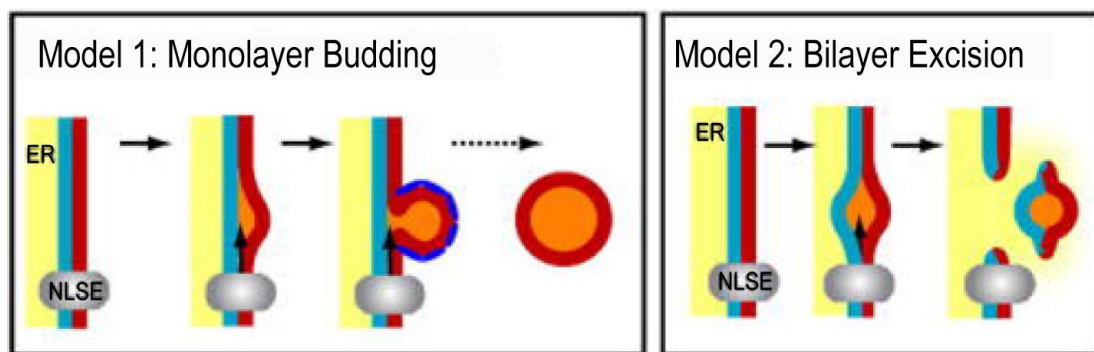


Figure 2. Models of LD biogenesis.

Model 1. LD biogenesis by ER monolayer budding. Neutral lipids (orange) are synthesized by enzymes located in the ER and accumulate between the two leaflets. A lipid lens bulges from the outer leaflet of the ER membrane (orange). Proteins localizing on the surface of the nascent droplet (dark blue) may facilitate the budding process. Model 2: Bilayer excision. In comparison to model 1 the entire lipid lens is excised from the ER, leaving a transient hole in the membrane. In this model, ER integrity cannot be maintained and ER contents (yellow) might leak into the cytosol (adapted from Walther and Farese, 2009).

Another point of current debate is whether LD biogenesis occurs all over the ER or is restricted to certain ER domains in which neutral lipid synthesis enzymes and other proteins for LD formation accumulate. For example, diacylglycerol acyltransferase (DGAT) enzymes catalyzing the last step of TG synthesis do not distribute evenly in the ER membrane but show a punctuate pattern (Shockey et al., 2006). Their distribution might reflect specialized regions in the ER for LD formation.

Another open point concerning LD formation is that it is not clear whether LDs completely detach from the ER after their formation or if the membranes of both organelles remain associated. Freeze-fracture electron micrographs revealed that many LDs remain surrounded with ER membranes, with the LD being held in an egg-cup (Robenek et al., 2006). Those sites of close apposition between LDs and the ER could correspond to specialized membrane contact sites, as they were previously described between the ER and mitochondria. Those contact sites could facilitate lipid and protein transfer between the ER and LDs (Holthuis and Levine, 2005).

2.2.2 LD breakdown

In contrast to LD biogenesis, processes involved in the breakdown of LDs to mobilize the stored lipids are better understood. Under conditions of elevated energy or metabolite needs for membrane synthesis lipolysis is induced. In adipocytes, this highly regulated process is mainly initiated by the release of catecholamines that bind to G-protein coupled receptors on the cell surface. Receptor binding subsequently induces activation of protein kinase A (PKA) by increasing cyclic adenosine monophosphate (cAMP) levels caused by enhanced adenylate cyclase activity (Steinberger D. and Huttunen, 1972). PKA activation is an important step for the regulation of several proteins involved in lipolysis by phosphorylation. One important target for PKA phosphorylation is perilipin, one of the best studied PAT-proteins and an important regulator of basal and induced lipolysis. Under basal conditions, perilipin localizes to the LD surface and shields the surface from lipases. However, after the induction of lipolysis, perilipin helps to assemble the required machinery on LDs in a phosphorylation dependent manner (Brasaemle, 2007; Tansey et al., 2001). In the basal state, perilipin binds comparative gene identification-58 (CGI-58), a coactivator of adipose triglyceride lipase (ATGL) on the LD surface. Upon phosphorylation, perilipin triggers the release of CGI-58, which then forms a complex with ATGL. Consequently, ATGL is activated and catalyzes cleavage of the first fatty

acyl chain from TG, thereby initiating TG hydrolysis on the LD surface (Lass et al., 2006; Zimmermann et al., 2009).

Another important target for PKA phosphorylation is hormone sensitive lipase (HSL) that removes the second fatty acyl chain from the glycerol backbone. HSL is targeted to LDs upon phosphorylation and interacts there with phosphorylated perilipin (Sztalryd et al., 2003). The last acyl chain is finally removed by monoacylglycerol lipase and glycerol released in the cell (Figure 3) can further be used for TG reesterification or be exported to the liver where it is further metabolized (Fredrikson et al., 1986).

To generate energy, the released fatty acyl chains are used as substrate for β oxidation to generate adenosine-5'-triphosphate (ATP) in mitochondria or peroxisomes. LDs are often found in close apposition to organelles involved in β oxidation. Regions of direct membrane contact between LDs and those organelles were suggested to facilitate the transfer of fatty acyl chains into mitochondria and peroxisomes (Murphy et al., 2009).

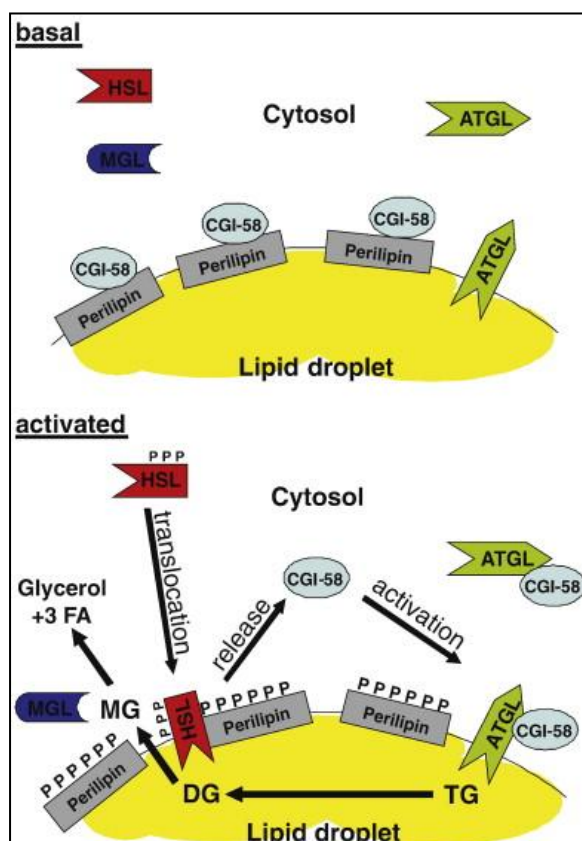


Figure 3. Model for the molecular mechanisms regulating lipolysis.

In the basal state, HSL is not bound to LDs. CGI-58 is bound to perilipin, thereby preventing ATGL activation by CGI-58. Consequently, lipase activity of HSL and ATGL on LDs is low. In the activated state phosphorylated perilipin releases CGI-58 resulting in ATGL activation. Phosphorylation of HSL leads to LD recruitment mediated by perilipin. ATGL cleaves one acyl chain from TG degrading it to DG, the substrate for HSL. HSL hydrolyses the second acyl chain, resulting in monoacylglycerol that is finally converted to free glycerol and free fatty acids by monoacylglycerol hydrolyse (adapted from Zimmermann et al., 2009).

Lipases catalyzing the breakdown of CEs have not been fully characterized yet. Several candidates were discussed to contribute to CE hydrolysis in different cell types, among them HSL or cholesterol ester hydrolase (CEH). However, none of the hydrolases identified so far provides total cellular CE hydrolase activity, suggesting that other unknown enzymes might be involved (Ghosh et al., 2010).

How the catalytic sites of different lipases access the substrate in the LD core is unknown. One possibility involves the help of other protein complexes, either to get access to neutral lipids in the core or by bringing the substrate to the lipase's catalytic site (Farese and Walther, 2009). Another hypothesis is that, depending on the LD phospholipid surface composition, a small portion of neutral lipids might be continuously exposed on the LD surface, thus being accessed easily by LD bound lipases.

Lipase access to LDs might also be facilitated by breakdown of larger droplets into smaller ones during lipolysis, thereby providing a larger surface area and offering more contact sites. However, LD fragmentation was only observed after addition of β receptor agonists to cells and it is still not clear whether this process also occurs under physiological conditions and how it is regulated (Brasaemle et al., 2004).

A completely new way to degrade LDs was discovered recently (Singh et al., 2009). It was found that in hepatocytes, under starvation conditions, LDs are degraded by macroautophagy. LDs are either completely taken up or get partially sequestered by autophagosomes, with their components being subsequently hydrolyzed in lysosomes. So far, it remains unclear how extensively macroautophagy contributes to lipid homeostasis under physiological conditions and if this mechanism is conserved between different cell types.

2.3 Protein targeting to LDs

To fulfil all the different biological functions that have been associated with LDs, many proteins were implicated to function on the LD surface (Guo et al., 2009). As LDs are the only organelle in the cell that is surrounded by a phospholipid monolayer instead of a bilayer, LD binding proteins must contain special structural features in comparison to other membrane proteins. Polytopic membrane proteins are suggested not to bind to the LD monolayer because it would be energetically unfavourable if the hydrophilic loops connecting the transmembrane would be located in the hydrophobic LD core rather than in an aqueous environment (Thiele and Spandl, 2008). Nevertheless, proteins with multiple transmembrane domains were found in different LD proteomes (Brasaemle et al., 2004; Beller et al., 2006) and it is still not clear whether these proteins localize to closely surrounding membranes rather than directly to LDs (Farese and Walther, 2009). Due to technical limitations, for example, diffraction limit in fluorescent microscopy or artefacts using immunogold labeling electron microscopy, it is impossible to distinguish between direct LD localization and targeting to surrounding membranes (Robenek et al., 2005). The development of new technologies such as super high resolution microscopy might enable scientists to answer those questions in the future (Toomre and Bewersdorf, 2010).

In contrast, there are several other hydrophobic structural features that might mediate direct targeting to the LD monolayer. For example, proteins with lipid anchors, such as Rab18 (Ras-related in brain 18) found on LDs, in addition to membranes (Figure 4) (Martin et al., 2005). Proteins also localize to LDs by binding of hydrophobic domains to the LD surface. These domains can be localized anywhere within the protein. For example, DGAT2 and caveolin were both shown to integrate into the LD monolayer by one long central hydrophobic hairpin structure with both N- and C-termini being exposed on the cytosolic side (Figure 4) (Robenek et al., 2004; Stone et al., 2009).

Many other proteins bind to LDs by amphipathic helices (Thiele and Spandl, 2008). One example for this is TIP47, which is structurally very similar to apolipoprotein E. Both proteins consist of four amphipathic α helices. In the unbound state the four helices form a closed bundle burying the hydrophobic parts in the core. When opening the bundle, the hydrophobic regions are exposed and the proteins can bind to LDs or lipoproteins, respectively. Thereby, the hydrophobic side of the helix embeds in the LD monolayer and the hydrophilic site remains exposed to the aqueous environment (Hickenbottom et al., 2004; Ohsaki et al., 2006).

Amphipathic helices are a common structural feature for membrane binding. However, most proteins with amphipathic helices exclusively bind to bilayers and not to LDs, whereas other amphipathic helices specifically mediate LD targeting. Several proteins can bind both, membranes and LDs and their localization is regulated in response to different cellular conditions (Ohsaki et al., 2006). How proteins can distinguish between bilayers and monolayers and which structural features target them either to membranes or LDs is not known. One possibility could be that neutral lipids from the LD core are partially exposed on the LD surface and thus induce the binding of certain amphipathic helices or other LD targeting domains.

Moreover, for proteins targeted to LDs from different cellular localization in response to different stimuli, it is not known what induces their LD targeting. Several mechanisms, including post-translational modifications or a special lipid composition on the LD surface, are possible (Walther and Farese, 2009).

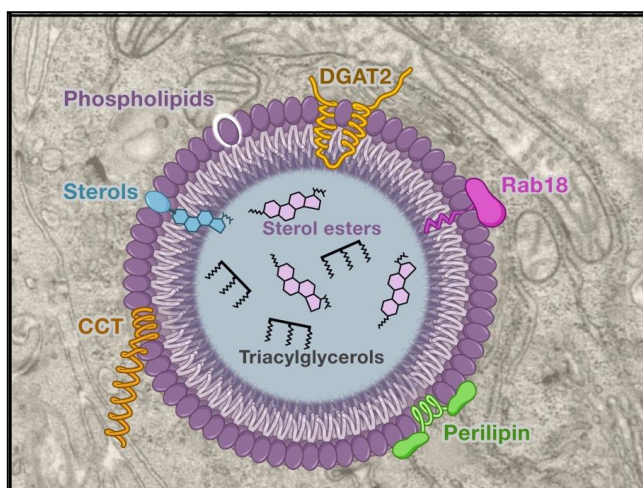


Figure 4. Different possibilities for LD protein topology.

Proteins, such as Rab18, can bind to LDs by a hydrophobic fatty acid anchor. CCT or PAT proteins bind by amphipathic alpha helices that embed into the LD monolayer. DGAT2 is targeted to LDs by a hydrophobic hairpin domain.

Despite those known structural features that mediate LD targeting, the general targeting process to the LD surface and its regulation are less understood than those for other organelles, such as mitochondria or the ER, for which specific targeting signal sequences were identified.

Besides the diversity in targeting sequences, targeting mechanisms for LD proteins also seem to differ. Some of the proteins localize exclusively to LDs, whereas others are targeted from different cellular locations, such as the ER, cytosol or caveolae, to the LD surface. Therefore, it is suggested that a couple of different targeting mechanisms might exist, depending on the structure and localization of the protein before LD targeting (Thiele and Spandl, 2008).

Several *trans* acting factors might be involved in some of those targeting pathways. One of those factors might be the Arf1/COPI (ADP ribosylation factor1/coat proteinI) machinery, as LD targeting of some proteins is dependent on Arf1/COPI. Knockdown of Arf1 or COPI components results in a very strong phenotype with larger and more dispersed LDs in *Drosophila* and also in mammalian cells (Beller et al., 2008; Guo et al., 2008). In Arf1 or COPI depleted cells, ATGL association with LDs decreases and ATGL accumulates in specialized ER exit sites (ERES) and ER-Golgi intermediate compartments (ERGIC), resulting in a reduction in lipolytic activity on LDs (Soni et al., 2009). The mechanism of Arf1/COPI dependent LD protein targeting is still not known. Vesicular transport to LDs is possible but presents a topological problem, as it would require vesicle bilayer fusion with the LD monolayer. As a solution of this problem, protein transfer by a “kiss-and-run” mechanism including a hemi-fusion event between the vesicle and the LDs was suggested (Walther and Farese, 2009). Another hypothesis describes a recruitment mechanism for proteins to the LD surface by LD localized Arf1/COPI components. However, experimental proof for any of those models is still missing (Walther and Farese, 2009).

2.4 Lipid synthesis for LD formation and growth

2.4.1 LD growth and neutral lipid synthesis

Many organelles regulate their abundance and size according to need under different cellular conditions. An especially dramatic example for that are LDs. When cells are confronted to an excess of fatty acids from *de novo* lipogenesis or extracellular sources, LDs can increase their volume and number by several orders of magnitude to protect cells from lipotoxicity (Listenberger et al., 2003). In other mammalian cell types, such as macrophages, large amounts of SE must be stored to prevent excessive amounts of sterols in membranes (Prieur et al., 2010). Thus, in a relatively short time LDs can deposit massive amounts of neutral lipids in their core.

Especially cell types specialized for lipid storage, such as mammalian adipose tissue or fly fat body react with rapid and dynamic changes in LD size and abundance to changes in nutrient intake and energy balance. Conditions of saturated lipid storage capacity in adipose tissue lead to accumulation of large amounts of TG in tissues that normally contain only a few small LDs, which is associated with obesity, type II diabetes and tissue steatosis (Savage et al., 2007). Thus, regulating LD size and abundance and preventing an excess of LD accumulation at the cellular level may play an important role in those complex metabolic diseases.

Mechanisms of LD expansion are mostly unknown. LD growth reflects deposition of large amounts of TG and SE in the LD core. CE synthesis is catalyzed by acyl coenzyme A:cholesterol acyltransferase (ACAT) (Buhman et al., 2000). TG synthesis mainly occurs from the glycerol phosphate pathway that is at least in part regulated by substrate availability and flux through the enzymatic reactions. In this pathway fatty acid moieties are sequentially added to the glycerol backbone. In the last step diacylglycerol (DG) and fatty acyl CoA are converted to TG in a reaction catalyzed by DGAT enzymes. Most of the enzymes involved in TG and in CE synthesis were found to localize to the ER or mitochondria and have several isoforms (Yen et al., 2008). How the newly synthesized neutral lipids are delivered to the cores of growing

LDs is not known. It is unclear how such highly hydrophobic neutral lipids could translocate from the ER to growing LDs, especially since components for a potential transfer mechanism have not been discovered yet. However, recent studies showed that DGAT2, catalyzing the final step of TG synthesis, localizes to LDs, thereby suggesting that neutral lipids might be locally synthesized on LDs (Kuerschner et al., 2008; Stone et al., 2009). Nevertheless, it still not known how TG is transferred to the LD core and whether only the reaction catalyzed by DGAT2, or maybe more steps of the TG synthesis pathway, occur directly on the LD surface or on the surrounding specialized membrane domains.

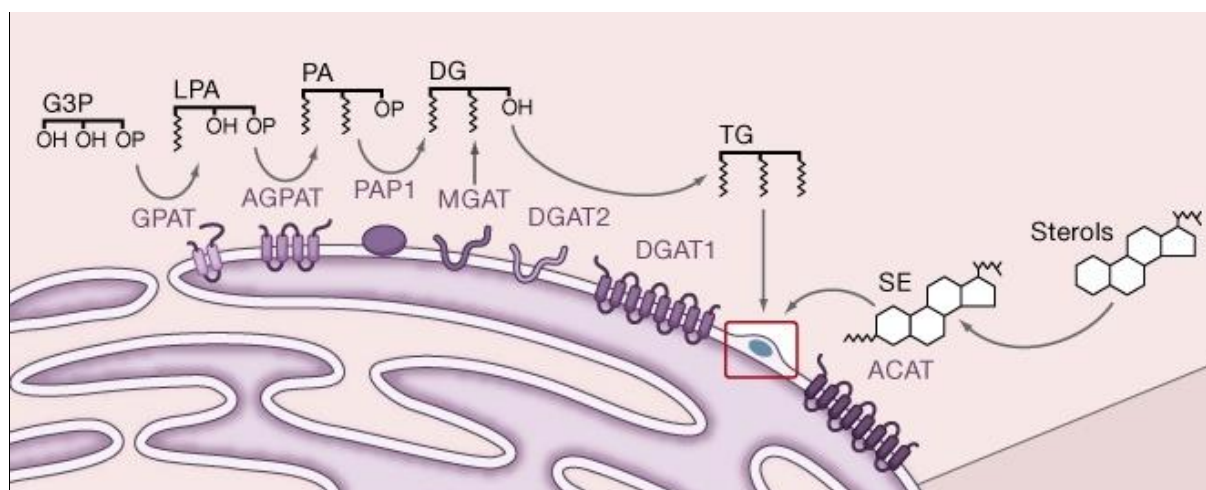


Figure 5. Neutral lipid synthesis.

The final step of TG synthesis, the transfer of a fatty acid from fatty acyl CoA to DG, is catalyzed by DGATs. DG the precursor of TG, is synthesized either by phosphatidic acid phosphatase 1 (PAP1) from phosphatidic acid (PA) or by monoacylglycerol acyltransferases (MGATs) from monoacylglycerol. PA is made from glycerol-3-phosphate by reactions catalyzed by glycerol-3-phosphate-acyltransferase (GPAT) and acylglycerol-3-phosphate-acyltransferase (AGPAT). Similarly, SEs are synthesized by ACATs, which transfer fatty acyl chains to free cholesterol. All those enzymes were found to localize to the ER. Newly synthesized TG and SE are thought to accumulate between the two leaflets of the ER membrane and form an oil lens that buds off the ER. How neutral lipids get on the LDs for LD growth after the budding is unknown. Specific isoforms of the enzymes involved in neutral lipid synthesis might localize to LDs or surrounding specialized membrane domains for localized neutral lipid synthesis on LDs.

LD may also grow by homotypic fusion of smaller droplets into larger ones. SNARE proteins were suggested to mediate those fusion events (Bostrom et al., 2007). Nevertheless, the mechanism of LD fusion remains unclear, as conclusive data is still missing. Moreover, in most cell types LD fusion is a rare event that can hardly be detected. Only in adipocytes LD fusion can widely be observed when small droplets form the characteristic unilocular large LD. In adipocytes, LD fusion is dependent on Fat-specific protein of 27 kDa (FSP27), a member of the Cell Death-Inducing DFF45-Like Effector (CIDE) family that localizes to LDs and enhances neutral lipid storage (Nishino et al., 2008). The three CIDE proteins, CIDEa, CIDEb and FSP27, containing an N-terminal CIDE-N domain that shares sequence similarity with the N-terminal of DNA fragmentation factor Dffa/Dff45/ICAD and a unique C-terminal CIDE-C domain, were discovered to localize to LDs and to be involved in many metabolic disorders (Gong et al., 2009). However, CIDE proteins are not found in all tissues. FSP27 expression is largely restricted to white adipose tissue and thus cannot provide a general mechanism for LD growth. Furthermore, any mechanistic understanding of protein catalyzed LD fusion is still missing (Nishino et al., 2008).

2.4.2 Phospholipid synthesis for LDs

Under conditions of energy excess, large amounts of neutral lipids are deposited in the hydrophobic LD core and the neutral lipid content can increase by several orders of magnitude within a relatively short time. This volume increase of the neutral lipid core has to be coordinated with the expansion of the surface monolayer. The LD monolayer contains mainly phospholipids and smaller amounts of free cholesterol. The phospholipid composition is very similar to that of the ER membrane, with minor differences, such as slightly increased lyso-PC content and small variations in the fatty acid composition (Tauchi-Sato et al., 2002). PC and phosphatidylethanolamine (PE) are the most abundant phospholipids, constituting more than 90% of total LD phospholipids. Besides PC and PE, small amounts of phosphatidylserine (PS),

phosphatidic acid (PA) and phosphatidylinositol (PI) can be found (Kuerschner et al., 2008).

PC and PE are mostly made through analogous pathways starting from choline or ethanolamine, respectively. These pathways were discovered by Eugene Kennedy in the 1950s and are thus called Kennedy pathways (Figure 6) (Kennedy, 1959). Alternatively PE can be made by decarboxylation of PS by PS decarboxylase (PSD) (Zborowski et al., 1983). The contribution of this pathway for total PE synthesis is cell type dependent (Vance and Vance, 2008). Also for PC synthesis an alternative pathway exists. PE can be converted to PC by sequential methylation by PE methyltransferase (PEMT). PEMT is mainly expressed in hepatocytes in which 30-40% of the total cellular PC is made from this pathway (Sundler and Akesson, 1975).

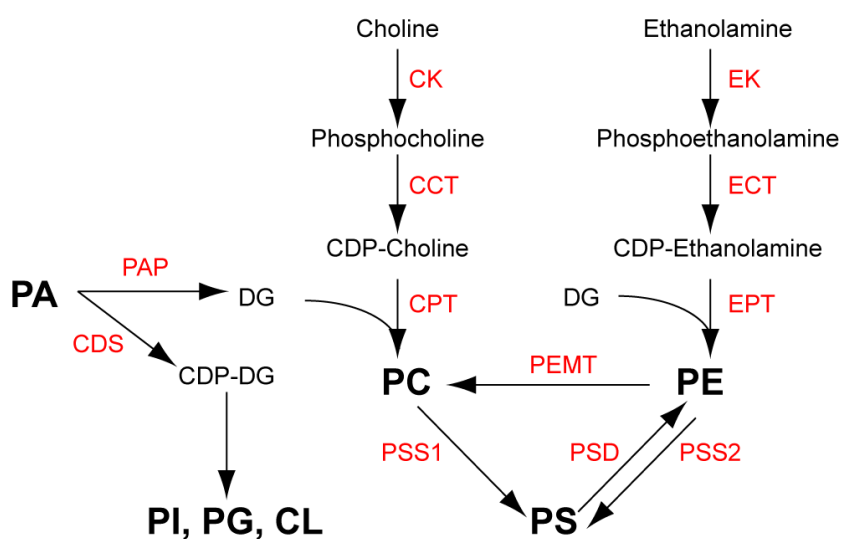


Figure 6. Overview of phospholipid synthesis pathways in mammalian cells.

PA serves as precursor for the synthesis of either DG by phosphatidic acid phosphatase (PAP) or CDP-DG by CDP-diacylglycerol synthetase (CDS). CDP-DG is used for the generation of PI, phosphatidylglycerol (PG) or cardiolipin (CL), whereas DG is necessary for the formation of PC and PE by analogous pathways [choline kinase (CK), CTP:phosphocholine cytidylyltransferase (CCT), choline phosphotransferase (CPT) ethanolamine kinase (EK), ethanolamine cytidylyltransferase (ECT), ethanolamine phosphotransferase (EPT)]. PE can be converted to PC by PEMT. PS is synthesized by head group exchange to serine by phosphatidylserine synthase (PSS). PE can be synthesized from PS by phosphatidylserine decarboxylase (PSD).

Little is known about how synthesis and addition of phospholipids to the LD monolayer are regulated during LD growth. A previous genome-wide RNAi screen showed that knockdown of enzymes involved in phospholipid biosynthesis increased LD size and promoted their fusion (Guo et al., 2008). Here, fatty acid synthase (FAS) and sterol regulatory element-binding protein (SREBP) that regulates fatty acid synthesis in *Drosophila* were among the strongest phenotypes. Moreover, giant LDs resulted from the knockdown of choline kinase (CK) that catalyzes the phosphorylation of choline in the first step of the Kennedy pathway for PC synthesis. The same phenotype was observed for the knockdown of both isoforms of CCT catalyzing the formation of CDP-choline, the second step of this pathway (Choy and Vance, 1976). Thus, phospholipids of the LD-delimiting monolayer may play an important role in regulating LD size, and the candidates identified in the screen that resulted in the formation in larger LDs might play an important role in adjusting cellular PC levels according to need.

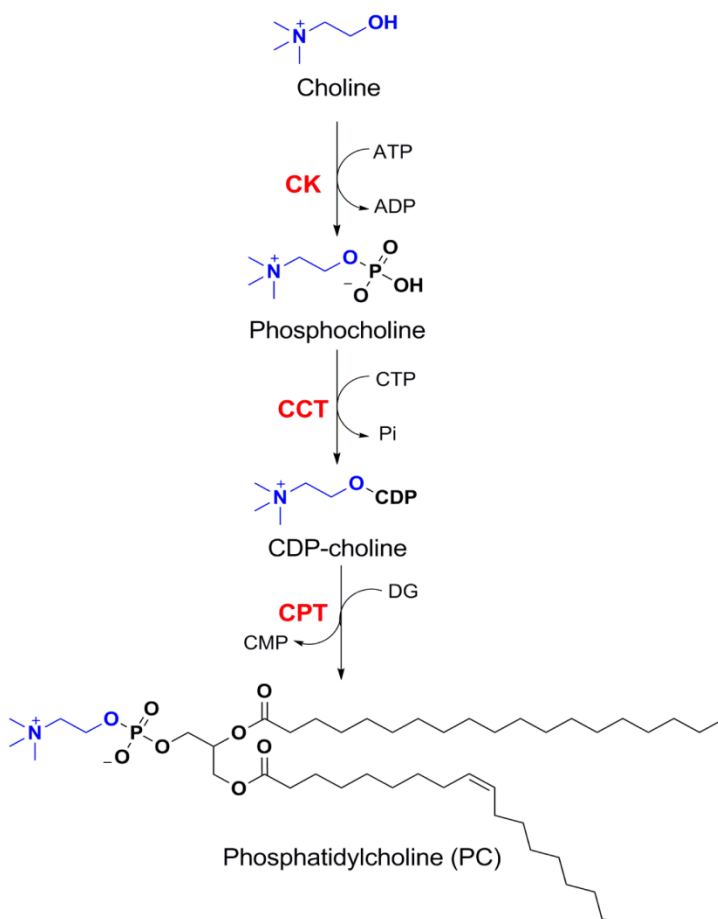


Figure 7. The Kennedy pathway for PC synthesis.

In most cell types PC is made from choline by the Kennedy pathway. First, choline is phosphorylated by CK. Then, CCT catalyzes the formation of CDP-choline from phosphocholine and CTP, in the rate-limiting step of this pathway. Finally, CPT catalyzes the formation of PC from one molecule of CDP-choline and one molecule of DG. PE is synthesized by an analogous pathway.

CK activity can only be regulated at transcriptional levels (Kent, 2005), whereas CCT is highly regulated by a combination of different posttranslational mechanisms. In mammals and in *Drosophila* two CCT genes exist, encoding CCT α and CCT β or CCT1 and CCT2, respectively (Helmink and Friesen, 2004). Whereas CCT β and CCT2 are localized in the cytosol, CCT α and CCT1 contain an N-terminal nuclear localization sequence (NLS) and are mainly found in the nucleus (Tilley et al., 2008). It was suggested that the nuclear pool might provide a sequestered inactive pool (Northwood et al., 1999). However, the function of nuclear localization remains still unclear.

CCT activity is highly regulated by reversible membrane binding. The enzyme was shown to convert between an inactive soluble form and an active membrane-bound form. Membrane binding is mediated by a helical domain that changes its structure from a random coil in the unbound form to an amphipathic alpha helix in the membrane bound state (Feldman et al., 1985; Vance and Pelech, 1984). In the unbound conformation, the helical domain exerts an autoinhibitory function on the catalytical domain that is relieved when the enzyme binds to membranes and thus CCT activity can increase up to 80-fold (Friesen et al., 1999). It was shown that changes in the lipid composition induce membrane targeting. The accumulation of different lipid types, such as PE, DG, anionic lipids or free fatty acids, were reported to increase CCT membrane localization. Moreover, an inverse correlation between PC levels in the membrane and membrane targeted CCT was observed, indicating a feedback inhibition of PC synthesis by PC (Mallampalli et al., 1993).

Furthermore, all CCT forms have a C-terminal phosphorylation domain containing multiple serine residues. It was shown that dephosphorylated CCT has higher membrane affinity and thus is easier to be activated than the phosphorylated form of the enzyme (Kent, 1997). So, it seems that phosphorylation is an additional mechanism to fine tune CCT activity and to provide a regulatory switch to modulate enzymatic activity.

Although cellular regulation of phospholipid synthesis, especially of PC, has been well characterized, nothing is so far known how phospholipid synthesis is coordinated with LD formation and growth. When LDs are formed and growing, large amounts of phospholipids are needed to cover the surface and to shield the neutral lipids in the core from the aqueous environment. A further characterization of genes involved in phospholipid biosynthesis showing a strong phenotype might provide a possibility to get more insight in these processes.

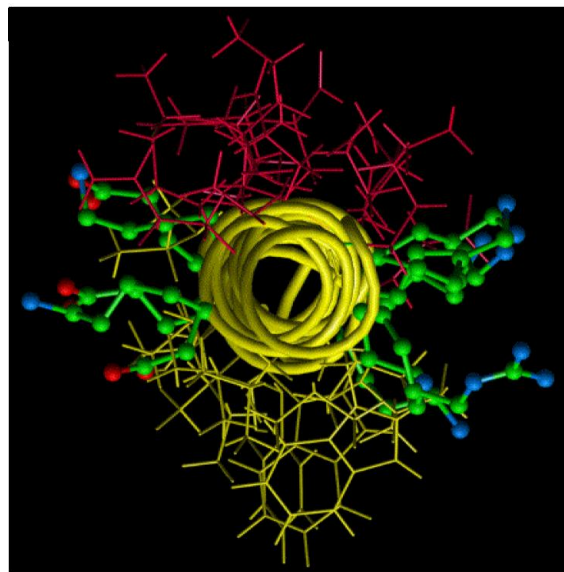


Figure 8. Domain structure of CCT1.

(A) CCT1 contains an N-terminal NLS, followed by a highly conserved catalytic core. A helical domain that mediates lipid binding and a C-terminal phosphorylation domain.

(B) Structure of the membrane-binding amphipathic α helix from CCT α , based on the atomic coordinates of two overlapping peptides. Side chains of the polar face are red; side chains of the nonpolar face are yellow. The carbon (green), nitrogen (blue), and oxygen atoms (red) of the interfacial side chains are in ball-and-stick representation (Cornell and Northwood, 2000).

3 AIMS OF THE THESIS

Many molecular mechanisms underlying the regulation of cellular fat storage are still poorly understood. Recently, LD proteins such as the PAT proteins and the CIDE family have been found to be key players in the regulation of LD abundance, morphology and function (Brasaemle, 2007; Gong et al., 2009). However, many of the proteins functioning on the LD surface and regulating important processes in cellular lipid homeostasis have not been identified yet and a reliable and quantitative characterization of the LD proteome is still missing. This is mainly due to technical and methodical limitations of existing proteomic studies (Bartz et al., 2007; Beller et al., 2006; Brasaemle et al., 2005; Cermelli et al., 2006). LDs are closely associated with other organelles, what makes it impossible to purify them to homogeneity. Previously used methods do not allow distinguishing between *bona fide* LD proteins and potential contaminants. Thus, the generated data sets are not reliable and contain contaminating proteins from other organelles.

Therefore, the first aim of this study was to generate a high confidence LD proteome of *Drosophila* S2 cells that allows a reliable characterization of LD localized proteins and excludes contaminants from other organelles. To this end, I used a strategy called “protein correlation profiling” that is based on a quantitative analysis of proteins in all fractions during organelle purification and allows the identification of specifically enriched proteins in the purified fraction. I compared the results of this proteomic study to data derived from genome-wide screens in *Drosophila* S2 cells (Guo et al., 2008; Beller et al., 2008) to identify proteins important for LD function localizing to the LD surface. One interesting candidate strongly enriched in the LD fraction and whose knockdown resulted in one of the strongest phenotypes detected in the screen was CCT, the rate-limiting step for PC synthesis. Also other proteins involved in the synthesis of phospholipids gave strong LD phenotypes, indicating that phospholipid biosynthesis pathways might play an important role during LD formation and for LD function.

Thus, in the second part of this study I focus on how phospholipid homeostasis is maintained during LD formation and growth, when large amounts of phospholipids are required to shield large amounts of neutral lipids added to the LD core. The aim of this part of the study was to elucidate the importance of different phospholipids for LD stability and to identify phospholipid biosynthetic enzymes that are crucial for LD phospholipid homeostasis. Among different phospholipid species, I identified PC as the most important detergent for LD stability and CCT, rate-limiting enzyme for PC synthesis, as key player in LD PC homeostasis in *Drosophila* S2 cells. As CCT localizes to the LD surface after the induction of LD formation (Guo et al., 2008), the next aim for me was to characterize the LD targeting signal and the targeting mechanism for CCT in S2 cells. The goal was to test what induces relocalization of the enzyme from the nucleus or cytosol to the LD surface and whether enzymatic activity is changed by LD targeting. Elucidating the CCT targeting mechanism led me discover that PC synthesis for LD formation is regulated by a homeostatic feedback loop that is controlled by CCT relocalization. Finally, I tested whether CCT function is also relevant *in vivo* and whether the mechanism of maintaining PC homeostasis during LD formation is conserved in different mammalian cell types.

4 RESULTS

4.1 High confident LD proteome by protein correlation profiling

4.1.1 Quantitative analysis of a PCP for LD proteins by SILAC labeling

The combination of subcellular fractionation and mass spectrometric analysis, referred to as organellar proteomics, is a powerful method that facilitates comprehensive characterization of subcellular structures (Andersen and Mann, 2006). However, due to increasing sensitivity of mass spectrometers and difficulties in purifying organelles to homogeneity, it is challenging to distinguish *bona fide* organellar proteins from those that are contaminants. This problem is particularly relevant for LDs. Purifying LDs to homogeneity is impossible, since LDs maintain close contacts to organelles, such as mitochondria or peroxisomes and have been shown to be tightly enwrapped by ER membranes.

To overcome these problems, I adapted a strategy called protein correlation profiling to generate a LD proteome from *Drosophila* S2 cells. Protein correlation profiling is based on the different behavior of proteins originated from different organelles during a purification process. The abundance of a protein is followed over all fractions of an organelle purification, which allows generating a purification profile for each protein. Proteins derived from the same organelle are expected to have very similar profiles. Thus, protein correlation profiling enables to determine the subcellular localization of proteins by comparing a protein's profile to profiles of known organellar markers (Andersen et al., 2003; Foster et al., 2006).

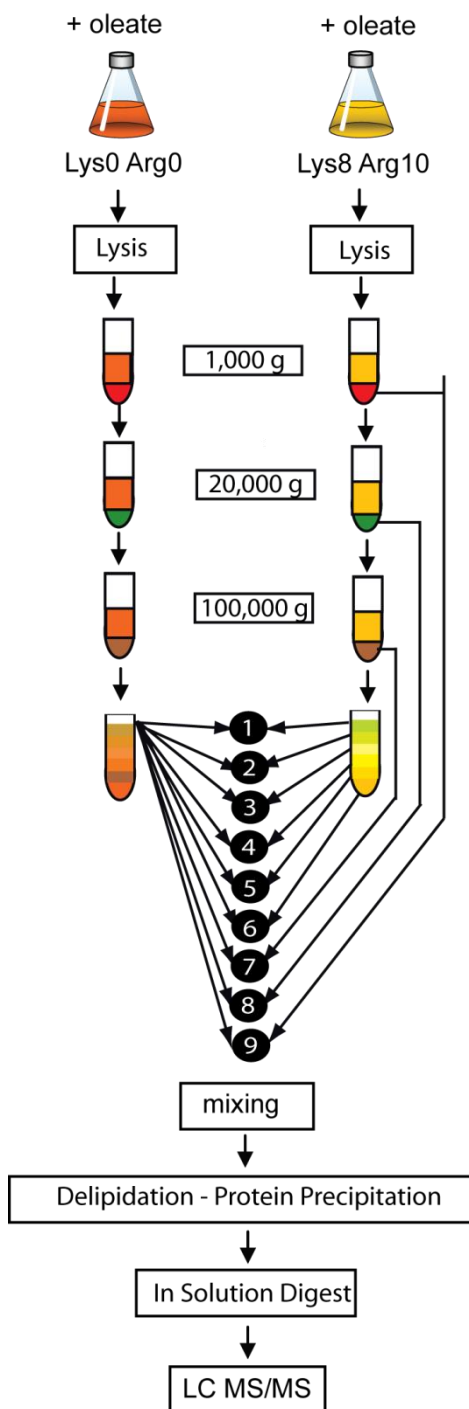


Figure 9. Experimental scheme of quantitative analysis of a LD proteome by protein correlation profiling.

LDs were purified from two populations of *Drosophila* S2 cells, one unlabeled and one labelled with heavy amino acids Arg10 and Lys8. After three steps of differential centrifugation, cell lysates were loaded on a sucrose step gradient. For quantitative analysis, light LD fraction was mixed in a 1:1 ratio with six fractions of the heavy sucrose gradient and three pellets from the centrifugation steps. Mixed fractions were delipidated and proteins precipitated. After in solution digest, samples were analyzed by high-resolution liquid chromatography–MS/MS (LC MS/MS).

Previously, LDs were purified by overlaying cell lysates with a sucrose layer and floating them on top (Brasaemle and Wolins, 2006). To get higher LD purity; I improved the protocol for several steps. Specifically, I included several differential centrifugation steps prior to loading S2 cell lysate to the sucrose gradient in order to remove stepwise unbroken cells, nuclei, mitochondria and membranes. Subsequently, I loaded the lysate on the bottom of a sucrose step gradient. I analyzed the three centrifugation pellets and six sucrose gradient fractions by LC MS/MS. For relative protein quantification, I applied stable isotope labeling with amino acids in cell culture (SILAC) and used a light LD fraction as internal standard that was spiked in a 1:1 ratio in each fraction of a purification from heavy labeled cells (Figure 9). Then, I delipidated and digested in solution the resulting protein mixtures (Olsen et al., 2006). Each fraction was analyzed by reverse-phase chromatography coupled to high-resolution, quantitative mass spectrometric analysis using a LTQ Orbitrap. In total, I identified 2,855 proteins at least once in triplicate analysis. 1,361 of them were detected in fraction1, containing LD heavy mixed with LD light. The average peptide ratio heavy/light in fraction1 was 1.36, indicating a high reproducibility of the experiment. Fraction 1 contains a 1:1 mixture of LD light and LD heavy fraction and thus, the average ratio heavy/light should be close to one if the fractions of the two biological replicates show strong overlap.

To confirm that proteins of different organelles can be distinguished by this method and diverge in their protein correlation profiles, I calculated averaged normalized peptide intensities of five characterized marker proteins of different organelles (Table S1) and compared their profiles (Figure 10). As expected LD proteins (red line) had their main abundance mainly in fraction1, the top fraction of the sucrose gradient and showed very low abundance in all other fractions. Nuclear and mitochondrial proteins (yellow and green line, respectively) had different PCPs with main peaks in fractions 8-9, representing the pellet fractions of differential centrifugation. In general, cytosolic proteins (purple line) showed a broad distribution between fractions 3-6, the bottom

fractions of the sucrose gradient. ER proteins (blue line) were detected with high abundance in the LD fraction but still had their main peak in microsomal fractions 7-9. Thus, proteins of different organelles diverge greatly in their behavior among the fractions of the gradient. The comparison of the PCPs shows that in general PCP allows distinguishing bona fide LD proteins from contaminants that might be detected in the LD fraction.

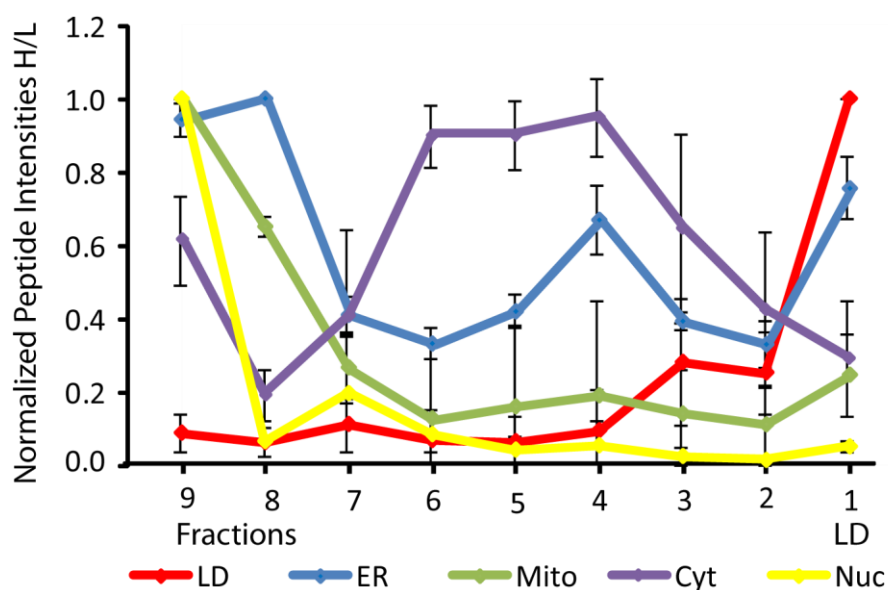


Figure 10. Averaged fractionation profiles for different organellar marker proteins.

The average normalized peptide intensities for marker proteins of the indicated cellular organelles, as determined by quantitative LC-MS/MS, are shown for fractions of a LD purification. Values are mean \pm SD of five proteins.

4.1.2 Identification of proteins specifically localizing to LDs by hierarchical clustering

To identify the proteins specifically enriched in the LD fraction among the 1,361 proteins detected in fraction1, I performed a hierarchical cluster analysis. Clustering revealed, consistent with the average protein correlation profiles (PCPs) (Figure 10) that proteins of same organelles show very similar behaviour during the purification process, as proteins of same organelles were strongly enriched in specific clusters (Figure 11A). One cluster contained proteins that were enriched only

in fraction 1 with no peaks in other fractions (Figure 11A, B yellow box). In total, this LD cluster 1 contained 45 proteins (Table S2). This set of proteins was considered to include proteins with the highest probability to localize to LDs, as they have their main abundance exclusively in the LD fraction, in contrast to potential contaminants that should also have strong additional peaks in other fractions. Three other clusters, named LD cluster 2, 3 and 4 also showed strong enrichment in fraction1, but had additional peaks in other fractions (Figure 11B, C, white boxes). These proteins might also contain LD proteins, however, with less confidence. Proteins from those clusters might be proteins with dual subcellular localization that are targeted to LDs but that also have a pool on some other organelle or otherwise be contaminants from other organelles in the LD fraction. LD cluster 2 contained 14 proteins, LD cluster 3 38 proteins and LD cluster 4 10 proteins (Table S3, S4, S5). Table 1 shows a selection of interesting candidates from certain biosynthetic pathways or special functions found in the LD proteome. In addition to the already characterized lipases brummer (homolog of ATGL) with its co-factor CGI-58 and HSL, I identified two so far uncharacterized lipases CG9186 and CG17292 on the LDs. CG9186 is highly evolutionary conserved from yeast to mammals, suggesting an important function for this protein in LD function. Moreover, several lipid transfer proteins, homologues of SEC14 and oxysterol binding proteins were strongly enriched in the LD fraction. In addition, I found some proteins involved in TG and phospholipid synthesis in the LD proteome.

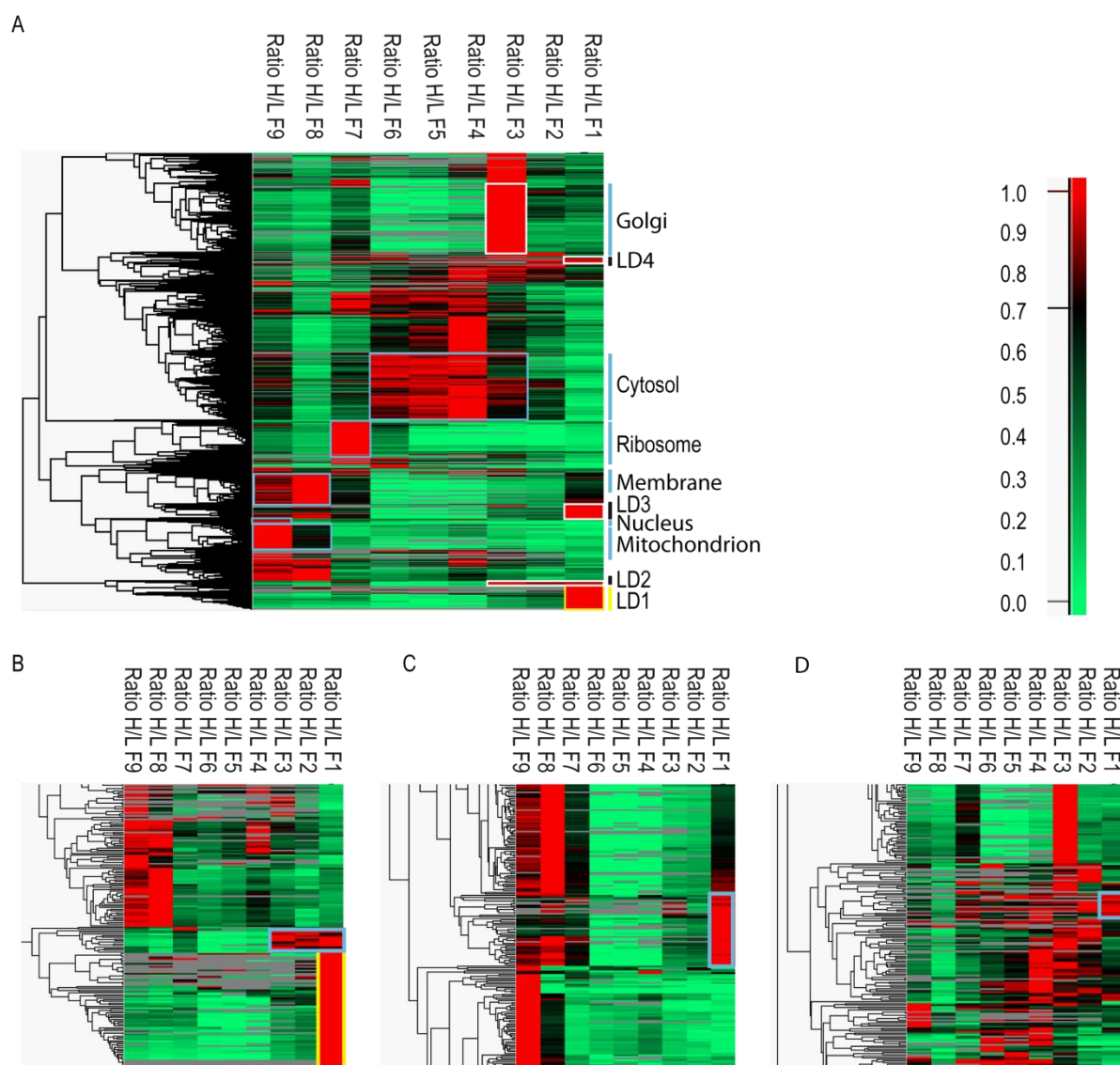


Figure 11. Hierarchical clustering of proteins identified in fraction1.

(A) Hierarchical clustering of 1,361 proteins identified in fraction 1 of LC MS/MS analysis of all fractions of a LD purification. The colour code represents the peptide ratio heavy/light normalized by the maximum value among the fractions. Grey indicates that the protein was not identified in that fraction. Cellular organelles whose proteins are enriched in a certain cluster are indicated on the right. Cluster with proteins having a single peak in fraction1 is marked in yellow. Cluster with proteins having their main peak in fraction 1 but also showing peaks in other fractions are indicated in white. (B), (C) and (D) Zoom of LD clusters 1+2, 3 and 4 from (A), respectively.

CG	Protein name	Pfam Descriptions
Lipid transfer proteins		
CG13848	Prolonged depolarization afterpotential (PDA) is not apparent	CRAL/TRIO domain
CG1513	Oxysterol-binding protein	Oxysterol-binding protein;PH domain
CG5077	Oxysterol-binding protein	Oxysterol-binding protein;PH domain
Triglyceride synthesis		
CG8709	CG8709	Lipin
CG3209	GPAT	Acyltransferase
CG4729	AGPAT	Acyltransferase
Phospholipid synthesis		
CG1049, CG18330	CTP:phosphocholine cytidyltransferase 1, 2	Cytidylyltransferase
CG9655	Transmembrane protein nessy; lyso-PA acyltransferase	MBOAT family
CG32699	Lyso-PA acyltransferase	Acyltransferase
CG4825	CG4825	Phosphatidyl serine synthase
Lipases and co-factors		
CG1882	CGI-58	Alpha/beta hydrolase fold
CG5295	Brummer (ATGL)	Patatin-like phospholipase
CG11055	Hormone-sensitive lipase (HSL)	Alpha/beta hydrolase fold
CG9186	CG9186	Uncharacterised conserved lipase1 (DUF2305)
CG17292	CG17292	Uncharacterized lipase2
ER shape		
CG10326	ARL-6-interacting protein 1 homolog	Reticulon
CG33113	Rtnl1	Reticulon
CG4775	Tango14, NogoB-receptor	Transport and golgi organization
CG6668	Atlastin	Guanylate-binding protein

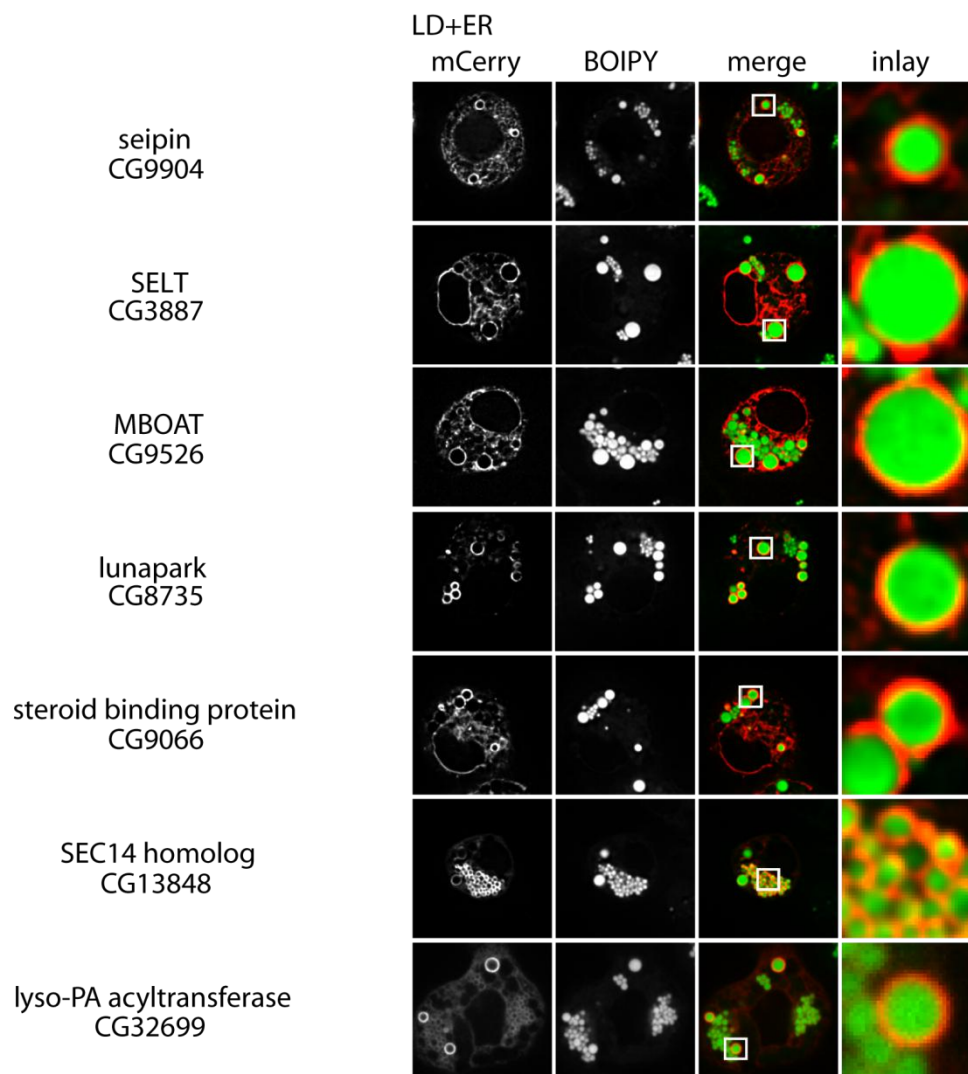
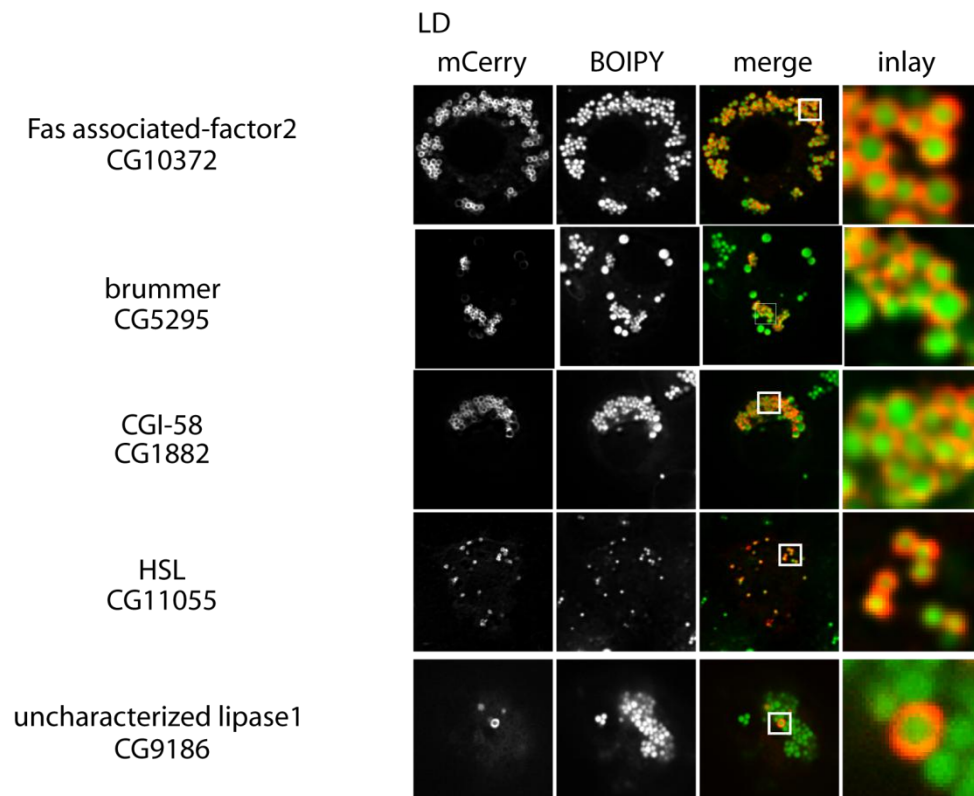
Table1. Examples for proteins identified as LD proteins by hierarchical clustering.

4.1.3 Correlation of protein correlation profiling with fluorescence microscopy

To independently confirm the localization of candidate LD proteins identified by protein correlation profiling and to test the reliability of the generated data set, I fluorescently tagged 20 proteins detected in the LD proteome and determined their subcellular localization in oleate loaded and BODIPY stained S2 cells by fluorescence microscopy. Among the 20 tagged proteins, 18 showed clear LD localization. This indicates that the confidence rate of the by protein correlation profiling identified LD proteins is very high, as the LD localization of about 90% of the tagged proteins was true. Several of the tagged proteins localized exclusively to LDs (Figure 12A). Those proteins were all found in the LD cluster 1 consistent with their PCPs that all showed a single strong peak in the LD fraction (Figure 13A). Among the proteins localizing to LDs, different interesting patterns were observed. For example, brummer (ATGL) was specifically enriched around smaller LDs or CG9186, the uncharacterized lipase1, was in some cells specifically targeted to very few LDs in the cell (Figure 12A).

Many of the tagged proteins showed dual subcellular localization to LDs and some other compartment. Those proteins were found in all four LD clusters. Many proteins were found to target to LD and ER membranes (Figure 12B). The PCPs for most of those proteins already indicated this dual cellular localization, because most proteins of this group had a strong peak in the microsomal fractions 7-9 in addition to the LD peak (Figure 13B). However, not all of the proteins classified by fluorescence microscopy as LD and ER proteins showed this second peak in their PCP. This potentially indicates that, in contrast to endogenous levels, overexpression of some of these tagged proteins saturates LD binding, resulting in an accumulation in other cellular compartments. Many of the dual localized LD-ER proteins, such as CG3887 (SELT) or CG9904 (seipin) specifically accumulated around larger LDs. Other proteins, such as CG8735 (lunapark) partially formed half rings around LDs and did not surround the complete LDs, what might indicate that those proteins do not localize directly to LDs but might be enriched in specialized membrane domains that enwrap LDs. An alternative that would explain this localization pattern would be an organization of specialized membrane domains on the LDs surface itself. Some other proteins localized to LDs and different other cellular compartments, such as the plasma membrane (CG17292, uncharacterized lipase2) or the cytosol (CG4775, Tango14) (Figure 12C). For most of those proteins, the dual subcellular localization was also reflected in their PCPs (Figure 13C).

Only for two of the tagged proteins, CG33113 (reticulon) and CG5014 (VAP-33-1), no characteristic rings around BODIPY stained LDs were detectable and they showed an ER like pattern (Figure 12D). PCPs for both proteins showed their main abundance in the LD fraction but they also had peaks in the microsomal fractions (Figure 13D). Thus, those proteins might either be contaminants in the LDs fraction or the endogenous proteins might localize to LDs and tagging interferes with protein function or the LD targeting mechanism.



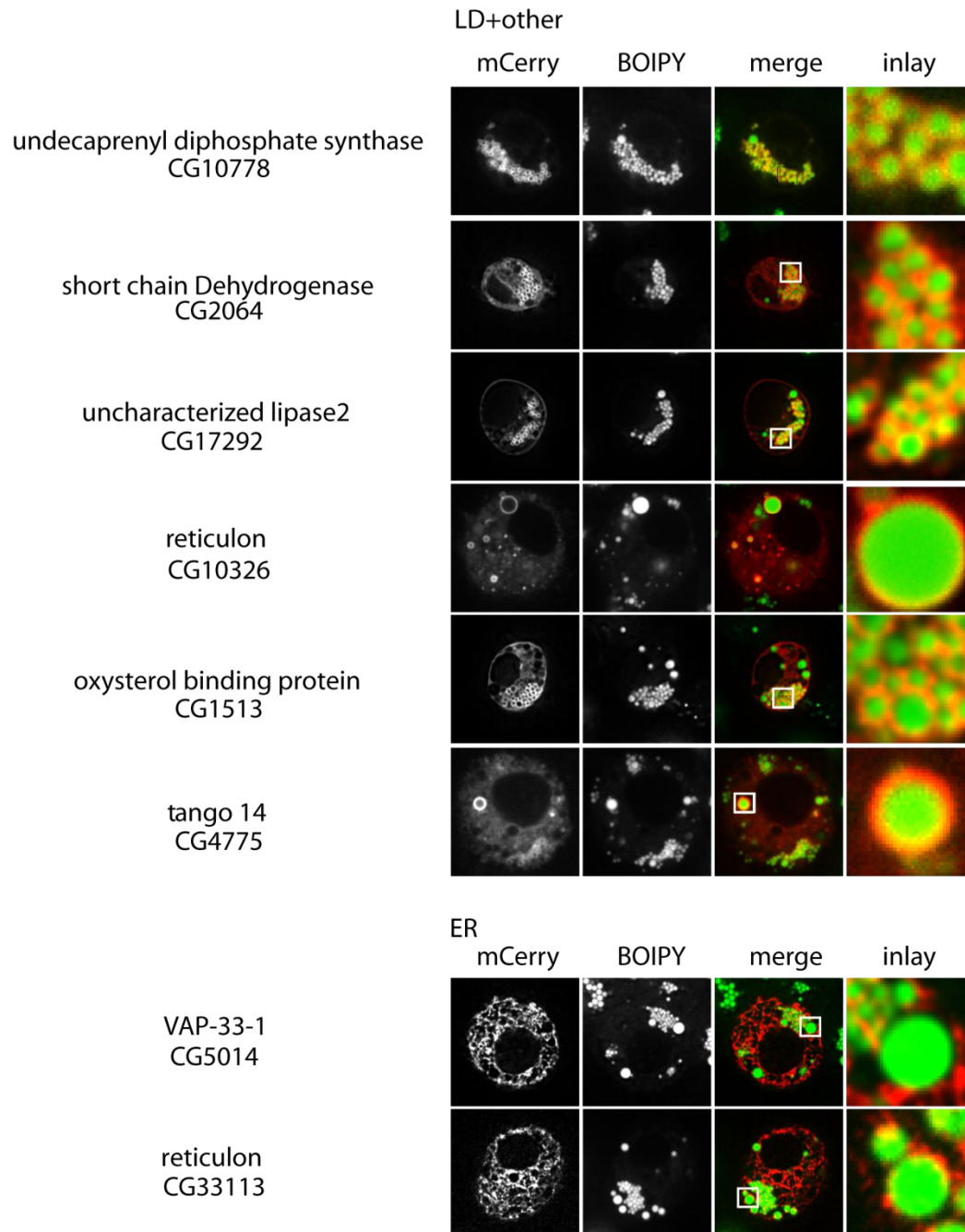


Figure 12. Localization of proteins found in LD proteome as determined by fluorescent microscopy.

The indicated fluorescent mCherry–tagged enzymes were transiently expressed in S2 cells (left panels, red), loaded with 1 mM oleate for 12 h. LDs were stained with BODIPY (middle panels, green). The overlays of the two channels and zooms of a representative LD section are shown (right two panels). Bar = 5 μ m (overview) or 1 μ m (inlay). (A) Proteins localizing exclusively to LDs. (B) Proteins localizing to LDs and ER. (C) Proteins localizing to LDs and other cellular compartments. (D) Proteins localizing to ER and not to LDs.

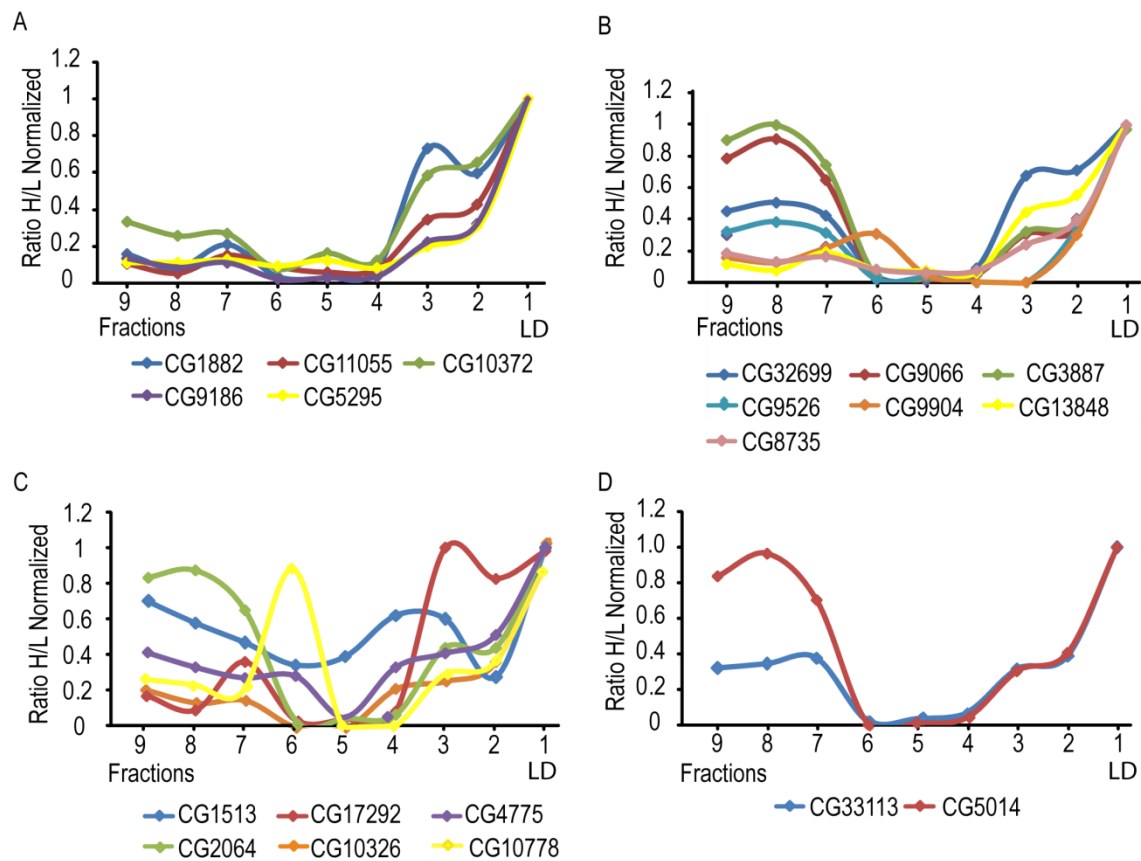


Figure 13. PCPs of proteins whose subcellular localization was determined by fluorescence microscopy.

(A) PCPs of proteins localizing exclusively to LDs, (B) PCPs of proteins localizing to LDs and ER. (C) PCPs of proteins localizing to LDs and other cellular compartments. (D) PCPs of proteins localizing to ER and not to LDs.

4.1.4 Comparison of proteomic data with genome-wide RNAi screens

To identify proteins that localize to LDs and additionally play an important role for LD function, I compared proteomic data to two genome-wide RNAi screens for genes important for LD function in *Drosophila* S2 cells (Beller et al. 2008; Guo et al., 2008). In the RNAi screen Guo et al. 227, genes were found by visual screening whose knockdown results in a phenotype with dramatically or moderately altered LD size, representing about 1,5 % of the complete *Drosophila* proteome.

Genes with the most striking alterations in LD morphology were categorized into five distinct phenotypic classes. Class I genes showed reduced numbers of LDs, Class II genes gave smaller, more dispersed LDs, Class III genes showed more dispersed

LDs of slightly larger size, Class IV genes yielded highly condensed clusters of LDs and Class V genes contained one or a few very large LDs. A comparison of the proteomic data with hits of the screen revealed surprisingly little overlap (Figure 14). From 106 proteins identified to be specifically enriched in the LD purification by hierarchical clustering, only knockdown of four of those proteins gave a phenotype in the screen. Thus, knockdown of about 4% of the proteins found in the proteome gives a LD phenotype, what represents only a small enrichment compared to 1,5% of the complete genome giving a phenotype. A comparison of the LD proteome with the data set from the screen (Beller et al., 2008) revealed another four candidates whose knockdown results in a LD phenotype.

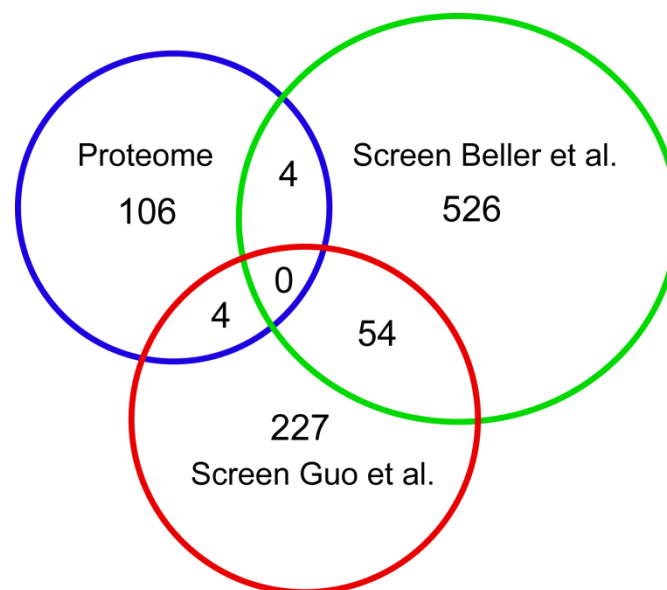


Figure 14. Venn diagram showing overlap between LD proteome and genomic RNAi screens. Four of the 106 proteins identified in the LD proteome were also detected in the RNAi screen Guo et al. to give a LD phenotype. Another four LD proteins overlapped with the screen Beller et al..

Among the proteins identified in both, the proteome and the screens, was brummer, the *Drosophila* ATGL homolog, whose knockdown resulted in an increase in LD number. Moreover, CG8732 (Table 2), a long-chain fatty acyl CoA ligase (ACSL), was found in the LD proteome. CG8732 knockdown resulted in fewer and smaller LDs. ACSL catalyzes the activation of fatty acids by conjugating them with CoA, a reaction required for fatty acids to be incorporated into various lipids, such as TG, CE and phospholipids. It was previously suggested that different ACSLs, localizing to different organelles in the cell, help channeling fatty acids toward a particular metabolic fate. Specifically, the mammalian homolog of CG8732 (ACSL3) is required for neutral lipid synthesis during LD formation (Fujimoto et al., 2007). Another protein from the LD proteome that gave a phenotype with fewer and smaller LD was CG3887, SEL T, a selenocysteine containing protein with unknown function. Moreover, both isoforms of CCT were found enriched in the LD fraction and gave one of the strongest phenotypes in the screen Guo et al. with fewer and much larger LDs. Most of those class V genes from this screen were linked directly or indirectly to phospholipid biosynthesis. Also in the Beller et al. screen knockdown of CG4825, encoding a phosphatidylserine synthase detected in the LD proteome, resulted in an overstorage phenotype. Thus, I hypothesized that phospholipid synthesis regulates LD size and abundance.

CG	Protein Names	Phenotype
Screen Guo et al.		
CG1049	CTP:phosphocholine cytidyltransferase 1	ClassV: fewer LDs, larger size
CG18330	CTP:phosphocholine cytidyltransferase 2	ClassV: fewer LDs, larger size
CG8732	Lethal 44DEa	ClassII: smaller LDs, more dispersed
CG3887	SELT-like protein	ClassII: smaller LDs, more dispersed
Screen Beller et al.		
CG11100	Mes2; Alcohol dehydrogenase transcription factor Myb	Overstorage
CG1884	CCR4-Not complex component, Not1	Overstorage
CG4825	Phosphatidyl serine synthase	Overstorage
CG5295	Brummer	Overstorage

Table 2. Proteins identified in the LD proteome with LD phenotype.

4.2 CCT binding to LDs activates synthesis of PC for their expansion

4.2.1 CCT is a principal enzyme regulating phospholipid homeostasis during LD formation

One important question in the field of LD biology is how phospholipid synthesis is regulated for LD formation and growth. As the knockdown of several genes involved in phospholipid synthesis, especially for PC synthesis gave strong phenotypes in the genome-wide screens (Beller et al., 2008; Guo et al., 2008), changes in LD phospholipid levels are suggested to be an important factor determining LD morphology and function. PE and PC are the most abundant phospholipids on the LD surface constituting more than 90% of total LD surface phospholipids (Bartz et al., 2007; Tauchi-Sato et al., 2002).

To determine which of the enzymes for PC and PE synthesis play a role in regulating LD size, I knocked down each Kennedy pathway enzyme for PC and PE synthesis in S2 cells (Figures 15A and 16A). The knockdown efficiency was always higher than 80%, as verified by quantitative PCR (Figure 15B, 16B). Due to the lack of antibodies against *Drosophila* CK, CPT and PE synthesis enzymes, I could verify knockdown efficiency for those enzymes only on mRNA and not on protein levels. Only for CCT1, I could show that protein levels were completely depleted by Western blot with antibodies against murine CCT α that also recognize *Drosophila* CCT1 (McCoy et al., 2006) (Figure 15C).

Although PE is the most abundant phospholipid in *Drosophila* and constitutes the main LD phospholipid in *Drosophila* S2 cells (Figure 17), knockdown of PE synthesis enzymes of both pathways for PE synthesis, the Kennedy pathway and the phosphatidylserine decarboxylase pathway, produced no phenotypes in LD morphology (Figure 16). In contrast, knockdown of several PC synthesis enzymes resulted in the formation of fewer and much larger LDs in the cells (Figures 15).

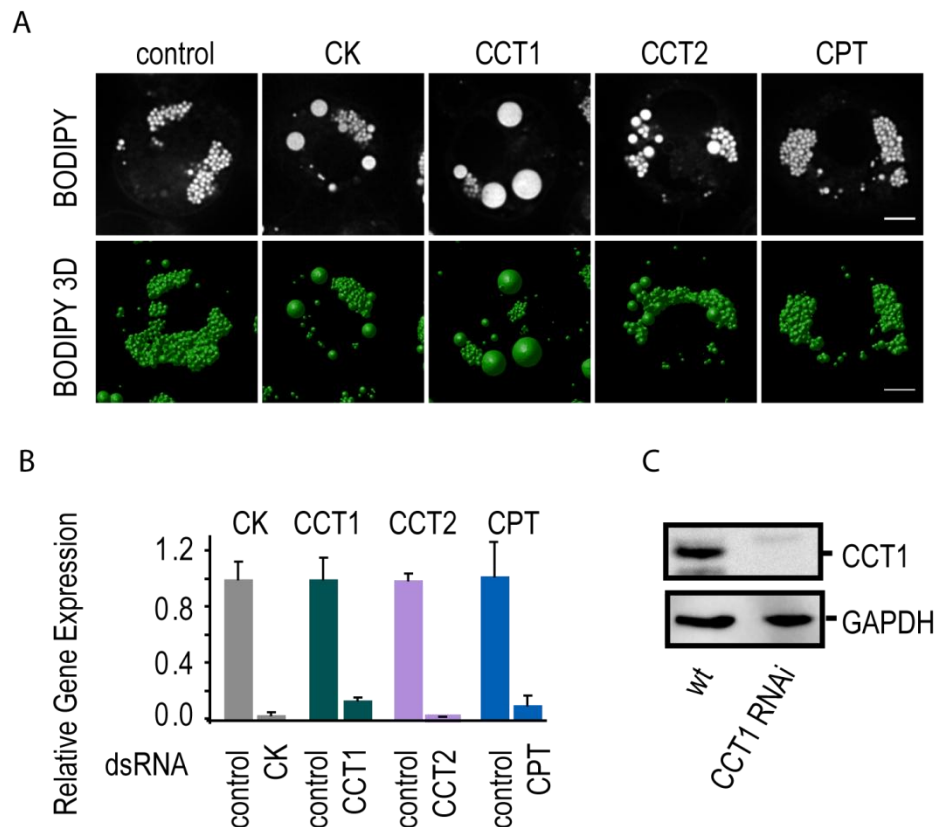


Figure 15. CCT is a major phospholipid synthesis enzyme required during LD expansion.

(A) Knockdown of several PC synthetic mRNAs results in giant LDs. The indicated enzymes were depleted by RNAi in *Drosophila* S2 cells. Cells were loaded with 1 mM oleate for 12 h, and LDs were stained with BODIPY. Representative confocal midsections from single cells are shown in the upper panels. 3-D reconstructions from image stacks are shown in the lower panels. Bar = 5 μ m.

(B) Enzymes of PC synthesis were efficiently knocked down. Expression levels were measured by quantitative RT-PCR. Total RNA was prepared with the Preparse Kit (USB); 3 μ g was used for first-stand cDNA synthesis with a kit (Fermentas). Real-time quantitative PCR was performed with the MyiQTM Single-Color Real-Time PCR Detection System (BioRad) and Mesa green (Eurogentec). Primers used are listed in Table S7. Values are mean \pm SD of three experiments.

(C) CCT1 protein was completely depleted by RNAi treatment. Western blot shows complete depletion of CCT1 in total lysate of S2 cells treated with dsRNA directed against CCT1, whereas no effect on CCT1 levels was observed in control treated S2 cells. GAPDH was used as loading control.

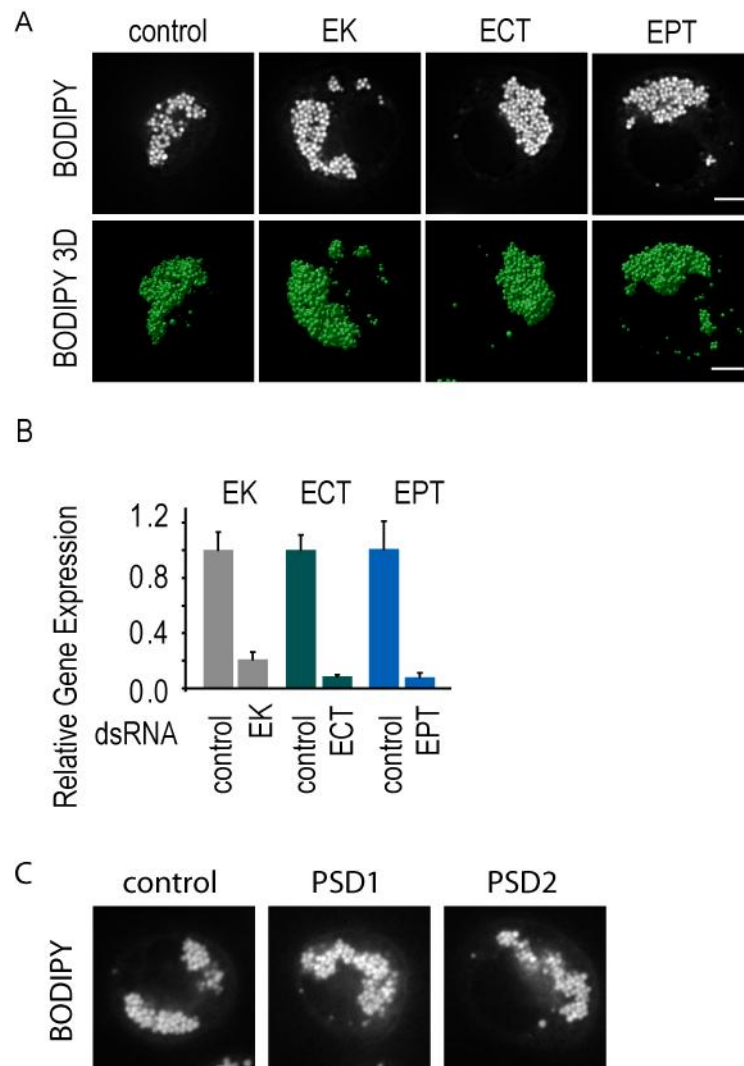


Figure 16. Depletion of PE synthetic enzymes does not affect LD morphology.

(A) Knockdown of Kennedy pathway enzymes for PE synthesis does not alter LD morphology. Enzymes were depleted by RNAi and cells were analyzed as in (15A). Bar = 5 μ m.

(B) Enzymes of PE synthesis were efficiently knocked down. Expression levels were measured and analyzed as described in (15B).

(C) Knockdown PSD1 or PSD2 does not affect LD morphology. Enzymes were depleted by RNAi and cells were analyzed as in (15A). Bar = 5 μ m.

Among PC synthesis enzymes, knockdown of CCT1 gave the strongest phenotype—with only few, giant LDs per cell (Figures 15A). This finding is supported by the fact that CCT1 knockdown also results in the largest decrease in PC levels among PC synthesis enzymes, as shown by thin layer chromatography (TLC) (Figure 17). Consistently, CCT1 catalyzes the rate-limiting step of PC synthesis and thus changes in enzyme level are expected to give the highest impact on PC levels in the cell.

Although CCT2 mRNA levels were efficiently reduced (Figure 16B), CCT2 knockdown showed smaller effects on LD morphology than CCT1 depletion. This suggests that CCT1 is the main isoform in S2 cells, especially since CCT1 expression levels are much higher than for CCT2 (Celniker et al., 2009). Hence, CCT1 provides the majority of cytidyltransferase activity for LD-directed PC synthesis.

CK depletion also reduced PC levels in LDs and induced formation of large droplets (Figure 15A, Figure 17). In contrast, depletion of CPT, the enzyme catalyzing the final step of PC synthesis had no effect on LD size and caused only minor reduction of PC levels (Figure 15A, Figure 17). Evidently, reduction of CPT mRNA levels by ~80% was not sufficient to reduce enzyme levels below the threshold required for PC synthesis during LD formation.

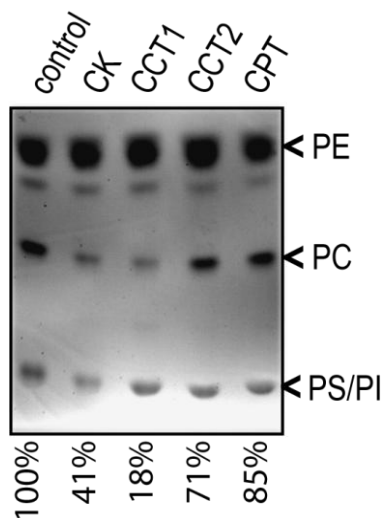


Figure 17. CCT1 Depletion causes the strongest reduction of LD PC levels among PC synthesis enzymes.

Knockdown of PC synthetic enzymes reduces PC levels in LDs. LDs from cells as in (15A) were purified, and extracted lipids were analyzed by TLC.

To further test whether the CCT phenotype is caused by PC deficiency on LDs or any other side effect of RNAi treatment against CCT, I added liposomes of different lipid compositions to CCT1 knockdown cells. In comparison to liposomes containing mostly PE, addition of PC liposomes fully rescued the phenotype (Figure 18). Thus, the formation of giant LDs resulted from PC deficiency.

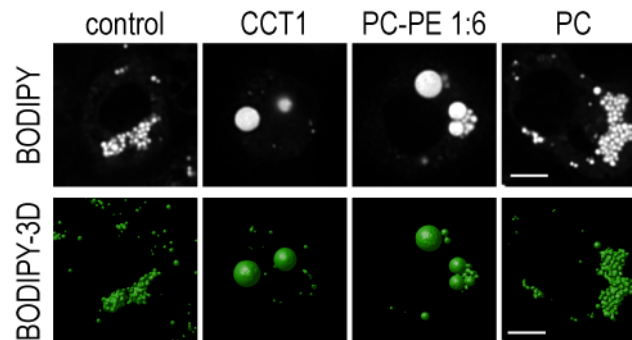


Figure 18. CCT1 phenotype is rescued by the addition of PC liposomes.

CCT1 knockdown can be rescued by addition of PC liposomes but not by liposomes consisting mainly of PE. *Drosophila* S2 cells treated with RNAi against CCT1 were incubated with 5 mM liposomes of the indicated lipid mixtures before LD morphology was analyzed 12 h after oleate treatment. LDs were stained with BODIPY. Representative confocal midsections from single cells are shown in the upper panels. 3-D reconstructions from image stacks are shown in the lower panels. Bar = 5 μ m.

Furthermore, treating S2 cells with miltefosine (hexadecylphosphocholine), caused a similar phenotype than that was seen during oleate loading of CCT1 RNAi treated S2 cells (Figure 19A). This inhibitor of CCT has been shown to decrease cellular PC levels (Geilen et al., 1992). Moreover, reducing flux through the Kennedy pathway by growing cells in choline deficient medium led to the formation of giant LDs resembling those after CCT1 depletion (Figure 19B).

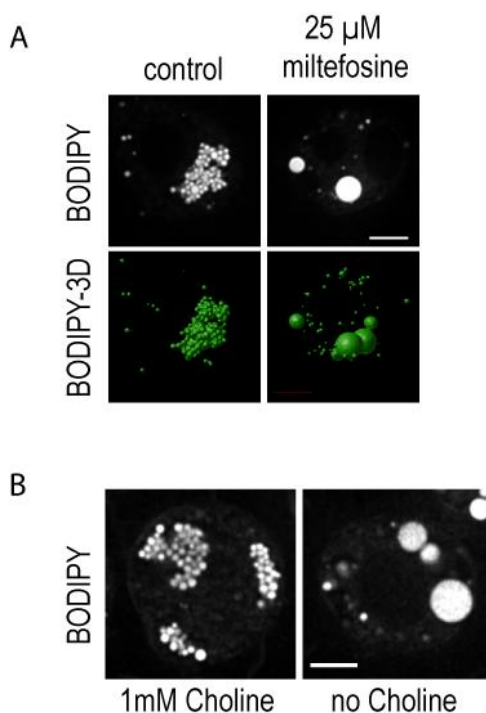


Figure 19. The formation of giant LDs is caused by PC deficiency.

(A) The CCT inhibitor miltefosine induces the formation of giant LDs. *Drosophila* S2 cells were treated with 25 μ M miltefosine for 48 h and oleate for 12 h. LDs were stained with BODIPY. Representative confocal midsections from single cells are shown in the upper panels. 3-D reconstructions from image stacks are shown in the lower panels. Bar = 5 μ m.

(B) Choline deficiency leads to giant LDs. S2 cells were grown in normal or choline-deficient medium, oleate loaded, and analyzed as in (A). Representative images of BODIPY-stained confocal midsections from a single cell are shown. Bar = 5 μ m.

Previous studies suggest that N-ethylmaleimide-sensitive-factor attachment receptor (SNARE) proteins might be involved in the fusion process of LDs (Bostrom et al., 2007). To test whether the formation of giant LDs upon reduction of PC levels on the LD surface was mediated by SNARE protein dependent fusion pathways, I co-depleted N-ethylmaleimide-sensitive-factor (NSF), α soluble NSF attachment protein (SNAP), or a series of SNAREs (SNAP23, syntaxin5) together with CCT1. However, knockdown of none of the mentioned proteins had an effect on CCT1's LD phenotype, implicating that LD coalescence under those conditions is not mediated by a SNARE protein dependent pathway (Figure 20).

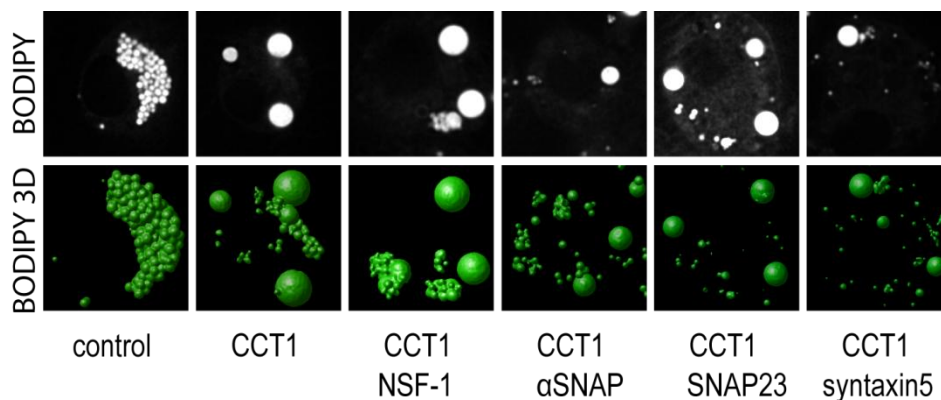


Figure 20. PC depletion promoted coalescence is independent of SNARE protein mediated pathways. Depletion of proteins involved in SNARE dependent membrane fusion does not rescue the CCT1 phenotype. The indicated enzymes were depleted by RNAi in *Drosophila* S2 cells. Cells were loaded with 1 mM oleate for 12 h, and LDs were stained with BODIPY. Representative confocal midsections from single cells are shown in the upper panels. 3-D reconstructions from image stacks are shown in the lower panels. Bar = 5 μ m

Together these results show that CCT1 has a main function in maintaining LD phospholipid levels during LD formation and growth. Depleting CCT1 has the strongest impact on LD morphology among all enzymes for PC and PE synthesis and results in the fusion of small LDs into fewer but giant ones due to PC deficiency arising on LDs.

4.2.2 PC serves as surfactant stabilizing LDs and preventing LD coalescence

As different phospholipid species have different surfactant characteristics (Kabalinov et al., 1996), I decided to test their capacities to act as stabilizers on the LD surface. As only knockdown of PC synthesis enzymes results in LD phenotypes, I hypothesized that PC plays a more important role in shielding neutral lipid emulsion in an aqueous environment and preventing LD coalescence than other phospholipids. To test the shielding effect of different phospholipids on the LD surface, I analyzed the stability of *in vitro* generated artificial droplets with different phospholipid compositions in an aqueous environment.

The stability of *in vitro* formed artificial droplets correlated with the characteristics of changes in the LD composition observed in S2 cells. Artificial droplets whose TG core is shielded by either PC or a PC/PE mixture, thereby resembling the composition of LDs in S2 cells (PC:PE 1:2.7), remained stable for at least 3 h. In contrast, LDs formed with TG alone or with TG and a PE monolayer rapidly coalesced, forming a continuous lipid phase (Figures 21A and 21B). Also other phospholipids that are normally found in smaller amounts on the LD surface, such as PI or PS, showed a weaker stabilizing effect compared to PC, even when added individually and in large excess (Figure 21B). Moreover, also PI and PS did not prevent artificial TG droplet coalescence when added together with PE in molar ratios similar to those in LDs (PE:PI:PS on artificial droplets: 9:1.3:1, corresponding to LD phospholipid ratio quantified by TLC (Figure 17), which yielded data similar to previous studies (Jones et al. 1992)). In contrast, addition of PC to this complex phospholipid mixture abolished droplet coalescence (PC:PE:PI:PS on artificial droplets: 1:2.7:0.4:0.3; Figure 21B). These findings, together with previous data on the stability of lipid-water emulsions (Saito et al., 1999), indicate that PC, but not PE, is necessary as a surfactant stabilizing LDs and preventing them from coalescence.

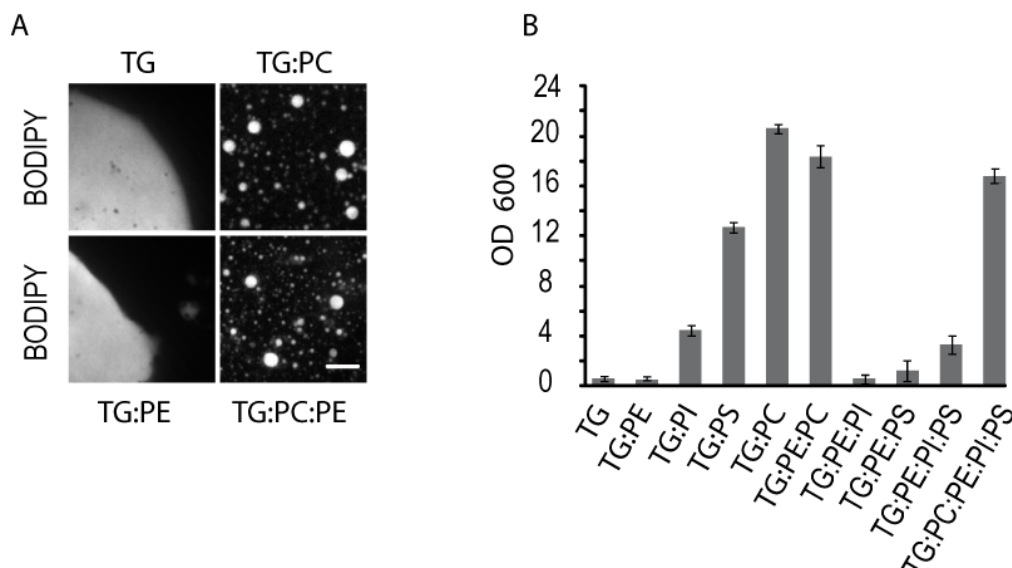


Figure 21. PC is a stronger stabilizer of artificial LDs than other phospholipids.

Stability and size of artificial droplets consisting of the indicated lipid mixtures were determined by fluorescence microscopy (A) and light scattering (B). The molar ratios of the phospholipids were calculated according to quantifications of TLC analyses of LD fractions (PC:PE 2.7:1; PE:PI 6.75:1; PE:PS 9:1; PE:PI:PS, 9:1.3:1; PC:PE:PI:PS:PC, 1:2.7:0.4:0.3). Values are mean \pm SD of three experiments.

4.2.3 Among PC synthesis enzymes, only CCT localizes to LDs

Overexpressed fluorescently tagged CCT1 and CCT2 localize to LDs (Guo et al., 2008). Moreover, protein correlation profiling suggests a strong enrichment of endogenous CCT enzymes in the LD fraction compared to other cellular fractions. In addition, I confirmed LD targeting of the endogenous protein by Western blot with antibodies against CCT. I compared CCT distribution over the gradient of a LD purification to the behavior of other well characterized organelle marker proteins, as well as a TG profile generated by TLC as indicator for the LD purification (Figure 22A).

CCT1 was highly enriched in the LD fraction with only minor amounts being found in fractions 8 and 9, representing protein either still localizing to the nucleus or to membranes. CCT abundance mirrored the distribution of TG over the gradient, indicating LD localization. In contrast, other organelle markers, such as the cytosolic GAPDH or the ER/Golgi marker KDEL-receptor, showed complete different profiles

over the gradient and were not detected in the LD fraction (Figure 22A). The amount of total cellular CCT1 localizing to the LD surface was at least 50% as quantified by comparison of its presence in the total and the LD fraction. In contrast, the cytosolic control protein GAPDH was excluded from the LD fraction (Figure 22B). This suggests that a major pool of the total endogenous cellular CCT1 is recruited to growing LDs.

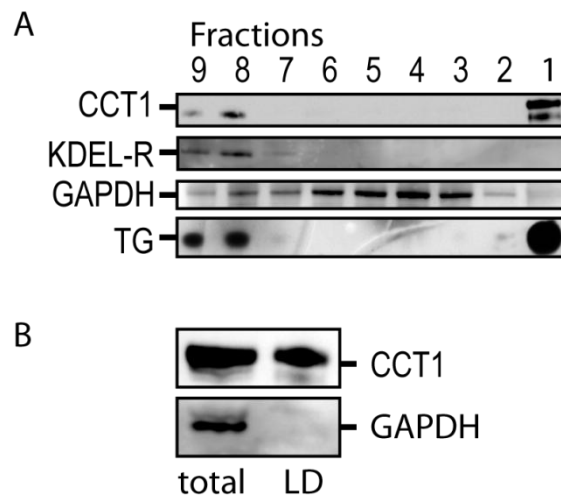


Figure 22. Endogenous CCT localizes to LDs.

(A) Western blots for CCT1, KDEL-receptor and GAPDH and a TLC for TG are shown for all fractions of a LD purification. Same amount of protein of each fraction was used.

(B) At least 50% of total cellular CCT1 localizes to LDs after oleate loading. The same percentage of total protein of total and LD fraction was blotted for CCT1 and GAPDH as a control.

My first hypothesis for the function of CCT targeting to the LD surface was that relocation of CCT and eventually other Kennedy pathway enzymes might facilitate localized PC synthesis on the LD surface. Under those conditions of extensive LD growth, large amounts of PC are required to stabilize the hydrophobic neutral lipid core. Thus, PC might be synthesized at the LD surface, the site in the cell where the additional PC would be required.

However, for localized PC synthesis also other Kennedy pathway enzymes, at least CPT, would have to localize to LDs. CPT was reported to localize under normal conditions to ER membranes (Coleman and Bell, 1978; Wilgram and Kennedy,

1963). It catalyzes the final step of PC synthesis by converting CDP-choline and DG into PC. Unlike all other precursor substrates of PC synthesis before this step, the substrate DG and the product PC of the CPT catalyzed reaction are not water-soluble and cannot diffuse freely in the cell to its site of use. Thus, CPT localization defines the site of PC production from the Kennedy pathway.

To test whether also CPT and CK are targeted to LDs under conditions of LD grow and thus, to the site of *de novo* PC synthesis, I analyzed subcellular distributions of fluorescently tagged Kennedy pathway enzymes during oleate loading of S2 cells. However, in contrast to CCT1 and CCT2, CK and CPT showed no LD localization (Figure 23). Also during oleate treatment, CPT was still found in the ER (Figure 23), whereas CK showed a diffuse cytoplasmic signal, consistent with its soluble characteristics. Thus, I only found CCT but no other Kennedy pathway enzymes for PC synthesis on the LD surface. This indicates that also under conditions of LD expansion *de novo* PC synthesis takes place in the ER, the site of CPT localization and not on the LD surface. This implicates that CCT is not targeted to LDs to participate in localized PC synthesis.

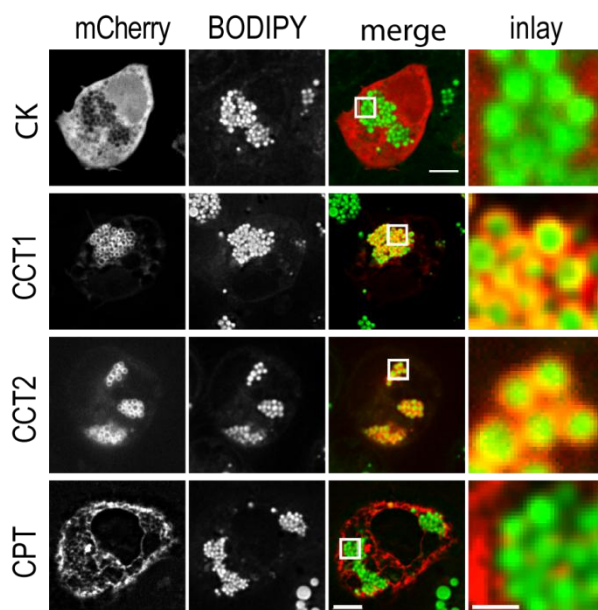


Figure 23. CCT1 and CCT2, but not CK and CPT, localize to LDs.

The indicated fluorescent mCherry-tagged enzymes were transiently expressed in S2 cells (left panels, red), loaded with 1 mM oleate for 12 h. LDs were stained with BODIPY (middle panels, green). The overlays of the two channels and zooms of a representative LD section are shown (right two panels). Bar = 5 μm (overview) or 1 μm (inlay).

4.2.4 CCT directly binds to LDs by an amphipathic alpha helix

As reported earlier, CCT directly binds to membranes and liposomes *via* an amphipathic alpha helix (Attard et al., 2000; Friesen et al., 1999; Taneva et al., 2003). However, it is not clear yet, whether the interaction with the LD phospholipid monolayer is direct or mediated by another protein. To approach this question, I affinity-purified CCT2 (Figure 24A) and incubated it with artificial droplets with a PC:PE ratio as found *in vivo* in S2 cells. Then, I purified the artificial droplets by floating them on a sucrose cushion and tested CCT binding by comparing the artificial droplet bound fraction with an adequate control fraction of the sucrose cushion. In contrast to a GFP control protein, a significant amount of CCT2 was floated with the artificial droplet fraction, indicating that CCT interacts directly with monolayer-bound droplets and no other proteins are required to mediate CCT LD targeting (Figure 24B).

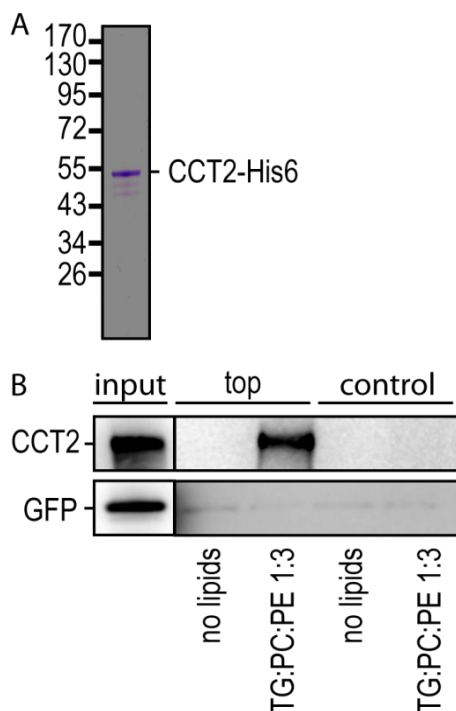


Figure 24. CCT directly binds to LDs

(A) CCT2-His₆ was affinity purified to high purity. Purity of affinity purified CCT2-His₆ was checked by SDS gel electrophoresis.

(B) CCT2 directly binds to artificial droplets. Purified CCT2 and purified GFP were mixed in a 1:1 ratio and incubated with artificial droplets with a phospholipid composition PE:PC 3:1, adjusted to 0.75 M sucrose and floated by centrifugation. The top fraction and a control fraction under the LDs were analyzed by Western blot and compared to a control sample without lipids.

Membrane binding of CCT was shown to be mediated by an amphipathic alpha helix. However, a C-terminal phosphorylation domain containing multiple serine residues was also implicated in modulating CCT regulation and localization (Arnold et al., 1997; Houweling et al., 1994; Wang et al., 1993a; Wieprecht et al., 1996). To

address which protein domains are responsible for LD targeting, I generated several CCT1 mutants and tested their ability to bind to the LD surface (Figure 25). A mutant lacking the C-terminal phosphorylation domain (ΔP) still targeted to the LD surface, whereas deletion of both the phosphorylation and the helical domain (ΔHP) abolished LD phospholipid monolayer localization. LD targeting was also completely abolished by introducing a single point mutation, W397E, into the amphipathic alpha helix which is predicted to disrupt the amphipathic structure of the helix. To test whether the amphipathic helix alone is already sufficient for LD localization, I expressed the helical domain alone (H) fused to mCherry in S2 cells. Strikingly, these 65 amino acids were sufficient for efficient LD targeting. These results show that the helical domain of CCT1 is both necessary and sufficient for LD targeting.

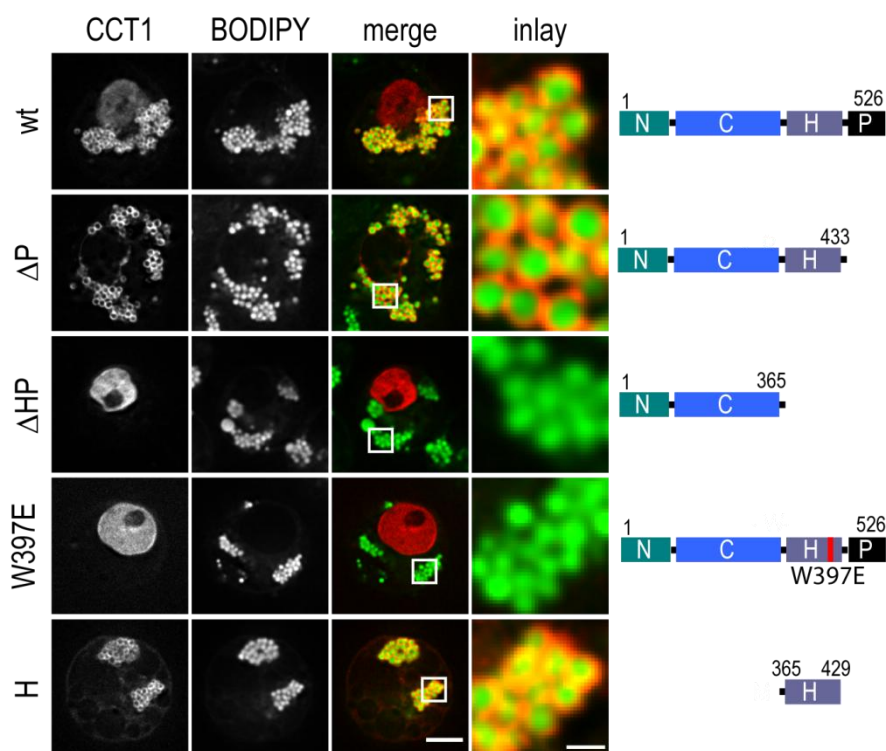


Figure 25. CCT1 binds to LDs through its helical region.

S2 cells expressing fluorescent mCherry-tagged mutants of CCT1 were oleate loaded for 12 h, and their localization was determined (left panels). LDs were stained with BODIPY (second left panels). Second right panels show overlays (merge) of the two channels. Far right panels show a zoom of a representative LD section. Bar = 5 μ m (overview) or 1 μ m (inlay). Design of the constructs is visualized on right side (N is N-terminal region containing NLS, C is catalytic core, H is helical domain, P is phosphorylation domain).

4.2.5 CCT is targeted to LDs when the PC to TG ratio decreases

An alternative model to CCT targeting for localized PC synthesis on the LD surface would be that CCT relocalization serves a regulatory function. This hypothesis would be consistent with previous studies showing increased CCT activity upon binding to membranes such as liposomes and large unilamellar vesicles (Cornell and Vance, 1987). Especially membranes with low PC content were shown to promote CCT binding (Weinhold et al., 1994).

A similar regulatory mechanism might exist during LD expansion. Under conditions of LD growth the surface increases dramatically and large amounts of phospholipids are required to shield neutral lipids within the core and to stabilize the phase interface with the cytosol (Farese and Walther, 2009). CCT, the rate-limiting enzyme for PC synthesis that regulates the flux through the pathway, could sense increasing PC deficiency on the expanding LD surface, bind there and thus being activated, thereby providing more substrate for PC synthesis. This hypothesis would include that CCT senses the lipid composition on the LD surface and localizes there when PC deficiency arises.

To test this, I analyzed CCT1 localization during a 24 h time course of oleate loading. Over time, the average and maximum size of LDs increased continuously (Figures 26A and 26B). Already 1 h after oleate loading numerous small LDs appeared in cells. However, in most of the cells, CCT fluorescent signal was detected in the nucleus and CCT was found to localize to LDs only in ~15% of cells (Figures 26A, C, D). Between 1h and 3h of oleate loading, I observed a strong increase in cells with LD targeted CCT. After 3 h almost 90% of cells showed CCT on the LD surface and after 5 h of oleate treatment, CCT was in almost all cells on the LD surface (Figures 26A, C).

If CCT serves a regulatory function by sensing PC deficiency on LD surfaces and consequently inducing its relocalization and activation, one would assume that the targeting process might be part of a homeostatic feedback loop. For a homeostatic

feedback loop, CCT LD targeting would be expected to be reversible. Specifically, under conditions when LD growth is stopped and the cellular conditions require less CCT activity, the enzyme would fall off LDs and either relocate back to the nucleus or be specifically degraded. To test this hypothesis, I induced LD formation by treating cells for 24 h with oleate so that in all cells CCT was found on the LD surface. Then, I replaced oleate containing medium by lipid-free medium (Figures 26A, C, D). 20h after this shift, I observed no further LD accumulation or growth and in more than 50% of the cells I detected no CCT1 on LDs any more but in the nucleus, similar to its location before oleate loading (Figures 26A, C).

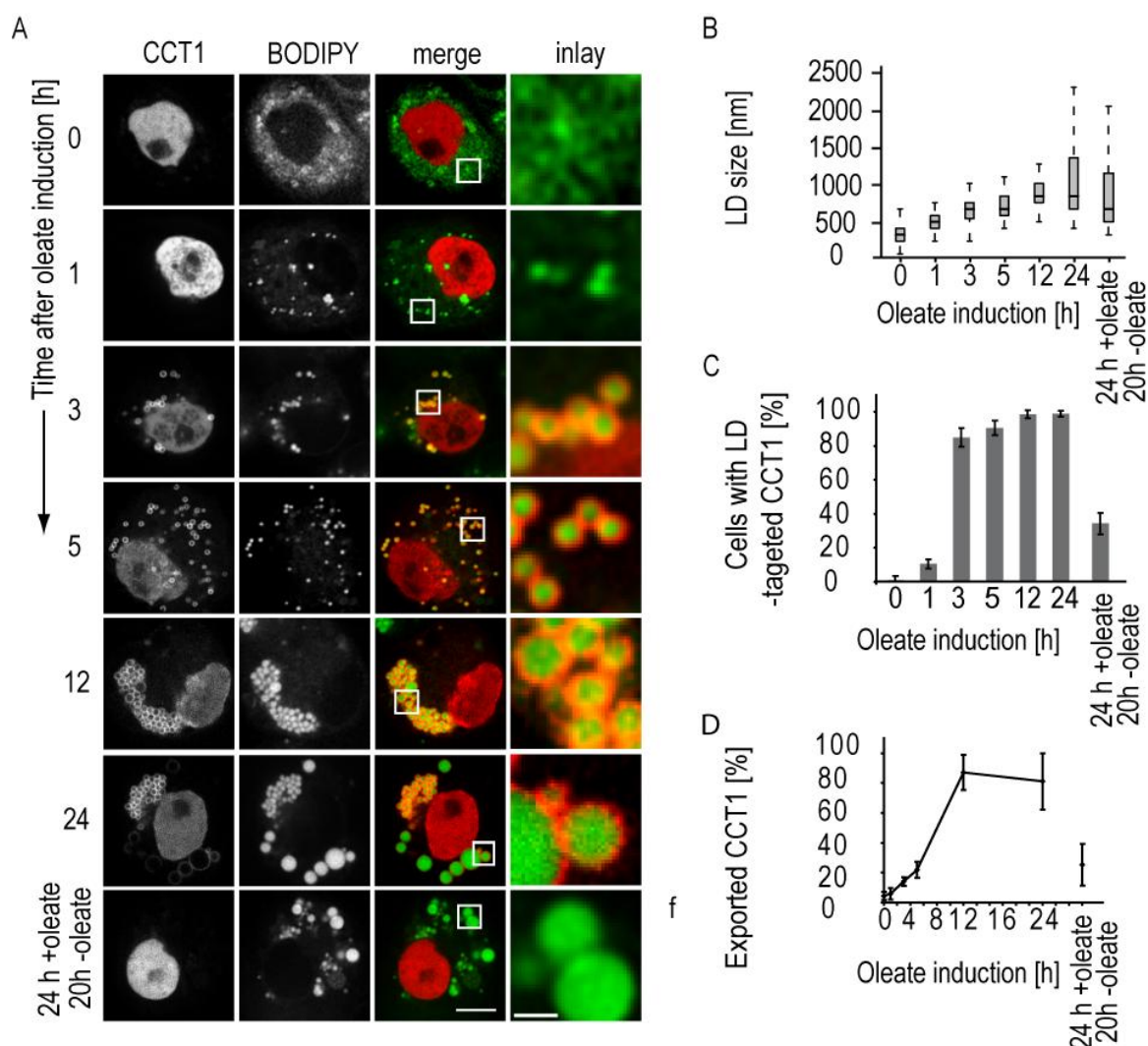


Figure 26. CCT1 is targeted to LDs after an initial delay and relocates to the nucleus when oleate is removed.

(A) CCT1 localizes to LDs after 3 h of oleate loading and relocates to the nucleus when cells are shifted to lipid-free medium. mCherry-CCT1 was expressed in S2 cells (left panels). LD targeting was followed by fluorescence microscopy after 1 mM oleate was added to the medium. LDs were stained with BODIPY (second left panels) and representative confocal midsections of each time point are shown. Second right panels show overlays of the two channels. Right panels show a zoom of a representative LD section. Bar = 5 μ m (overview) or 1 μ m (inlay).

(B) Number of cells with targeting of CCT1 to LDs increases strongly between 1 and 3 h of oleate loading and decreases after oleate removal. The number of cells in which CCT1 is targeted to LDs at indicated time points was quantified. Values are mean \pm SD of three independent experiments.

(C) The amount CCT1 on LDs increases in the first 12 h of oleate loading and decreases after oleate removal. Quantification of the fluorescence intensity of mCherry-CCT1 outside the nucleus. Values are mean \pm SD of three independent experiments.

(D) LDs grow during oleate loading. Box plots representing the median, the upper and lower quartiles, and 1.5-fold inter-quartile range (IQR) of LD diameters at different time points of oleate loading are shown ($n > 100$ for each time point).

In comparison to CCT1, CCT2 is localized in the cytosol in unloaded cells, as I observed in the same time course experiment. When LD formation is induced by incubation with oleate, small droplets already appear after 1h. However, only after 3 h, I detected CCT2 on LDs in most of the cells (Figure 27), thus CCT2 shows the same delay in LD targeting as CCT1.

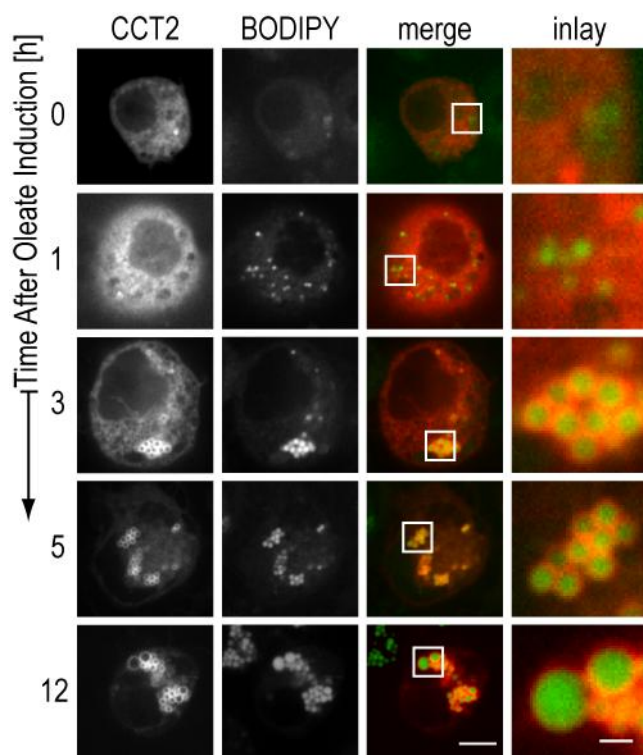


Figure 27: CCT2 is targeted to LDs with an initial delay

3 h after oleate loading, CCT2 localizes to LDs. mCherry-CCT2 was expressed in S2 cells (left panels). LD targeting was followed after the addition of 1 mM oleate to the medium. LDs were stained with BODIPY (second left panels). Second right panels show overlays of the two channels. Right panel shows a zoom of a representative LD section. Bars = 5 μ m (overview) or 1 μ m (inlay).

To address what induces LD targeting after the initial delay, I analyzed the changes in lipid composition in growing LDs. I isolated LDs at different times during oleate loading and measured their TG and PC content by enzymatic assays (Figure 28A). In the initial phase of oleate loading the PC:TG ratio strongly decreased, only after 5h, when all CCT1 was targeted to LDs, the PC:TG ratio stabilized at a new, lower level and remained constant during the remaining 24 h of oleate loading. During the time course the total cellular TG levels continuously increased until they reached a plateau after 12h (Figure 28B). Also the total cellular PC content increased during 24 h of oleate loading more than two-fold. In contrast to TG levels that start to increase immediately after oleate loading, PC levels increased after an initial lag-phase of 3-5

h. Thus the increase of cellular PC levels starts at those time points when CCT is relocated to LDs (Figure 28C).

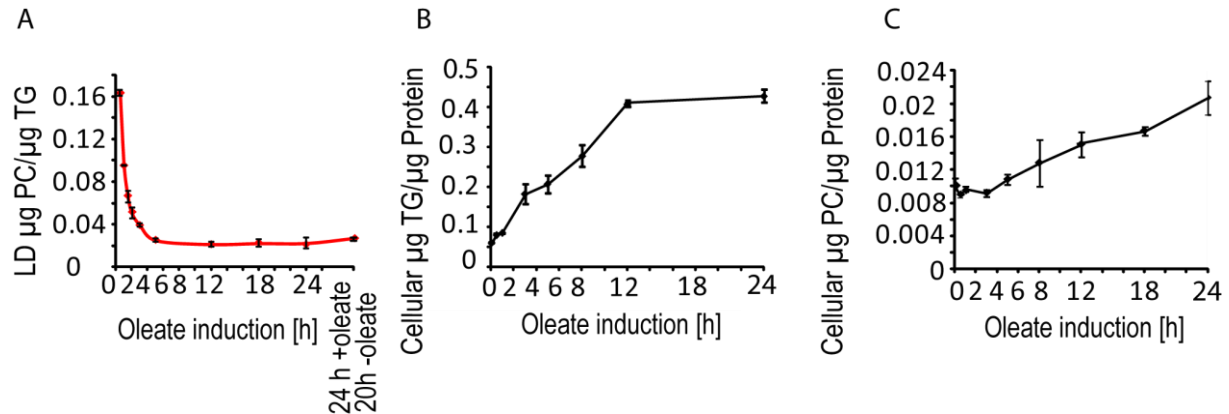


Figure 28. CCT is targeted to LD when the PC/TG ratio decreases

(A) PC/TG ratio of LDs decreases for up to 5 h of oleate loading but stabilizes afterwards. LDs were isolated at indicated time points after oleate loading, and PC and TG in LD fractions were measured by enzymatic assays. Values are mean \pm SD of three independent experiments.

(B) Cellular TG levels increase steadily over time in oleate-loaded cells. TG content of total cell lysate was measured enzymatically at indicated time points after oleate loading and normalized to protein levels. Values are mean \pm SD of three independent experiments.

(C) After an initial delay, cellular PC levels increase linearly over time in oleate-loaded cells. PC content of total cell lysate was measured enzymatically at indicated time points after oleate loading and normalized to protein levels. Values are mean \pm SD of three independent experiments.

CCT targeting to LDs may be part of a homeostatic feedback response: when LD increase their size, PC deficiency on LDs increases so that more CCT activity is required in order to produce PC. CCT then senses the PC deficiency and is targeted to LDs thereby being activated. When LD growth reaches an equilibrium and PC levels stabilize, CCT1 no longer binds to LDs and is localized mostly in the nucleus.

4.2.6 CCT1 is highly mobile and shuttles between nucleus and cytosol before oleate loading

The previous data indicate that CCT binds to the LD surface when PC deficiency arises. But how can CCT monitor PC levels on LDs and react to changes, if the enzyme resides in the nucleus under basal conditions? One possibility is that CCT1 shuttles between the nucleus and cytosol, thereby having continuous access to the LD surface and being able to survey PC levels.

I examined the mobility of CCT1 in oleate untreated cells by fluorescence-loss-in-photobleaching (FLiP) experiments, when most of the CCT1 is in the nucleus. I approached the question whether CCT1 shuttles between the nucleus and the cytosol by repeatedly bleaching mCherry-CCT1 at one spot in the cytosol, while monitoring the loss in nuclear fluorescence (Figure 29A). The results indicate a rapid loss of fluorescence within ~30 s in the nucleus of bleached cells (Figure 29B), whereas the signal of mCherry-CCT1 in nuclei of other cells at a similar distance from the bleached spot was not decreased. This shows that cytoplasmic continuity is required for CCT1 to be bleached over time. This strongly suggests that CCT1 shuttles rapidly between the nucleus and the cytosol under basal conditions, since almost all nuclear CCT1 at steady state migrated through the cytoplasmic bleaching spot within 30 s.

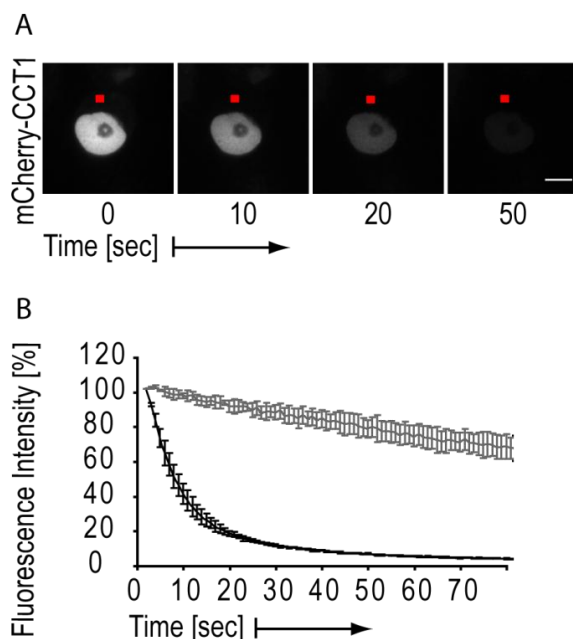


Figure 29. CCT1 shuttles between nucleus and cytosol before oleate loading

(A) CCT1 shuttles between nucleus and cytosol. Representative time course images of a FLiP experiment in which a spot in the cytosol of a cell expressing mCherry-CCT1 was bleached repeatedly. Bar = 5 μm .

(B) Normalized fluorescence intensity of mCherry-CCT1 in the nucleus of both bleached and nonbleached cells in the same experiment. Values are mean \pm SD of three independent experiments.

Moreover, at steady-state CCT1 is extremely mobile within the nucleus and does not bind to any nuclear structure. This finding is in contrast to previous studies that found CCT binding to the nuclear envelope (Lagace and Ridgway, 2005). FLiP experiments show that repeated bleaching of a small nuclear spot led to a loss of nuclear mCherry fluorescence within seconds (Figure 30).

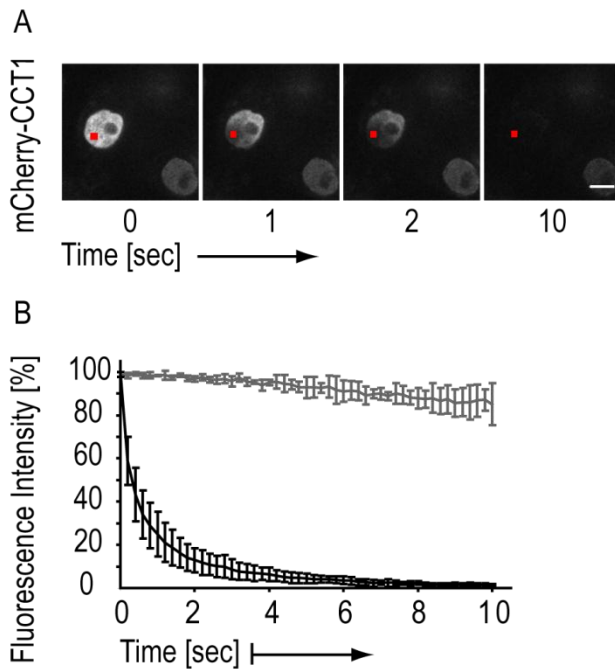


Figure 30. CCT1 freely diffuses in the nucleus

(A) CCT1 freely diffuses in the nucleus. The mobility of mCherry-CCT1 in the nucleus was assayed by repeatedly bleaching the indicated spot (FLiP). Selected time frames from one experiment are shown. Bar = 5 μ m.

(B) Quantification of FLiP experiments shown in (A). Normalized fluorescence intensity of mCherry-CCT1 in the nucleus of both bleached and nonbleached cells of the same experiment. Values are mean \pm SD of three independent experiments.

Earlier studies suggested that the phosphorylation domain or the helical domain of CCT might be required to mediate nuclear export of the protein (Gehring et al., 2009). Thus, I analyzed the mobility of the mutant CCT1 proteins (Δ P, Δ HP, and W397E) using the same FLiP experiments as for full-length CCT1. The behavior of all of tested mutants was the same as for full-length CCT1 and all mutants were still able to shuttle between the nucleus and the cytosol (Figure 31). This indicates that neither the phosphorylation domain, nor the helical domain is necessary for nuclear export. Thus, under steady-state conditions, CCT1 rapidly shuttles between a major nuclear and a minor cytosolic pool, thereby having access to LD surfaces and other membranes and being able to survey PC levels on those sites.

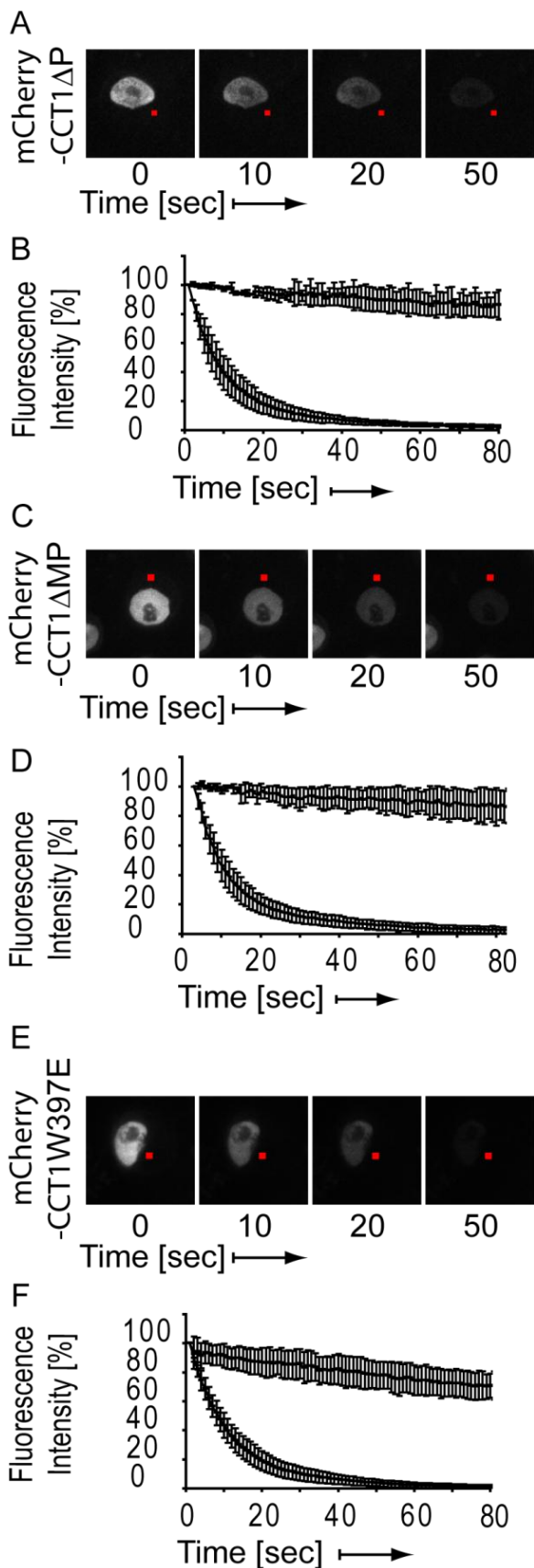


Figure 31. CCT1 mutants shuttle between the nucleus and the cytosol

(A) CCT Δ P shuttles between nucleus and cytosol. Representative time course images of a FLIP experiment in which a spot in the cytosol of a cell expressing mCherry-CCT1 Δ P was bleached repeatedly. Bar = 5 μ m. (B) Normalized fluorescence intensity of mCherry-CCT1 in the nucleus of both bleached and nonbleached cells of the same experiment. Values are mean \pm SD of three independent experiments. (C) and (D) Experiments as described in (A) and (B) for CCT1 Δ MP. (E) and (F) Experiments as described in (A) and (B) for CCT1 W397E.

4.2.7 CCT binds stably to LDs during their expansion

CCT1 is highly mobile in untreated cells, as it freely diffuses within the nucleus and shuttles between the nucleus and the cytosol. Thus, I wanted to test whether CCT is stable once bound to the LD surface. If CCT targeting to the LD surface would be part of a regulatory feedback loop and serves to activate the enzyme, CCT binding to LDs should be stable until adequate PC concentrations are reached.

To test this, mCherry-CCT1 was bleached on one LD in oleate treated cells and the fluorescence recovery was subsequently monitored over more than 20 min. For this fluorescence-recovery-after-photobleaching (FRAP) experiment I specifically chose cells showing complete CCT1 targeting to the LD surface in order to exclude any complications due to continuous retargeting from the nuclear pool. After initial bleaching the mCherry-CCT1 signal was completely depleted from the selected LD and no recovery was observed during the following 24 min (Figure 32A, B). This shows that CCT1 is stable once bound to the LD surface. The same FRAP experiment for CCT2 revealed that also CCT2 binds stably to the LD surface because its signal on a LD also did not recover after bleaching (Figure 32A, B).

To confirm these findings, I measured the release rate of CCT1 from LDs by using inverse FRAP (iFRAP). To do so, I bleached the mCherry-CCT1 signal of a whole cell except for one LD in the beginning of the experiment (Figure 32C). Then, I measured the loss of fluorescence on the unbleached LD over 20 min. I used the signal of a LD in an unbleached cell in the same image to correct for bleaching due to imaging. Over 20 min the mCherry signal on the unbleached LD remained stable (Figure 32D). This confirms that CCT1 is stably bound to LDs during this time period. I observed the same finding for CCT2 (Figures 33C, D), as there was no loss in signal intensity on an unbleached LD, following 20 min after bleaching the rest of the cell. Thus, during LD growth, CCT enzymes are stably bound to LDs and do not exchange with CCT bound to other LDs or in other circulating pools.

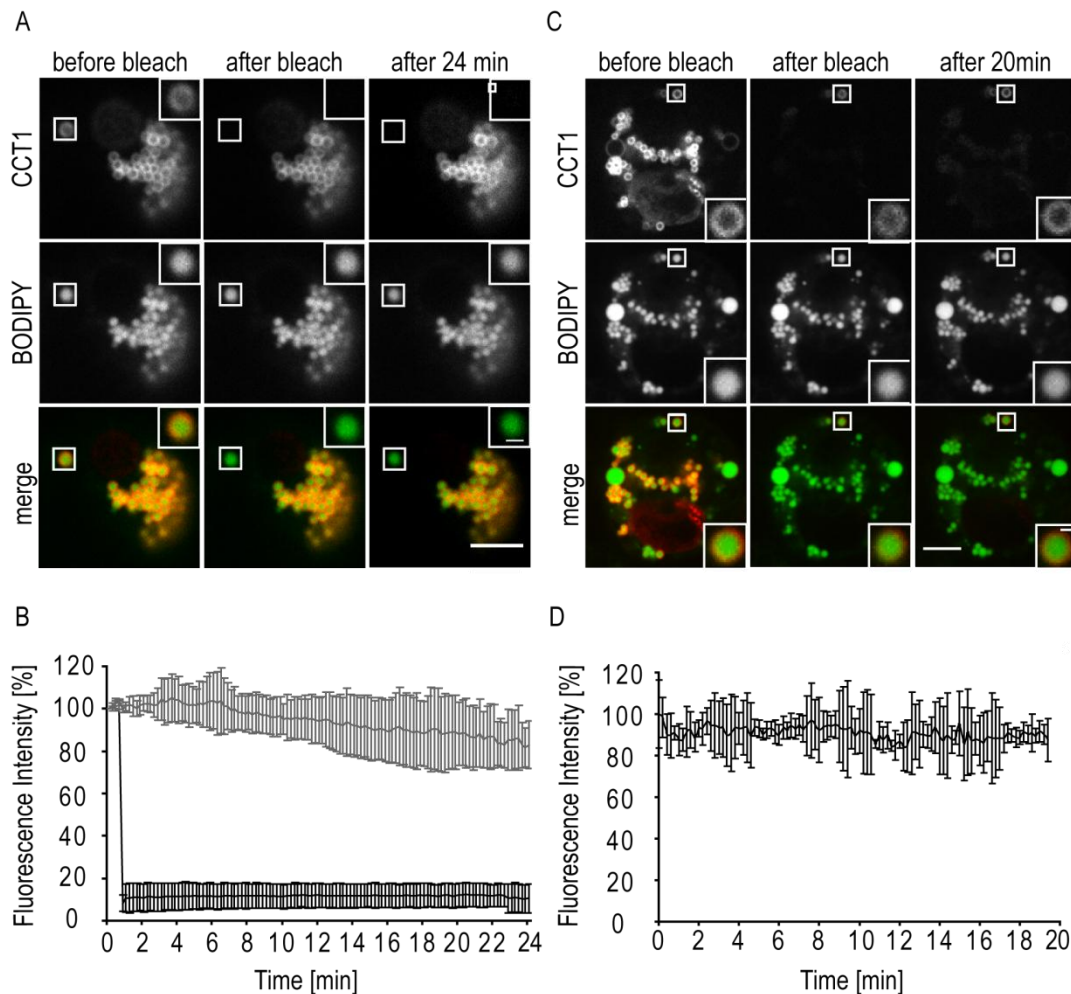


Figure 32. CCT1 stably binds to LDs

(A) CCT1 fluorescence of a bleached LD does not recover. CCT1 was tagged with mCherry (upper panels), LDs were stained with BODIPY (middle panels). Lower panels show overlays of the two channels. The box indicates the LD that was photobleached (FRAP). Insets show the indicated part of the image at higher magnification. Prebleach (left), immediately after bleach (middle), and postbleach (right) images of the FRAP experiment are shown. Bar = 5 μm .

(B) Normalized fluorescence intensity of mCherry-CCT1 on a bleached LD as in (A) over time in black. In grey, fluorescence of mCherry-CCT1 of a LD in an unbleached control cell during the same experiment. Values are mean \pm SD of three independent experiments.

(C) CCT1 fluorescence remains stable on LD in a bleached cell (iFRAP). CCT1 was tagged with mCherry (upper panels), and LDs were stained with BODIPY (middle panels). The lower panels show overlays of the two channels. At time 0 min, all signal except on the LD in the box was photobleached. Insets show the indicated part of the image at higher magnification. Pre-bleach (left), immediately after bleach (middle), and postbleach (right) images of the FRAP experiment are shown. Bar = 5 μm . (D) Fluorescence intensity of mCherry-CCT1 of experiments as in (C) over time normalized for photobleaching caused by imaging. Values are mean \pm SD of three independent experiments.

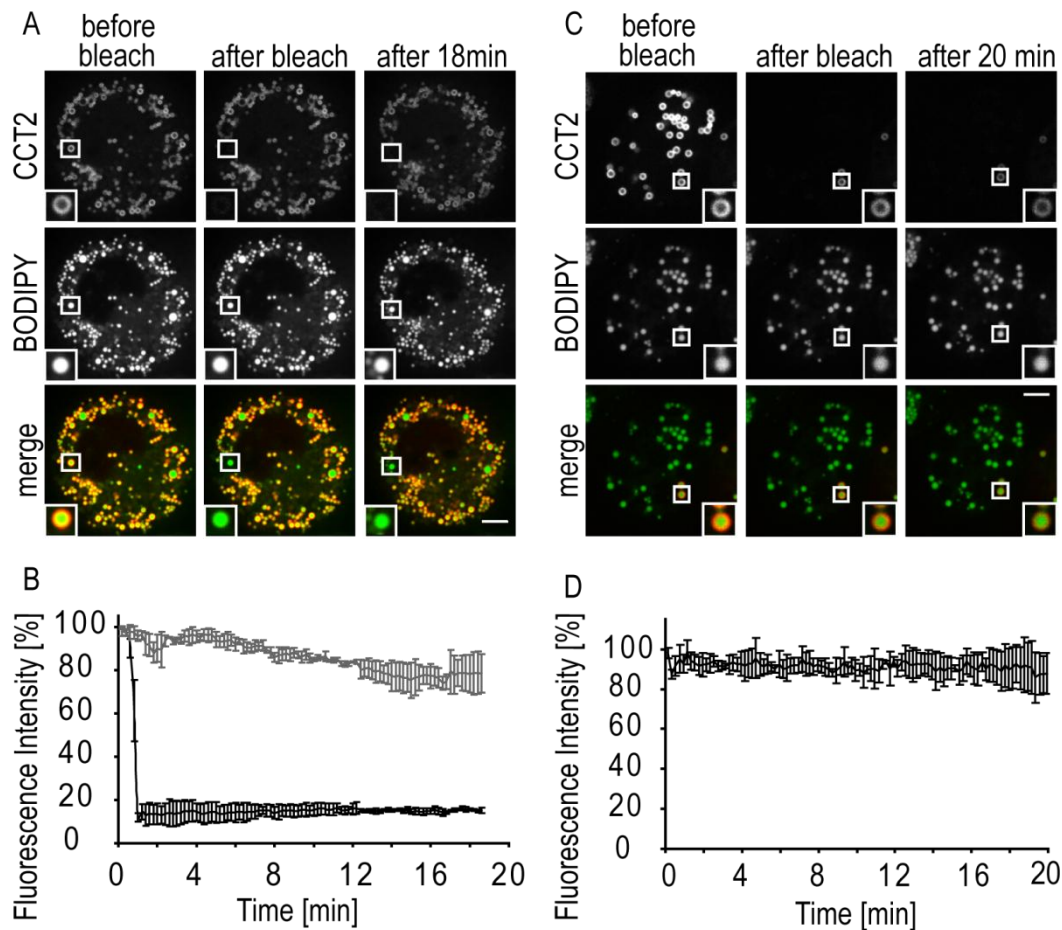


Figure 33. CCT2 binds stably to LDs

(A) CCT2 fluorescence does not recover on a bleached LD. FLIP of mCherry-CCT2 treated with oleate for 12 h. CCT2 was tagged with mCherry (upper panel), LDs were stained with BODIPY (middle panels). The lower panels show overlays of the two channels. The box indicates the LD that was photobleached in the cell. Insets show the indicated part of the image at higher magnification. Prebleach (left), immediately after bleach (middle panels), and postbleach (right) images of the FRAP experiment are shown. Bar = 5 μ m.

(B) Fluorescence intensity of mCherry-CCT2 on the LD shown in (A) at the beginning of the experiment was set to 100%. An LD in an unbleached cell was used as control to monitor photobleaching during the experiment (grey). Values are mean \pm SD of three independent experiments.

(C) CCT2 fluorescence remains stable on a single LD in a bleached cell. FLIP of mCherry-CCT2 in cells treated with oleate for 12 h. CCT2 was tagged with mCherry (upper panels), LDs were stained with BODIPY (middle panels). The lower panels show overlays of the two channels. Box indicates the LD that was not photobleached in the cell. Insets show the indicated part of the image at higher magnification. Prebleach (left), immediately after bleach (middle), and postbleach (right) images of the FRAP experiment. Bar = 5 μ m. The fluorescence of the non-bleached LD was subsequently monitored.

(D) Normalized fluorescence intensity of mCherry-CCT2 of experiments as in (C) over time. Values are mean \pm SD of three independent experiments.

4.2.8 CCT is activated by LD targeting

Among enzymes localizing to LDs some are active on the LD surface, whereas others are sequestered there in an inactive state (Leber et al., 1998). The hypothesis that CCT localization has a regulatory function in upregulating PC synthesis according to the increased need during LD growth suggests that CCT activity increases by LD binding. Since it was shown before that CCT activity increases upon membrane binding, its enzymatic activity was tested after recruitment to LDs. To exclude that CCT is sequestered on LDs in an inactive state, I measured its activity before and after oleate loading and normalized it to its abundance determined by Western blot.

After oleate loading of S2 cells, I observed a strong increase in specific activity for the endogenous protein, as well as for mCherry-CCT1 (Figures 34A, B). Endogenous CCT activity and mCherry-CCT1 activity increased more than fourfold and more than threefold, respectively. Moreover, when I replaced oleate containing medium by lipid free medium what stops LD growth and CCT1 is released from the LD surface (Figure 26A), its activity returned to near basal levels (Figure 34A).

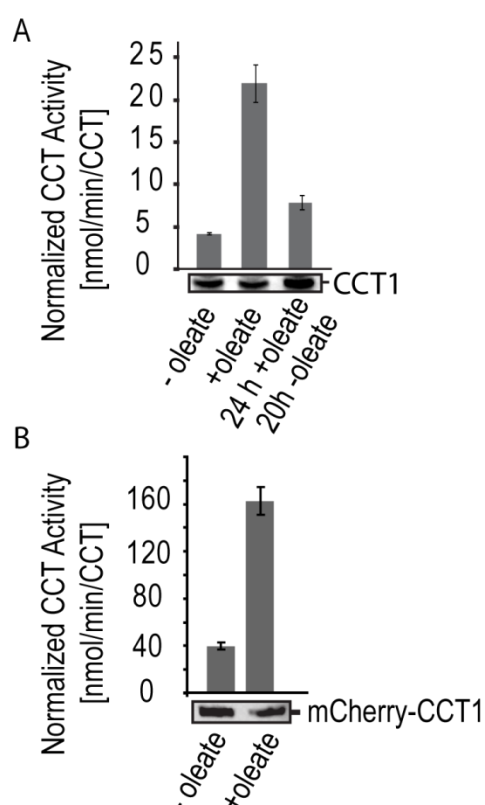


Figure 34. CCT is activated by LD binding.

(A) Endogenous CCT activity increases when cells are loaded with oleate and decreases again when cells are shifted to lipid free medium. CCT activity of total cell lysate was measured before oleate loading, after 12 h of oleate loading, and after removal of oleate for 20 h after 24 h of oleate loading. CCT activity was normalized to the amount of CCT1 measured by Western blot analysis. Lower panel shows a representative Western blot of CCT1 expression levels in samples used for activity assays (equal amounts loaded onto blot and activity assay). Values are mean \pm SD of three experiments.

(B) mCherry-CCT1 activity increases when cells are loaded with oleate. mCherry-CCT1 activity was measured and normalized as described in (A). Endogenous CCT activity was measured and subtracted before and after oleate loading. Values are mean \pm SD of three independent experiments.

To test whether CCT induction was due to targeting of the enzyme to LDs or any other cellular fraction, I measured CCT activity in soluble, membrane, and LD fraction. In the soluble and the membrane fraction, I detected only low levels of specific CCT activity and there was no increase in those fractions during oleate loading. However, in the LD fraction, I measured a strong increase in CCT-specific activity after the induction of LD formation (Figure 35). Strikingly, CCT activity started to increase with a 3-5 h delay after oleate induction, which resembles the time when CCT targeting to the LD surface starts (Figure 26 and 35). Thus, CCT activity increases concurrently with more and more CCT recruitment to LDs.

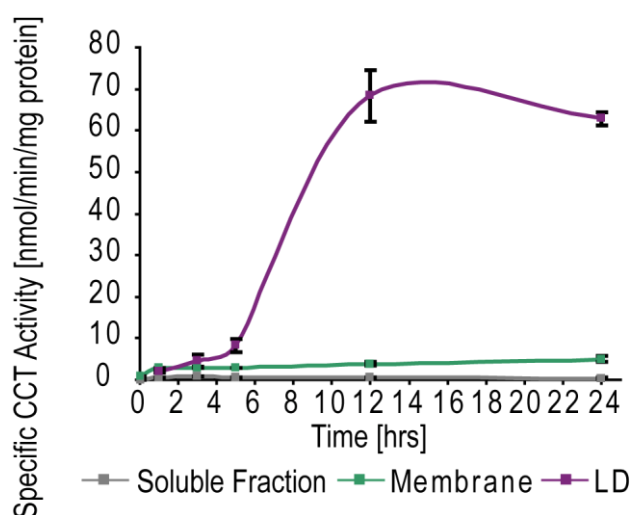


Figure 35. CCT is active on LDs.

Lysates of S2 cells loaded with oleate for the indicated times were fractionated into cytosol, membrane, and LDs, and specific CCT activity was measured. Values are mean \pm SD of three experiments.

Previously obtained results suggest that CCT1 relocation to LDs is induced by PC deficiency on the LD surface, as the targeting of the enzyme coincides with a dramatic decrease of the PC:TG ratio (Figure 28A). To directly address whether PC-deficient LDs recruit and activate CCT, I mixed S2 cell extracts with artificial droplets of different compositions. Droplets stabilized by PC alone did not induce CCT activity compared to basal activity levels without the addition of artificial droplets or TG alone (Figure 36A). However, CCT activation was inversely correlated with the molar PC:PE ratio. Additionally, artificial droplets shielded by other phospholipid species (e.g., PS or PI) strongly activated CCT (Figure 36A). To confirm that CCT activation was in fact caused by specific binding to the phospholipid monolayer by its

amphipathic alpha helix, I used the LD binding impaired CCT1 mutant (W397E) as a control (Figure 25). As shown before, this mutant cannot bind to droplets anymore and thus could not be activated by the addition of artificial droplets that activated WT CCT (Figure 36B). Thus, CCT is activated by PC deficiency on LDs *in vivo* and *in vitro*. This further supports the model in which CCT binds to PC and is activated by PC deficiency during LD formation in cells.

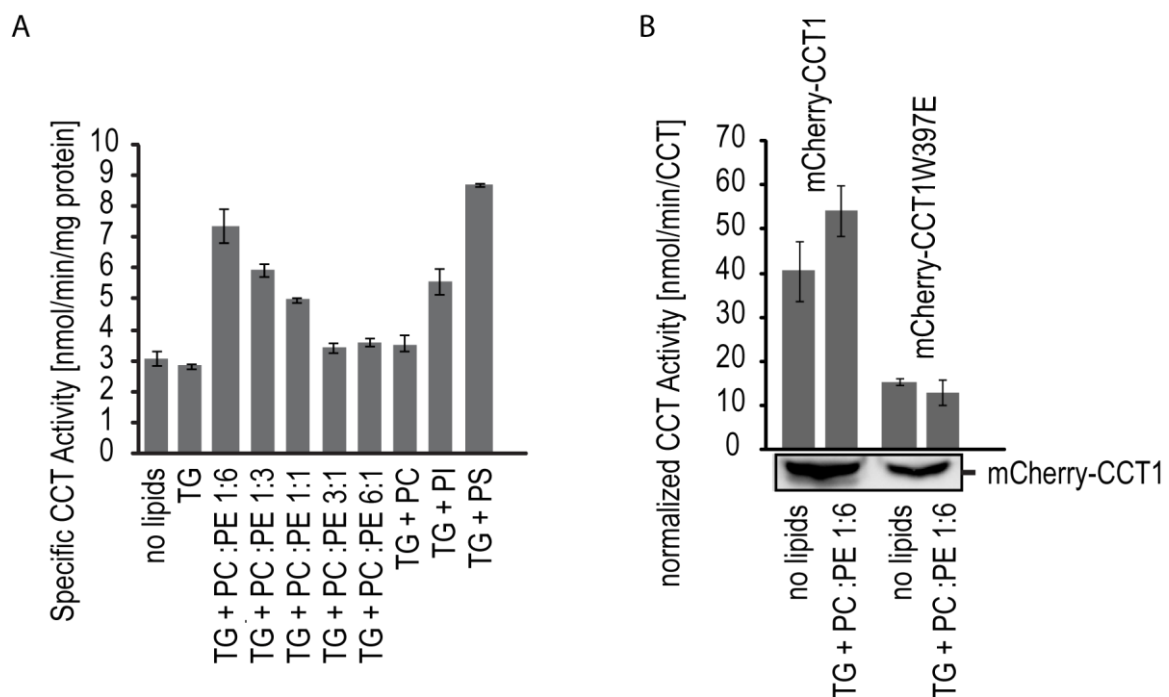


Figure 36. CCT is activated by PC deficient artificial droplets

(A) CCT activity inversely correlates with PC content of *in vitro* generated artificial droplets. Artificial droplets of the indicated phospholipid compositions were generated, added to total lysate of wild type cells, and CCT activity was determined. Values are mean \pm SD of three experiments.

(B) mCherry-CCT1, but not mCherry-CCT1W397E, is activated by artificial droplets with low PC. Artificial droplets containing PC and PE in a 1:6 ratio were generated and added to total mCherry-CCT1 and mCherry-CCT1W397E cell lysate and the CCT activity was determined. Values are mean \pm SD of three independent experiments.

4.2.9 LD binding is essential for CCT1 function in LD biogenesis

The hypothesis that PC synthesis during LD biogenesis is regulated by CCT subcellular relocalization predicts that LD binding is crucial for the enzyme's function. To further test this prediction, I determined the requirement of CCT1 for normal LD formation. As expected, depleting the endogenous CCT1 by RNAi against the 3'UTR of its mRNA led to the formation of giant LDs after oleate loading. Moreover, I expressed different RNAi-resistant mCherry-CCT1 constructs to determine whether they can rescue the depletion phenotype of the endogenous protein. Expressing full-length mCherry-CCT1 or mCherry-CCT1 Δ P completely rescued the phenotype (Figure 37), whereas mutants that are unable to bind to LDs, such as the constructs lacking the amphipathic helix (Δ HP) or the point mutant (W397E) had no effect on the formation of giant LDs (Figure 37). As shown before by FLIP experiments (Figure 32), both Δ HP and W397E CCT1 shuttled normally between nuclear and cytoplasmic compartments and had access to cytoplasmic LDs (Figure 31). These results indicate that LD binding is necessary for normal function of CCT in LD biogenesis

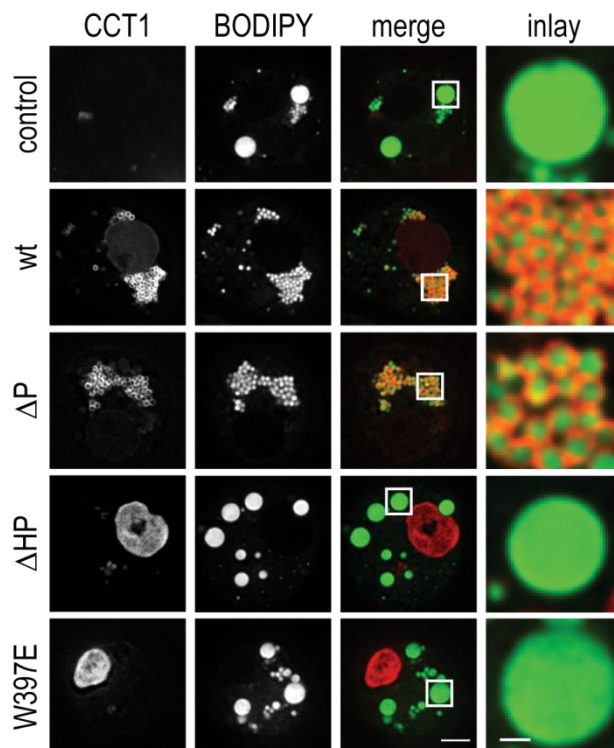


Figure 37. LD binding is essential for CCT1 function and biogenesis.

mCherry-CCT1, mCherry-CCT1 Δ P, mCherry-CCT1 Δ MP, and mCherry-CCT1W397E were expressed in cells with endogenous CCT1 knocked down by RNAi against its 3'-UTR, and the ability of the mutants to rescue the LD phenotype was tested in oleate loaded cells.

To analyze the function of CCT1 nucleocytoplasmic shuttling during LD expansion, I overexpressed CCT2, which is normally only present in low amounts, in CCT1 depleted S2 cells. CCT2 is highly homologous to CCT1 but in contrast contains no N-terminal nuclear localization signal (NLS) and is thus cytosolic under steady state conditions. Overexpression of cytosolic CCT2 fully rescued the phenotype of CCT1 depletion resulting in normally sized LDs (Figure 38). This suggests that continuous shuttling of CCT1 between the nucleus and the cytoplasm is necessary for CCT1 to survey LD PC levels and react to changes on the LD surface. However, this continuous shuttling is important only for enzyme localization and not its inherent function in PC synthesis during LD expansion.

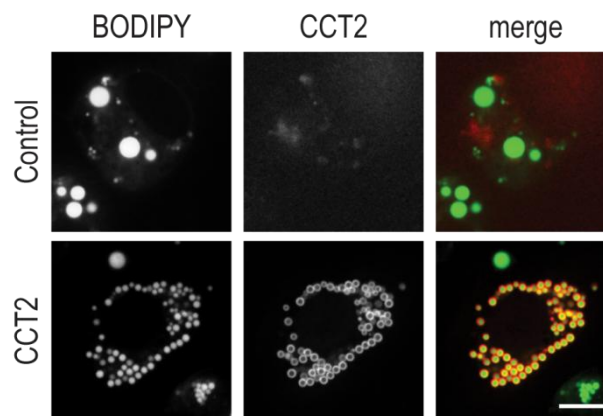


Figure 38. Nucleocytoplasmic shuttling is not necessary for CCT1 function during LD expansion.

mCherry-CCT2 (lower panels) was transiently expressed in cells with endogenous CCT1 knocked down by RNAi against its 3'-UTR and the ability of the CCT2 to rescue the LD phenotype was tested in oleate loaded cells. Untransfected control cell of the same sample is shown in the upper panel

4.2.10 CCT regulates LD size *in vivo*

To test whether regulation of PC synthesis by CCT1 activity also plays an important role during LD formation *in vivo*, I analyzed LD morphology in *Drosophila* expressing CCT1-directed shRNA in larval fat body. CCT1 depletion resulted in a similar phenotype as observed in S2 cells. Larvae expressing the CCT1-directed shRNA had significantly larger LDs as larvae expressing red fluorescent mCherry

protein alone. Fluorescent mCherry protein under the same driver was used as a control for demonstrating expression of the short hairpin RNA (shRNA) in the fat body (Figure 39). This shows that CCT1 function for the regulation of LD morphology is conserved in whole flies.

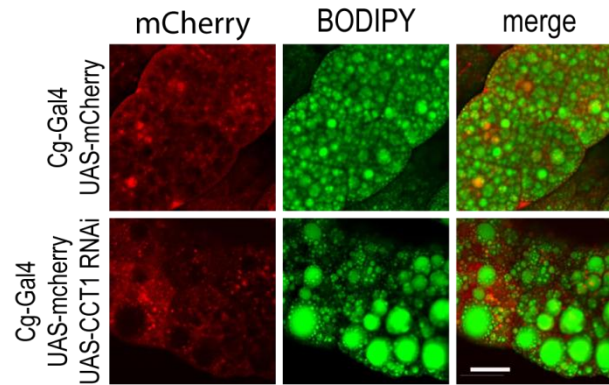


Figure 39. CCT is important for LD homeostasis *in vivo*.

CCT1 knockout flies have giant LDs in larval fat body. Fat body of Cg-Gal4 UAS-mCherry and Cg-Gal4 UAS-mCherry/UAS-CCT1 RNAi flies were stained for LDs with BODIPY (middle). Expression of the UAS-Gal driver was monitored by mCherry levels (left). Right panels show overlay of the two channels. Bar = 10 μ m.

4.2.11 CCT targeting and function in LD stabilization is conserved in mammalian cells

To address whether CCT function in LD biology and its regulation by relocalization is evolutionarily conserved in mammals, I expressed murine CCT α in S2 cells. As the *Drosophila* protein, murine CCT α localized to LDs after oleate treatment (Figure 40).

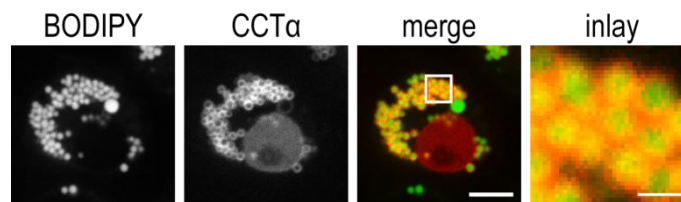


Figure 40. CCT α localizes to LDs in S2 cells.

Murine mCherry-CCT α was transiently expressed in S2 cells (left panels, red), which were loaded with 1 mM oleate for 12 h. LDs were stained with BODIPY (middle panels, green). The overlays of the two channels and zooms of a representative LD section are shown (right two panels). Bar = 5 μ m (overview) or 1 μ m (inlay).

Also in an oleate treated murine macrophage cell line (Raw267.4) CCT α formed rings around LDs (Figure 41A). However, in contrast to *Drosophila* S2 cells, Raw267.4 cells formed less LDs and CCT localization to reticular structures, likely ER membranes was observed besides LD localization (Figures 41A). This relocation in response to oleate loading was reflected in the localization of endogenous CCT α in different cellular fractions of primary bone marrow–derived macrophages (BMDMs) (Figure 41B). Under basal conditions CCT α was mostly detected in the soluble fraction and shifted after oleate loading to the LD and microsomal fractions.

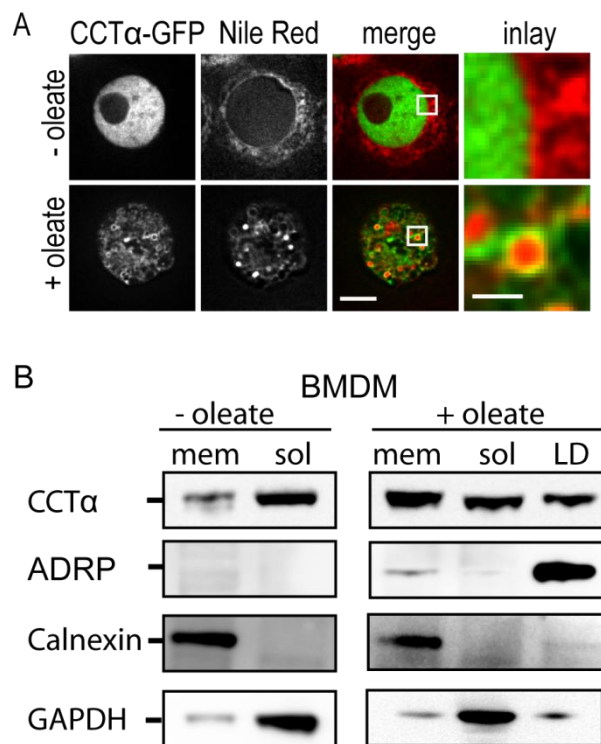


Figure 41. CCT function is conserved in mammalian cells.

(A) CCT α targets to LDs and membranes in oleate-loaded Raw 267.4 macrophages. CCT α -GFP was expressed in Raw 267.4 cells (left) loaded with oleate for 12 h. LDs were stained with Nile Red (middle). Second right panel shows overlays of the two channels. Right panels show a zoom of representative LD sections. Bar = 5 μ m (overview) or 1 μ m (inlay).

(B) Oleate loading causes CCT α to move from the soluble fraction to membranes and LDs in BMDM. The indicated cellular fractions were probed for CCT α , and the marker proteins ADRP, calnexin, and GAPDH.

To test whether CCT α relocalization to LDs and membranes is coupled to CCT α activation, similar to what was observed in S2 cells; I compared CCT activity to normalized enzyme levels before and after oleate loading. In BMDMs and Raw267.4 cells CCT activity increased more than nine- and three-fold, respectively (Figures 42A, B). These results indicate that also in mammalian cells CCT α is activated after oleate treatment and is mediated by enzyme relocalization.

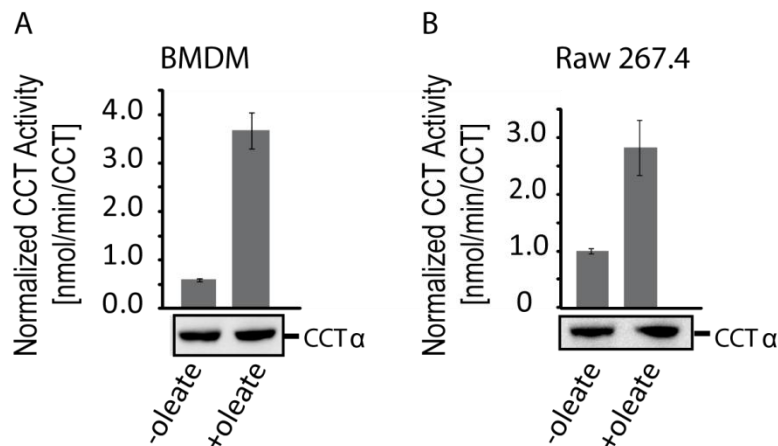


Figure 42. CCT α is activated by oleate loading in BMDMs and Raw 267.4 macrophages.

(A) and (B) CCT activity in total cell lysates was measured before and after 12 h of oleate loading and normalized to CCT levels measured by Western blot. Lower panels show a representative Western blot of CCT α expression in samples used for activity assays (equal amounts were loaded onto the blot and in the activity assay). Values are mean \pm SD of three experiments.

I observed the mechanism of CCT α activation by relocalization not only in macrophages, since neuronal N2a cells showed an even more pronounced recruitment and activation of CCT (Figures 43A, B, C). In untreated N2a cells CCT α was found in the membrane and soluble fraction as detected by Western blot. After oleate loading, CCT α redistributed from the soluble to the LD fraction (Figure 43A). Moreover, total CCT activity increased ~two-fold (Figure 43B) and specific CCT activity was highest in the LD fraction compared to other cellular fractions (Figure 28C). Also *in vitro* assays using N2a cell lysate showed similar results as observed for *Drosophila* CCT (Figure 37). CCT was strongly activated by artificial droplets consisting of PS and PI or with low amounts of PC, whereas almost no induction of CCT was detected with artificial droplets containing high PC levels (Figure 43E).

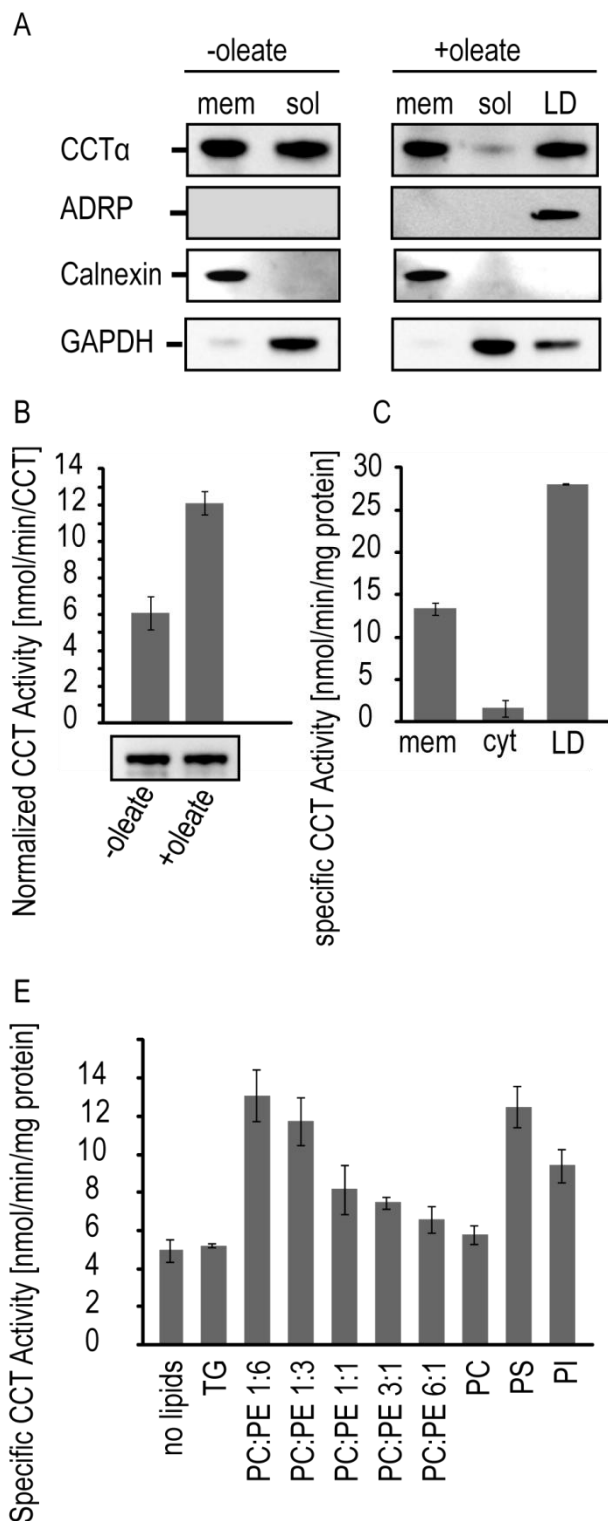


Figure 43. CCT α relocates to LDs and membranes in N2a cells and is activated by oleate loading and PC deficient artificial droplets.

(A) Same protein amount of the indicated cellular fractions was blotted against CCT α , and the marker proteins ADRP, calnexin and GAPDH.

(B) Oleate loading increases CCT α activity in N2a cells. CCT activity was measured in total cell lysate before and after 12h of oleate loading and normalized to enzyme levels measured by Western blot. Lower panels show a representative blot of CCT α expression in samples used for activity assays (equal amounts were loaded onto the blot and in activity assay). Values are mean \pm SD of three independent experiments.

(C) In oleate loaded cells CCT α activity is highest in the LD fraction. The specific CCT activity was measured for the indicated fractions purified from N2a cells after oleate loading. Values are mean \pm SD of three independent experiments.

(D) Mammalian CCT activity inversely correlates with the PC content of *in vitro* generated artificial droplets. Artificial droplets of the indicated phospholipid compositions were generated and added to total N2a cell lysate, and CCT activity was determined. Values are mean \pm SD of three experiments.

To determine whether a loss of CCT function during LD biogenesis has the same effect in mammalian cells as in *Drosophila*, I analyzed LD morphology in CCT α depleted BMDMs. I treated BMDMs from mice homozygous for a conditional *Ccta* allele (*Ccta*^{F/F}) or control mice (R26R-eYFP) with a fusion protein consisting of a His-tag-Tat peptide from human immunodeficiency virus, a nuclear localization sequence

and a membrane-permeable Cre recombinase (HTNC). This fusion protein catalyzes the site-specific recombination of DNA between loxP sites and thus deletes the *CCT α* gene after its entry into the nucleus (Peitz et al., 2007). As determined by FACS sorting of the R26R-eYFP BMDMs, recombination efficiency by HTNC treatment was >90%. In BMDMs from conditional *Cct α ^{F/F}* mice treated with HTNC, *CCT α* mRNA levels were 89% lower than in untreated control cells and 86% lower than in treated control cells (Figure 44B), which led to complete depletion of the protein, as tested by Western blot (Figure 44C). Upon *CCT α* depletion, I observed a similar phenotype as in the *Drosophila* S2 cell. Of the BMDMs deleted in *CCT α* , 66% had highly enlarged LDs in response to oleate loading (Figure 44A). Thus, CCT function is important for the regulation of LD formation and size also in mammalian cells, pointing to an evolutionarily conserved function for CCT in LD biology.

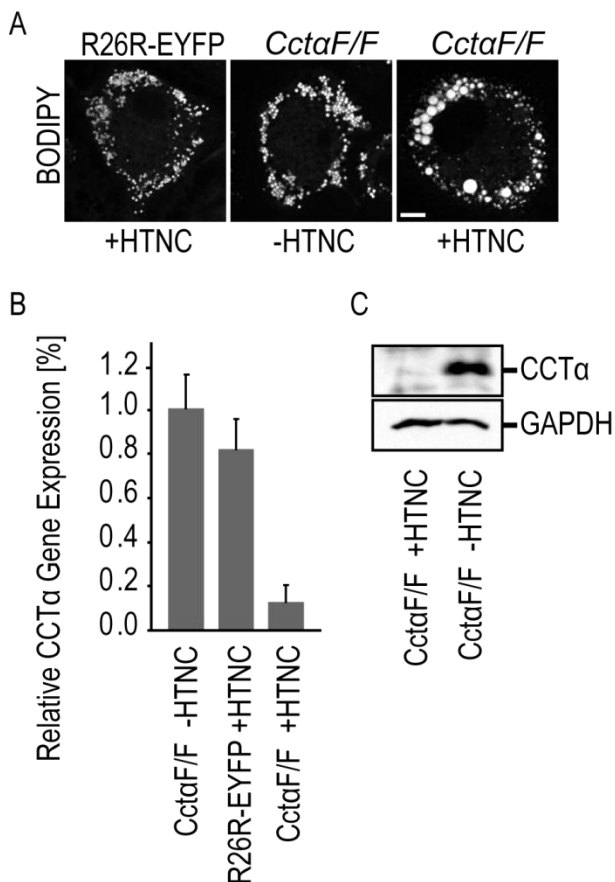


Figure 44. *CCT α* knockout in BMDMs results in giant LDs.

(A) LD morphology was analyzed in HTNC-treated BMDM from *Cct α F/F* mice. Untreated BMDM of *Cct α F/F* mice and of HTNC-treated R26R-EYFP mice were used as controls. Representative midsections of BODIPY-stained cells are shown. Bar = 5 μ m. (B) and (C) *CCT α* protein was completely depleted in HTNC-treated BMDMs from *Cct α F/F* mice. *CCT α* mRNA levels were 89% lower than in untreated control cells and 86% lower than in treated control cells. Western blot shows complete depletion of *CCT α* in total cell lysate from HTNC-treated BMDMs from *Cct α F/F* mice. GAPDH was used as a loading control.

5 DISCUSSION

5.1 *Protein correlation profiling identifies LD proteins with high confidence*

This thesis contains a first high confident LD proteome that allows distinguishing between *bona fide* LD proteins and contaminants from other cellular organelles. A number of LD proteomes from different cell types and organisms are published (Bartz et al., 2007; Beller et al., 2006; Brasaemle et al., 2005; Cermelli et al., 2006) but the reliability of those studies is limited. In these studies, the number of identified proteins was mainly dependent on the sensitivities of the mass spectrometers used for analysis. However, the abundance of a protein in the LD fractions does not provide enough information to determine whether a protein is indeed a LD-specific protein or whether it merely is a contaminant. Intracellularly highly abundant proteins, such as ribosomal proteins, might be found in larger amounts in the LD fraction than very low abundant LD proteins. This might explain the identification of large numbers of ribosomal and mitochondrial proteins in previous proteomes (Bartz et al., 2007; Beller et al., 2006; Brasaemle et al., 2005; Cermelli et al., 2006). Moreover, all existing proteomic studies show very little overlap. For example, in two previous *Drosophila* LD proteomes roughly three hundred proteins were identified in total. However, less than 10% of proteins were found in both proteomes (Beller et al., 2006; Cermelli et al., 2006).

1,361 proteins were detected in the LD fraction in this study. This number of identified proteins is much higher than in the proteomes published before. However, as expected, the main part of those identified proteins are contaminants from other organelles and only protein correlation profiling allowed me to identify 106 proteins that are specifically enriched in the LD fraction. Indeed, these numbers highlight the importance of incorporating an unbiased method, such as protein correlation profiling, to reduce false positives.

By fluorescence microscopy I confirmed the LD localization of 20 proteins found to be highly enriched in the LD fraction by protein correlation profiling. More than 90% of the tagged proteins localized to LDs confirming the high confidence of the mass spectrometry-based identification of LD proteins (Figure 12). For most of the tested proteins, PCPs highly correlated with their cellular localization determined by fluorescent microscopy. Protein correlation profiling potentially advantageous over ectopic expression of fluorescently tagged proteins, since addition of a tag and higher protein levels might alter protein localization, whereas protein correlation profiling is applied to endogenous proteins.

The results from this study open up a new perspective on protein targeting to LDs, as PCPs of the identified proteins contain more information than their mere localization. The determination of certain groups of LD proteins that share common PCPs might allow identification of proteins that are targeted to LDs from the same cellular compartments and thus might achieve this by similar mechanism. This may lead to a more general approach to study protein LD targeting. Another intriguing question that arises from the proteomic and microscopy data is, whether LD proteins with several predicted transmembrane domains localize directly to the LD monolayer or if they are enriched in specialized membrane domains that wrap around LDs. Novel techniques such as super high resolution light microscopy will provide new possibilities to address such questions in the future (Toomre and Bewersdorf, 2010).

In addition several previously characterized LD proteins, many new and so far unknown LD proteins were identified in the proteome, which might lead to new discoveries in the field of LD biology. For example, a current subject of research is how neutral lipids enter LDs during their growth. It was recently discovered that DGAT2, which catalyzes the final step of TG synthesis, localizes to LDs (Stone et al., 2009), suggesting that TG is generated directly on the LD surface. The LD proteome reveals that also certain homologues of enzymes catalyzing the preceding steps of the TG synthesis pathway (Figure 5) localize to LDs. Thus, it would be interesting to

test, whether the complete TG synthesis pathway is organized on the LD surface or closely opposed membranes. Another interesting discovery originating from the LD proteome is that several proteins involved in the formation of tubular ER, such as reticulons and atlastin (Park and Blackstone, 2010), are highly enriched in the LD fraction. Colocalization of tubular ER markers with LDs may indicate that LDs are associated preferentially with tubular ER. The identification of these proteins enriched in the LD fraction raises the question whether LDs are associated with specialized ER regions and might point to new aspects regarding the mechanism of LD budding from the ER. Moreover, the generated data set provides a basis for further analysis of changes in the LD proteome under varying cellular conditions, such as different time points after the induction of LD formation or starvation. The generated data set can also be used to compare effects of the knockdown of specific proteins on the LD proteome and thus allow studying certain LD targeting pathways.

5.2 Identification of key players for LD phospholipid homeostasis by comparing proteomic data with genome-wide screens

Integration of data from the PCP-derived LD proteome with results from global, genome-wide screens (Beller et al., 2008; Guo et al., 2008) revealed several proteins that localize to LDs and whose knockdown results in an alteration of LD morphology. However, the overall overlap of the data sets was unexpectedly low. Proteins with LD phenotypes were only slightly enriched in the LD proteome compared to the complete cellular proteome (Figure 14). This does not mean that proteins enriched in the LD fraction play no functional role on the LD surface; in fact other reasons might be responsible for lacking phenotypes of LD proteins in the genome-wide screens. One reason could be redundancy of proteins that have important cellular functions. An example is TG synthesis, where several homologous enzymes exist for every step in the pathway. When knocking down one protein, the enzymatic activity of the remaining homologues might be sufficient to maintain proper LD morphology (Yen et

al., 2008). Another reason for the low overlap between the LD proteome and the genome-wide screens is that in the latter some phenotypes could have been missed, since RNAi conditions were not optimized for each individual protein. Low knockdown efficiency for certain candidates or long protein half-life limit the detection of some of those phenotypes. Moreover, some proteins might only give phenotypes under specific conditions other than those used in the screen.

Among the LD proteins showing a strong LD phenotype, CCT could be identified as key player in phospholipid homeostasis during LD expansion. This led me to study further the mechanism of PC levels adjustment according to need during LD growth.

5.3 PC is a crucial surfactant stabilizing LDs and preventing their coalescence

The RNAi screen data implies that phospholipid levels and composition of the LD surface are important for normal LD morphology and function. However, nothing has been known so far about the role different phospholipids play in LD size determination and fusion, as well as how their synthesis is regulated during expansion.

Cells that are exposed to large amounts of free fatty acids start to extensively synthesize TG. At the same time, this process leads to an accumulation of LDs, as well as a dramatic increase in LD diameter up to ten-fold (Figure 28). In most cells types, including *Drosophila* S2 cells, LDs are always in close association and form grape-like clusters. Despite such close contacts between single LDs, fusion events are rarely, if ever, observed (Guo et al., 2008). This state persists as long as growth of the neutral lipid core of LDs is coordinated with the addition of stabilizing phospholipids to their surface. Only in cells with impaired phospholipid synthesis, conditions under which insufficient amounts of stabilizing phospholipids are present on the LD surface, LDs tend to coalesce resulting in few giant LDs per cell (Guo et al., 2008).

This phenomenon can be explained by the biophysical characteristics of a liquid-liquid biphasic system, such as a TG emulsion in an aqueous environment. For such a biphasic system it is thermodynamically most favorable to coalesce into a single oil layer separated from the aqueous phase, as this minimizes interface contacts between the phases and reduces surface tension (Kabalnov and Wennerstrom, 1996). Indeed, TG droplets generated *in vitro* coalesced rapidly (Figure 21). To prevent phase coalescence between a hydrophobic and a hydrophilic phase, sufficient amounts of amphipathic molecules are required that are able to separate the two phases and thus act as surfactants. This explains why sufficient amounts of phospholipids are required on the LD surface to shield the neutral lipid core from the aqueous environment and to prevent coalescence of smaller LDs into larger ones.

Phospholipid species differ in their ability to shield and stabilize LDs (Kabalnov et al., 1996). PC in particular is crucial for stabilizing growing LDs and is required to limit their size during expansion. Inhibition of PC synthesis in cells with expanding LDs leads to coalescence and formation of one or a few giant LDs per cell (Figure 15B) (Guo et al., 2008).

Sufficient amounts of PC prevented coalescence of artificial TG droplets *in vitro*. Consistently, addition of PC liposomes rescued the phenotype of a CCT knockdown in S2 cells (Figure 18). The surfactant property responsible for this stabilizing effect is specific to PC, since PE or physiological levels of other phospholipids (e.g. PS and PI) did not prevent coalescence of TG droplets (Figure 21). Also knockdown of enzymes for PE synthesis did not result in a LD phenotype, although PE is the most abundant phospholipid of LDs in *Drosophila* S2 cells (Figure 16, 17).

Described differences in stabilizing lipid emulsions are likely explained by the biophysical properties of these phospholipids. In contrast to PC, which has a large head group and thus a cylindrical shape, PE has a smaller head group and is conical (Vance and Vance, 2008). It was found that the stability of macroemulsions, such as LDs is strongly correlated to the surfactant lipid shape (Kabalnov et al., 1996;

Kabalnov and Wennerstrom, 1996; Saito et al., 1999), a fact that can be explained by the different behavior of surface lipids in the transition state during monolayer coalescence. During this transition state strong bending of the monolayer occurs at the interface of the coalescing droplets. For monolayers containing the conical, curvature inducing PE, it is much easier to enter this transition state than for monolayers containing cylindrical PC. The higher energy of the transition state for monolayers with PC increases the required activation energy and prevents coalescence (Kabalnov and Wennerstrom, 1996).

Another factor contributing to differential behaviors of phospholipid species is that phospholipids differ in their ability to shield TG. For example, in emulsion droplets consisting of PE and triolein, 28% of the interphase surface is exposed TG, whereas in PC and triolein mixtures, only 3% of the surface is TG (Saito et al., 1999). Since higher amounts of exposed highly hydrophobic TG increase the propensity for droplet coalescence in emulsions, it might explain why PC shielded TG droplets are much more stable and show a lower tendency to coalesce into larger droplets in cells.

However *in vivo*, additional factors, such as proteins on the LD surface, likely influence LD stability and size. Good candidates for a stabilizing function are PAT proteins in animals and the oleosins in plants. They are suggested to bind to exposed TG patches on the LDs with their amphipathic helices. Thus, they potentially help to shield such hydrophobic patches and increase LD stability (Siloto et al., 2006; Wolins et al., 2006). However, this study shows that proteins by themselves are not sufficient to prevent LD coalescence under PC deficient conditions in *Drosophila* cells, larval fat body, or murine macrophages.

5.4 CCT adjusts PC synthesis during LD expansion by a homeostatic feedback loop

Studying the targeting of CCT to LDs revealed an elegant homeostatic feedback mechanism to adjust PC synthesis according to elevated needs during LD growth. Relocalization of CCT to LDs, the site of relative PC depletion under conditions of LD growth, activates CCT and upregulates the Kennedy pathway. Thus, the cellular PC pool available to coat growing LDs increases and their coalescence is prevented. This mechanism of PC homeostasis is apparently evolutionarily conserved, as similar findings in *Drosophila* and mammalian cells were observed.

During lipid loading, average LD diameters increased from 300 nm to more than 900 nm, representing a more than nine-fold surface expansion (Figure 26). Thus cells are confronted with a huge demand for PC at the LD surface in a relatively short period of time. Indeed, during a time period of 24 hours of lipid loading, total cellular PC levels increase almost three-fold (Figure 26). Thus the questions arise how the required PC amounts can be provided and how PC synthesis is adjusted according to need? Data from this study suggest a model in which regulation of PC synthesis *via* the Kennedy pathway is achieved by activating its rate-limiting enzyme CCT, which relocates to PC deficient membranes on the LD surface. LD targeting activates CCT and thereby increases PC synthesis (Figure 45). At steady-state, before oleate loading, CCT is in its inactive soluble state. CCT1, the most abundant isoform in *Drosophila* S2 cells, shuttles between the nucleus and the cytoplasm, without being associated to any cellular membranes (Figure 29, 30). Circulation between the two compartments allows CCT1's access to cytosolic LDs and thereby enables the enzyme to survey PC levels on the LD surface. Under conditions when LDs expand, an increasing PC deficiency on the expanding LDs generates stable binding sites for CCT. As more and more CCT accumulates on the LDs instead of shuttling back to the nucleus, the equilibrium is shifted from the main nuclear pool towards the LD surface, slowly depleting the nuclear CCT1 pool (and the cytoplasmic CCT2 pool) is.

Previous studies showed that membrane association greatly induces CCT activity (Feldman et al., 1985; Vance and Pelech, 1984) and I found consistently that CCT is activated by binding to LD monolayers. Since CCT catalyzes the rate-limiting step of PC synthesis, its activation increases flux through the Kennedy pathway, and thus increases its *de novo* synthesis on the ER (Johnson et al., 2003). PC is then potentially trafficked to LD surfaces and prevents their coalescence into larger droplets.

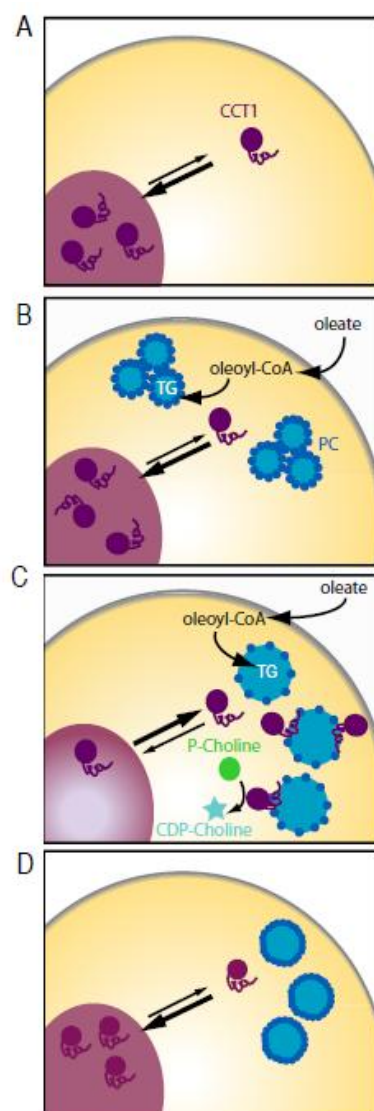


Figure 45. Model of CCT Regulation during LD Expansion.
See discussion for details.

Several lines of evidence support the hypothesis that CCT regulation by relocalization is part of a homeostatic control of PC synthesis. First, CCT is targeted to LDs after an initial delay and not immediately upon their formation. This is expected for a homeostatic control mechanism, as after budding of stable LDs from the ER the system is initially in equilibrium and sufficient amounts of PC are present on the LD surface. Only when LDs start to expand and more and more TG accumulates in the LD core, PC deficiency arises on the LD surface. Under those conditions the PC/TG ratio strongly decreases and CCT binds to the LD surface (Figure 28A). Second, once CCT has been recruited to the LD surface, the PC/TG ratio of LDs begins to stabilize and is then maintained at a constant level, even though LDs further expand and TG continues to accumulate. Interestingly, the amount of CCT1 targeted to LDs during the first 12 h of oleate loading increases roughly in proportion to the square of the diameter, similar to the changes in LD surface area (Figure 26). A third point supporting a homeostatic feedback loop is that CCT1 targeting is reversible. After removal of lipids from cells, LD expansion stops. There is no more need to increase cellular PC levels and after some time the system returns to equilibrium. Under those conditions in the cell, CCT1 no longer binds the LD surface and its activity returns to almost basal levels (Figure 34). At this point the main CCT pool relocalizes to the nucleus. This redistribution of CCT1 might either be caused by reimport into the nucleus after release from the LD surface or alternatively by specific degradation of LD-associated CCT1 and replacement of the nuclear pool by new protein synthesis.

5.5 CCT surveys PC levels on the LD surface and binds to PC deficient LDs

What induces CCT LD binding and how does CCT sense PC deficiency on expanding LD surfaces? Previous studies found that CCT binding to membranes and its activation is dependent on their lipid composition. It was found that CCT preferentially binds to membranes and liposomes containing DG, oleate, and PE. Moreover CCT targeting to membranes is inversely correlated with increasing PC content in S2 cells and *in vitro* (Arnold et al., 1997; Sleight and Kent, 1983; Utal et al., 1991; Weinhold et al., 1994; Yao et al., 1990).

Similar to these results, CCT was activated by PC-deficient LDs. Initially, when there are still sufficient amounts of PC on the LD surface, CCT remained in the nucleus. CCT is only targeted to LDs when the PC/TG ratio on its surface strongly decreases and is then activated there (Figure 26, 28). This could also be recapitulated *in vitro* as artificial droplets shielded by PC alone did not increase CCT activity. In contrast artificial droplets having high levels of other phospholipids like PE, PS or PI strongly activated CCT. Moreover, CCT activation is inversely correlated with decreasing PC levels in PC:PE consisting artificial droplets (Figure 36).

But how does PC deficiency induce CCT LD targeting? Previously it was suggested that some properties of membranes could promote CCT membrane targeting. Interfacial packing defects as might occur when lipids with small head groups such as PE are in the membrane or curvature strain that occurs when membranes are enriched in hexagonal phase-preferring lipids such as PE and DG. Synthesis of PC would reverse these properties of membranes resulting in a more stable bilayer (Vance and Vance, 2008). Another hypothesis is that exposed TG on the LD surface might favor the interaction between CCT and LDs. Exposure of TG might be closely correlated with the PC content of the LD monolayer, as deficiency of PC on expanding LDs would likely increase the area of exposed TG because of insufficient amounts of detergent available to shield the neutral lipid core. Thus, highly hydrophobic patches could form on the LD surface, likely providing stable binding

sites for the CCT helical domain. Such a mechanism would be similar to what has been described for apolipoproteins, which bind to oil/water interphases with their amphipathic alpha helices (Small et al., 2009). Binding of amphipathic alpha helices to exposed TG patches on the LD surface might even be a more general mechanism for targeting of different proteins to LDs, a process that is in general still poorly understood.

The model of CCT surveying PC levels on LDs to be activated when PC deficiency arises implies that the enzyme has access to the cytoplasm and the surface of LDs. Consistent with this model, in the basal state before oleate loading, CCT1 is soluble, diffusing rapidly in the nucleus, and continuously shuttling between the nucleus and cytoplasm (Figure 29, 30). So far, the mechanism for nuclear export remains unknown. It was previously suggested that in mammalian cells the amphipathic helix mediates CCT α nuclear export (Gehrig et al., 2009). However, a *Drosophila* CCT1 mutant lacking the amphipathic helix still shuttled between the nucleus and cytoplasm (Figure 31). Therefore it seems unlikely that the alpha helical sequence of CCT1 contains the nuclear export signal; rather it might mediate CCT1 retention in the cytoplasm when a stable binding site, such as a PC-deficient LD surface, is present and thus might be necessary to shift the equilibrium toward nuclear export. Nuclear import of *Drosophila* CCT1 and mammalian CCT α is mediated by a putative N-terminal nuclear localization signal present only in CCT1 and CCT α , but not in CCT2 and CCT β (Wang et al., 1993b). In *Saccharomyces cerevisiae* the α importin Kap60 and the β importin Kap95 were reported to bind the CCT homolog Pct1 and to escort it into the nucleus (MacKinnon et al., 2009).

5.6 PC must be transported from its site of *de novo* synthesis in the ER to the LD surface

However, the mechanism of phospholipid transport to the LD surface has not been studied yet and is so far unclear. One possibility is that phospholipid transport from membranes, such as the ER, to the LD surface is mediated by phospholipid binding proteins. In the LD proteome several lipid transfer proteins were found to be specifically enriched in the LD fraction and for some of them LD localization could be confirmed by microscopy (Figure 12). Also the *Drosophila* homolog of the mammalian PC transfer protein (PCTP) containing a steroidogenic acute regulatory (START) domain for PC binding, was found to localize to LD surfaces by fluorescent microscopy (unpublished data) and thus might be a candidate for PC transport to LDs. Thus, PC could be trafficked from the ER, the site of *de novo* PC synthesis to LDs, which would be similar to the transport mechanism of ceramides from the ER to Golgi membranes by CERT, another START domain protein. Since lipid transfer proteins can only transport a single molecule at a time, to ensure sufficient efficiency, the transport might occur at sites of close contact between the ER and LDs to minimize the transport distance (Holthuis and Levine, 2005). However, experimental evidence for a transport mechanism by lipid binding proteins is still lacking.

Another possibility could be a mechanism similar to the transport of PC to mitochondrial membranes in plant cells (Testet et al., 1996). It was found that one way to provide the mitochondrial outer membrane with PC is acylation of lyso-PC to PC. Lyso-PC is less hydrophobic than PC and can partially diffuse between closely apposed membranes, such as mitochondrial associated membranes. Thus the Lyso-PC that is derived from degradation of PC in the ER by phospholipase A2 can diffuse to mitochondria where it is then converted into PC again by lyso-PC acyltransferases. Two lyso-PC acyltransferases were also found in the LD proteome and suggest a similar mechanism to transport PC to the LD surface *via* lyso-PC diffusion.

5.7 Regulating PC synthesis by CCT relocalization might be a general mechanism to maintain cellular PC levels

Since PC is one of the main phospholipids in all cellular membranes, not only on the LD monolayer, PC homeostasis is also important during other cellular processes when organelle membranes expand and higher PC levels are required. Also in those processes, CCT activation by relocalization to such membranes might provide a way to adjust PC levels according to requirements by a feedback mechanism.

One intriguing example for such a situation might be the cell cycle when expansion of the ER requires synthesis of new phospholipids. Indeed, CCT was reported to localize to ER membranes for PC synthesis during the cell cycle (Northwood et al., 1999). However, this finding was not confirmed by other reports, which found no link between the cell cycle and CCT localization (DeLong et al., 2000). As previously suggested, CCT may sense PC deficiency arising in membranes during this process (Attard et al., 2000; Jamil et al., 1990; Johnson et al., 2003), similar to its relocalization during LD formation. This suggests that regulation of CCT activity by targeting to PC deficient membranes might have a broad cellular function in membrane homeostasis. However, the mechanisms of CCT targeting to other cellular membranes under different conditions are still poorly understood. CCT enzymes could have sufficient basal activity to provide PC for most normal cellular processes and its activation by targeted relocalization may occur only under conditions of extreme expansion of an organelle, such as LD expansion.

The regulation of PC synthesis during LD formation is not only important in isolated cell culture models, but also in whole organisms, since depletion of CCT1 in *Drosophila* larval fat body resulted in giant LDs similar to what was observed in S2 cells. In mammals the importance of PC levels for lipid metabolism was discovered decades ago. Already in 1932, it was shown that dietary supplementation with choline can reduce symptoms of hepatic steatosis, an accumulation of large amounts of TG droplets in the liver, induced by a high-fat diet in rats (Best et al., 1932).

Moreover, choline-deficient diet is thought to reduce PC synthesis *via* the Kennedy pathway and thus is commonly used to induce fatty liver in animal models. Similarly, a tissue-specific knockout of CCT α in liver, where it is responsible for roughly 70% of PC synthesis (Sundler and Akesson, 1975), leads to hepatic accumulation of TG, reminiscent of the CCT1 knockdown phenotype in S2 cells (Guo et al., 2008; Jacobs et al., 2004). Those findings suggest that the adjustment of PC levels according to need is important for TG storage in organisms and that changes in PC levels might have an impact on the lipid metabolism of the whole body.

5.8 The regulation of PC synthesis by CCT relocalization during LD formation may be conserved in mammalian cells

The general mechanism of regulating PC synthesis during LD formation by CCT relocalization is probably conserved in mammalian cells. Depletion of CCT α in primary BMDMs results in giant LDs as in *Drosophila*. Although it was shown that loss of CCT α is partially compensated by upregulation of CCT α (Zhang et al., 2000), knockdown of CCT α induces a strong phenotype.

Moreover, CCT α is at least partially recruited to growing LDs. However, in comparison to *Drosophila* S2 cells, where I detected no CCT targeting to membranes, in mammalian cells I observed a combination of LD and ER targeting. The proportion of CCT localizing to either ER membranes or LDs was varying among different cell types. This might be dependent on the different phospholipid compositions of the tested cell types, since a larger portion of total CCT was targeted to LDs for example in neuronal N2a cells, which have higher PE:PC ratios and thus less PC available for LD biogenesis (Hicks et al., 2006). The variation in targeting supports the hypothesis that organelle binding of CCT is determined by phospholipid composition of the delimiting membrane. In *Drosophila* cells membranes have a higher PE content than most mammalian membranes resulting in a lower PC:PE ratio

(Jones et al., 1992; van Meer et al., 2008), which could explain why CCT targeting to LDs is more prominent in *Drosophila* than in mammalian cells.

The mechanism of how PC levels are regulated by CCT relocalization during LD formation might even have clinical relevance. A hallmark in the formation of atherosclerotic lesions is the formation of foam cells, when macrophages accumulate large amounts of LDs and change their morphology into a foamy like cell. It was shown before that under those conditions CCT is activated and it was suggested that upregulation of PC synthesis helps to protect macrophages from apoptosis caused by elevated levels of unesterified cholesterol during this process (Zhang et al., 2000). Previous studies imply that dephosphorylation of CCT might partly be responsible for this increase in activity (Wang and Kent, 1995). However, CCT activation could also occur in coordination with targeted activation of the enzyme.

In summary, LD expansion is a fascinating and likely evolutionarily conserved paradigm for studying mechanisms of organelle homeostasis. By studying the phospholipid requirements for LD expansion, a novel regulatory mechanism was discovered. The described mechanism elucidates how the conditional subcellular relocalization of a rate-limiting enzyme controls enzymatic activity and thus the production of organellar components. Thereby, the activity of a biochemical pathway can be coupled directly to the organelle's expansion.

6 EXPERIMENTAL PROCEDURES

6.1 Cell culture

Drosophila S2 cells

Drosophila S2 cells were cultured in Schneider's *Drosophila* medium (Invitrogen) supplemented with 10% fetal bovine serum and antibiotics (100 unit/ml penicillin and 100 µg/ml streptomycin) at 27°C as described (Guo et al., 2008).

RNAi treatment of S2 cells was performed as previously described (Guo et al., 2008). In short PCR products with a length of 300-600 base pairs, containing the T7 promotor were generated from genomic DNA isolated from S2 cells (Quiagen, genomic DNA isolation kit). Ds RNAs were synthesized from purified PCR products (Quiagen, PCR purification kit) by *in vitro* transcription using T7 polymerase (Fermentas) in a reaction containing 40 mM Tris/HCl (pH 8.0), 6 mM MgCl₂, 15 mM DTT, 2 mM spermidine, 0.5 mM of each NTP. DNA was removed by incubation with DNase (Fermentas) for 15 min at 37°C and dsRNAs were annealed by heating for 5 min to 90°C and slowly cooling down over 2-3 h. Cells were incubated with dsRNA in serum free media. After 50 min incubation time the same volume of medium containing 20% fetal bovine serum was added. After three days cells were incubated for 12h with 1 mM oleate prepared as described (Guo et al., 2008). A segment of pBluescript backbone was used as template for control RNAi (referred as control RNAi thereafter). A list of primers to generate dsRNAs for RNAi experiments is given in Table S7. Knockdown efficiency was tested by Real-time quantitative PCR. Total RNA from a dsRNA treated 6-well was prepared with the RNeasy Lysis Kit (Qiagen); 3 µg was used for first-stand cDNA synthesis with a kit (Fermentas). Real-time quantitative PCR was performed with the MyiQ™ Single-Color Real-Time PCR Detection System (BioRad) and Mesa green (Eurogentec). Primers used are listed in Table S8. For protein localization in S2 cells vesicle interacting protein VAP-33-1-mCherry (CG5014), reticulon-mCherry (CG33113), torsin-mCherry (CG3204), mCherry-seipin

(CG9904), selenoprotein SELT-mCherry (CG3887), membrane bound O-acyl transferase MBOAT-mCherry (CG5926), lunapark-mCherry (CG8735), mCherry-steroid binding protein (CG9066), mCherry-SEC14 homolog (CG13848), Lyso-PA acyltransferase (CG32699), mCherry-short chain dehydrogenase (2064), uncharacterized lipase1-mCherry (CG17292), mCherry-phospholipase D (CG7718), oxysterol binding protein-mCherry (CG1513), tango 14-mCherry (CG4775), mCherry-FAS associated factor 2 (CG10372), fatty acid transferase-mCherry (CG7400), CGI-58-mCherry (CG1882), mCherry-HSL (CG11055), mCherry-uncharacterized lipase 2 (CG9186); mCherry-CK (CG2201), mCherry-CCT1(CG1049), mCherry-CCT1 Δ P (amino acids 1–433), mCherry-CCT1 Δ MP (amino acids 1–365), mCherry-CCT1 M (amino acids 365–429), mCherry-CCT2 (CG18330) and mCherry-CPT (CG7149) expression vectors (actin promoter) were cloned using the Gateway system (Invitrogen). mCherry-CCT1W397E was generated by QuickChange II mutagenesis (Stratagene).

Transfection of S2 cells was performed using Effectene (Qiagen) reagent according to manufacturer's instructions.

For choline deficiency and SILAC labeling, S2 cells were grown in custom Schneider medium (Bonaldi et al., 2008), with or without 1 mM choline, or 0.4 g/l $^{13}\text{C}_6^{15}\text{N}_4$ L-arginine and 1.65 g/l $^{13}\text{C}_6^{15}\text{N}_2$ L-lysine (Sigma Isotec), respectively.

Raw 264.7 cells

Raw 264.7 cells (American Type Culture Collection) were cultured in RPMI (Biochrom) with 10% fetal bovine serum and 100 unit/ml penicillin/ streptomycin in uncoated dishes at 37°C. For protein localization Raw 264.7 cells were transfected with Lipofectamine 2000 (Invitrogen) according to manufacturer's instructions. CCT α -GFP was provided by Dr. Neale Ridgway (Gehrig et al., 2008).

N2a cells

N2a cells (American Type Culture Collection) were cultured in DMEM (Invitrogen) supplemented with 10% fetal bovine serum and 100 unit/ml penicillin/streptomycin. When cells were 50% confluent differentiation was induced by changing the medium to 1% fetal bovine serum and 1 mM dibutyryl cAMP for 48h as described (Tremblay et al., 2010).

Bone marrow derived macrophages (BMDMs)

CCT α -deficient BMDMs from *Cct α ^{F/F}* mice (Jackson Laboratory) and R26R-EYFP mice (Srinivas et al., 2001) were generated as described (Granucci et al., 2001). In brief, tibia and femur were isolated from the indicated mice and sterilized in 70% ethanol. Bones were cut on both sides with sterile scissors and bone marrow was flushed with a syringe in RPMI supplemented with 10% fetal bovine serum and 100 unit/ml penicillin/ streptomycin. Cells were washed two times in medium and filtered to remove pieces of bone. 3×10^6 cells were plated per 10 cm dish in medium containing 10% macrophage colony stimulating factor (MCSF) in uncoated dishes for 3-5 days.

For Tat-Cre (HTNC) treatment, 5×10^6 cells were plated in 10-cm untreated cell culture plates, washed three times with phosphate-buffered saline (PBS), and incubated for 1 h at 37°C in 5 ml of serum-free medium (Hyclone) containing 1 μ M recombinant HTNC [expressed and purified as described (Peitz et al., 2007)], 200 μ M chloroquin (Sigma), 50 μ g/ml polymyxin (Calbiochem), 2 μ M leupeptin (Sigma). Five days later, cells were incubated with 1 mM oleate for 24 h and imaged. To quantify BMDM purity and HTNC recombination efficiency, cells were stained with PE-labeled anti-CD11b antibody (eBioscience) and analyzed for EYFP expression by flow cytometry (FACSCalibur, BD). CCT α knockdown efficiency was tested by real-time quantitative PCR and by Western blot. Primers used for real-time quantitative PCR are listed in table S8.

6.2 *Transgenic flies*

Fly stocks were raised on standard cornmeal-agar medium at room temperature. The UAS-mCherry line was from Dr. Thomas B. Kornberg (UCSF). Male UAS-RNAi CCT1 transgenic flies (transformant ID 18628) from the Vienna *Drosophila* RNAi center were crossed with CgGal4 (Asha et al., 2003) UAS-mCherry reporter strain virgins. Third instar larvae of the progeny were dissected in PBS, stained with BODIPY 493/503, and imaged with a confocal microscope (LSM 510, Carl Zeiss MicroImaging).

6.3 *Microscopy*

Cells were then mounted on glass bottom dishes coated with concanavalin A, stained with 1 µg/ml BODIPY493/503 (Invitrogen) or 1 µg/ml Nile Red (Invitrogen) for 10 min and washed two times with cell culture medium. Cells were imaged with a spinning-disk confocal microscope (TiLL iMIC CSU22, Andor) using a back-illuminated EM charge-coupled device camera (iXonEM 897; Andor) and a 100× 1.4 NA oil immersion objective (Olympus); 16-bit images were collected with Image iQ (version 1.9; Andor), deconvoluted (Huygens, SVI), and cropped (ImageJ <http://rsbweb.nih.gov/ij/>).

6.4 *Lipid biochemical methods*

TLC and lipid measurements

Lipids were extracted as described (Folch et al., 1957). 0.8 volume parts of aqueous sample were mixed with 2 parts of a chloroform/methanol 1:2 (v/v) and incubated for 1h at room temperature. 3 volumes chloroform and 0.7 volume parts of 0.2 M KCl were added for phase separation. After mixing the sample was centrifuged at high speed for 15 min and the lower chloroform phase containing the lipids was isolated.

Lipids were separated on silica TLC plates (Merck) with chloroform/methanol/ammonia solution (25%) (50:25:6; per vol.) for phospholipids or petroleum ether/diethyl ether/acetic acid (70:30:2; per vol.) for neutral lipids and detected by cerium molybdate staining. Bands were identified by comparison with standards. PC and TG levels were quantified from extracted lipids as described (Nanjee and Miller, 1996).

Emulsion and liposome preparation

To prepare lipid emulsions and liposomes, lipids were mixed in chloroform/methanol (2:1), dried under a stream of N₂, resuspended in buffer (150 mM NaCl, 50 mM Tris/HCl, pH 7.5, 1 mM EDTA, 1 mM DTT, 50 mM PMSF), and sonicated. For emulsions, the molar ratio of TG to total phospholipids was 2:5. Contaminating vesicles were removed and LDs were concentrated by ultracentrifugation at 100,000 *g* for 15 min. For light scattering, lipid concentration was 25 mM phospholipids and 10 mM TG before centrifugation.

6.5 Protein biochemical methods

LD purification

Drosophila S2 cells were harvested, washed with ice-cold PBS, resuspended in 2 ml of buffer (200 mM Tris/HCL, pH 7.5, 2 mM MgAc, and Complete Protease Inhibitor (Roche)), lysed with a tissue homogenizer and fractionated by three centrifugation steps at 3,000, 20,000, and 100,000 *g*. The supernatant was adjusted to 1 M sucrose, layered under a sucrose step-gradient with 2 ml steps (0.75, 0.5, 0.25, 0.125, 0 M) and centrifuged for 12 h at 200,000 *g*. Six fractions of the gradient and the three pellet fractions of the differential centrifugation steps were analyzed by MS-based proteomics and Western blot with the following antibodies CCT α (McCoy et al., 2006), GAPDH (LSBio), KDEL-receptor (Abcam), Calnexin (Abcam).

Cellular fractionation

Cells were harvested, washed with ice-cold PBS, resuspended in 2 ml of buffer (150 mM NaCl, 50 mM Tris/HCl, pH 7.5, 1 mM EDTA, 1 mM DTT, 50 mM PMSF). Cells were lysed by sonication. Unbroken cells were removed by centrifugation at 800 *g* for 3 min. The supernatant was fractionated into floating LDs and soluble and membrane fractions by centrifugation 100,000 *g* for 1 h. The LD fraction was washed in buffer to remove cytosolic contamination. The resulting fractions were used for CCT activity assay or analyzed by Western blot with the following antibodies CCT α (McCoy et al., 2006), ADRP (Novus Biologicals), GAPDH (Calbiochem), Calnexin (Abcam).

Protein binding to artificial droplets

CCT2-His₆ was expressed using pFASTBACHTb-CCT2 (provided from J. Friesen) as a donor plasmid for baculovirus expression as described (Helmink and Friesen, 2004).

For affinity purification the cell pellet was resuspended in lysis buffer [20 mM Tris and 100 mM NaCl (pH 7.5)] and lysed by sonication. After centrifugation at 27,000*g* for 30 min at 4 °C, the pellet was discarded and the supernatant, containing soluble cellular components, was incubated with Ni Sepharose™ 6 Fast Flow (GE Healthcare) for 3 h. Proteins that did not bind to the column were collected as flow-through. The column was washed successively with 5 column volumes of lysis buffer, lysis buffer containing 500 mM NaCl, 1 mM imidazole, 1% NP-40 and 1% glycerol and lysis buffer containing 10 mM imidazole. Elution of CCT2 from the metal affinity column was accomplished using lysis buffer containing 200 mM imidazole. Protein was quantified by the method of Bradford using a Bio-Rad protein assay kit and bovine serum albumin as standard.

Purified CCT2-His₆ (100 μ M) was incubated with artificial droplets (2.5 mM phospholipids and 1 mM TG) in a 1 ml reaction for 1 h on ice in buffer (150 mM NaCl, 50 mM Tris/HCl, pH 7.5, 1 mM EDTA). The reaction mix was adjusted to 0.75 M sucrose, overlaid with 10 ml of buffer and artificial droplets were floated for 1 h at 100,000 g. The top fraction was collected with a tube slicer and an adjacent control fraction was taken below the floating lipid fraction. An input fraction, the control fraction and the droplet fraction were analyzed by Western blot.

CCT activity assay

CCT activity in total cell lysate or cellular fractions was determined in the absence or presence of artificial droplets by monitoring the conversion of phospho-[³H]choline to CDP-[³H]choline as described (Pelech et al., 1981). Briefly, the substrate phospho-[³H]choline was prepared by incubation of [³H]-choline chloride with CK for 1h at 37°C in a reaction containing 10mM ATP, 100 mM Tris/HCl pH 8.0, 10 mM MgCl₂. The reaction product was purified by TLC with methanol /0.6% NaCl/ NH₄OH (10:10:0.9). The band for phospho-[³H]choline was detected by scintillation counting. Phospho-[³H] choline was scraped from the plate and eluted in 15 mM unlabeled phosphocholine to a specific activity of 10 μ Ci/ μ mol. To measure CCT activity, 25-50 μ g protein was incubated in 60 mM Tris/HCl pH7.5, 40 mM NaCl, 1.8 mM EDTA, 9 mM MgAc, 3 mM CPT, 1.5 mM phospho-[³H]choline for 15 min at 37°C. The reaction was stopped by heating for 2 min at 80°C. Substrate and products of the reaction were separated on a TLC with methanol /0.6% NaCl/ NH₄OH (10:10:0.9). The band for the reaction product CDP-choline was identified by co-migration of a cold CDP-choline standard that was visualized under UV-light after fluorescein staining. Specific CCT activity was finally determined by measuring radioactivity from the scraped CDP-choline band and compared to radioactive substrate with defined molarity to determine the amount (nmol) of converted

substrate per reaction. Specific activity was calculated by dividing the amount of converted substrate by reaction time and amount of protein input. Specific CCT activity was normalized to the amount of CCT as determined by Western blot.

6.6 Mass spectrometry–based proteomics

Protein digestion

100 µg of each heavy SILAC sucrose gradient fraction was mixed with equal amount of the light SILAC LD standard. Combined samples were acetone precipitated with four volumes of ice cold acetone. Precipitated proteins were collected by centrifugation, dissolved in 6 M urea, 2 M thiourea and 10 mM Tris and subjected to in-solution digestion. Protein sample were then reduced with 1 mM DTT for 45 min at RT, alkylated with 5.5 mM iodoacetamide for 30 minutes and digested with 1/50 endopeptidase Lys-C (Waco) per protein for 3 h. The resulting peptide mixtures were diluted with four volumes of 50 mM ammonium bicarbonate and digested with 1/50 sequencing grade modified trypsin (Promega) per protein over night at RT. Trypsin was inactivated by acidification with trifluoroacetic acid pH<3 and subsequently 5 µg peptides was concentrated and desalted on reversed phase C₁₈ STAGE tips (Rappsilber et al., 2003; Rappsilber et al., 2007).

LC-MS/MS analysis

Peptides were eluted from STAGE tips by 30 µL buffer B (80% acetonitril in 0.5% acetic acid) solution into a 96 sample well plate (Abgene), concentrated in a speed-vac until removal of the organic solvent and reconstituted with a one-to-one mix of buffer A (0.5% acetic acid) and buffer A* (2% acetonitril in 0.1 % trifluoroacetic acid). Eluted peptides were analyzed by a nanoflow HPLC system (Agilent Technologies or Proxeon Biosystems) coupled on-line via a nanoelectrospray ion source (Proxeon Biosystems) to a LTQ-Orbitrap mass spectrometer (Thermo

Scientific). Peptide samples were loaded onto a C₁₈-reversed phase column (15 cm long and 75 µm inner diameter, packed in-house with ReproSil-Pur C₁₈-AQ 3-µm resin) in buffer A (0.5 % acetic acid) with a flow rate of 500 nl/min and eluted with a linear gradient from 2% to 40% buffer B (80% acetonitril and 0.5% acetic acid solution) at a flow rate of 250 nl/min over 2 h.

Mass spectra were acquired in the positive ion mode applying a data-dependent automatic switch between the acquisition of one Orbitrap survey scan (mass range of m/z 300-1700) and tandem mass spectra (MS/MS) of the ten most intense ions in the LTQ ('top 10' method).

The target value in the LTQ-Orbitrap was 1,000,000 for the survey scan at a resolution of 60,000 at m/z 400 using lock masses. Fragmentation in the LTQ was performed by collision-induced dissociation with a target value of 5,000 ions. Ion selection threshold was 1000 counts. Selected sequenced ions were dynamically excluded for 90 seconds.

Data analysis

Raw mass spectrometric data were analyzed with MaxQuant (version 1.0.14.6) (Cox and Mann, 2008). Precursor and fragment ions were searched with a maximal initial mass deviation of up to 7 ppm and 0.5 Da, respectively. In the mascot search trypsin allowing for cleavage N-terminal to proline was used as enzyme specificity. Cysteine carbamidomethylation was selected as a fixed modification, while protein N-terminal acetylation and methionine oxidation were chosen as variable modifications. Depending on a priori knowledge about the number of Arg and Lys in the precursor ion determined by MaxQuant before the search, Arg10 and Lys8 were used as additional fixed or variable modifications. Maximally two missed cleavages and three labeled amino acids were allowed.

MaxQuant automatically quantified and normalized peptides and proteins based on the light SILAC LD standard. A false discovery rate (FDR) of 0.01 was required for proteins and peptides with a minimum length of 6 amino acids.

For cluster analysis Perseus software (version 1.1.1.34) was used. Data was filtered for contaminants, reverse identifications and one unique peptide. Proteins were removed that were not identified in fraction 1 or that were identified in less than three fractions. For cluster analysis the peptide ratio heavy/light was divided by the maximal value among all nine fractions. For fraction 1 the normalized ratio was used. The ratios were analyzed by hierarchical clustering with Euclidian row distance and average row linkage. To ensure reproducibility only proteins were considered as LD proteins that had a normalized heavy/light ratio between 0.25-4 in fraction1.

7 REFERENCES

- Alvarez, H.M., Mayer, F., Fabritius, D., and Steinbuchel, A. (1996). Formation of intracytoplasmic lipid inclusions by *Rhodococcus opacus* strain PD630. *Arch Microbiol* 165, 377-386.
- Andersen, J.S., and Mann, M. (2006). Organellar proteomics: turning inventories into insights. *Embo Rep* 7, 874-879.
- Andersen, J.S., Wilkinson, C.J., Mayor, T., Mortensen, P., Nigg, E.A., and Mann, M. (2003). Proteomic characterization of the human centrosome by protein correlation profiling. *Nature* 426, 570-574.
- Arnold, R.S., DePaoli-Roach, A.A., and Cornell, R.B. (1997). Binding of CTP:phosphocholine cytidyltransferase to lipid vesicles: diacylglycerol and enzyme dephosphorylation increase the affinity for negatively charged membranes. *Biochemistry-U S* 36, 6149-6156.
- Asha, H., Nagy, I., Kovacs, G., Stetson, D., Ando, I., and Dearolf, C.R. (2003). Analysis of Ras-induced overproliferation in *Drosophila* hemocytes. *Genetics* 163, 203-215.
- Attard, G.S., Templer, R.H., Smith, W.S., Hunt, A.N., and Jackowski, S. (2000). Modulation of CTP:phosphocholine cytidyltransferase by membrane curvature elastic stress. *Proc Natl Acad Sci U S A* 97, 9032-9036.
- Bartz, R., Li, W.H., Venables, B., Zehmer, J.K., Roth, M.R., Welti, R., Anderson, R.G., Liu, P., and Chapman, K.D. (2007). Lipidomics reveals that adiposomes store ether lipids and mediate phospholipid traffic. *J Lipid Res* 48, 837-847.
- Bartz, R., Zehmer, J.K., Zhu, M.F., Chen, Y., Serrero, G., Zhao, Y.M., and Liu, P.S. (2007). Dynamic activity of lipid droplets: Protein phosphorylation and GTP-Mediated protein translocation. *J Proteome Res* 6, 3256-3265.
- Beller, M., Riedel, D., Jansch, L., Dieterich, G., Wehland, J., Jackle, H., and Kuhnlein, R.P. (2006). Characterization of the *Drosophila* lipid droplet subproteome. *Mol Cell Proteomics* 5, 1082-1094.
- Beller, M., Sztalryd, C., Southall, N., Bell, M., Jackle, H., Auld, D.S., and Oliver, B. (2008). COPI Complex Is a Regulator of Lipid Homeostasis. *Plos Biol* 6, 2530-2549.
- Beller, M., Thiel, K., Thul, P.J., and Jackle, H. (2010). Lipid droplets: A dynamic organelle moves into focus. *Febs Lett* 584, 2176-2182.
- Best, C.H., Hershey, J.M., and Huntsman, M.E. (1932). The effect of lecithine on fat deposition in the liver of the normal rat. *J Physiol-London* 75, 56-66.
- Bonaldi, T., Straub, T., Cox, J., Kumar, C., Becker, P.B., and Mann, M. (2008). Combined use of RNAi and quantitative proteomics to study gene function in *Drosophila*. *Molecular Cell* 31, 762-772.

- Bostrom, P., Andersson, L., Rutberg, M., Perman, J., Lidberg, U., Johansson, B.R., Fernandez-Rodriguez, J., Ericson, J., Nilsson, T., Boren, J., *et al.* (2007). SNARE proteins mediate fusion between cytosolic lipid droplets and are implicated in insulin sensitivity. *Nat Cell Biol* 9, 1286-U1139.
- Boutet, E., El Mourabit, H., Prot, M., Nemani, M., Khallouf, E., Colard, O., Maurice, M., Durand-Schneider, A.M., Chretien, Y., Gres, S., *et al.* (2009). Seipin deficiency alters fatty acid Delta 9 desaturation and lipid droplet formation in Berardinelli-Seip congenital lipodystrophy. *Biochimie* 91, 796-803.
- Bradley, C.K., Takano, E.A., Gothert, J.R., Gottgens, B., Green, A.R., Begley, C.G., and van Eekelen, J.A.M. (2007). Temporal regulation of Cre-recombinase activity in Scl-positive neurons of the central nervous system. *Genesis* 45, 145-151.
- Brasaemle, D.L. (2007). Thematic review series: adipocyte biology. The perilipin family of structural lipid droplet proteins: stabilization of lipid droplets and control of lipolysis. *J Lipid Res* 48, 2547-2559.
- Brasaemle, D.L., Dolios, G., Shapiro, L., and Wang, R. (2004). Proteomic analysis of proteins associated with lipid droplets of basal and lipolytically stimulated 3T3-L1 adipocytes. *Journal of Biological Chemistry* 279, 46835-46842.
- Brasaemle, D.L., and Wolins, N.E. (2006). Isolation of lipid droplets from cells by density gradient centrifugation. *Curr Protoc Cell Biol Chapter 3*, Unit 3 15.
- Brown, M.S., Goldstein, J.L., Krieger, M., Ho, Y.K., and Anderson, R.G.W. (1979). Reversible Accumulation of Cholesteryl Esters in Macrophages Incubated with Acetylated Lipoproteins. *J Cell Biol* 82, 597-613.
- Buhman, K.K., Accad, M., Novak, S., Choi, R.S., Wong, J.S., Hamilton, R.L., Turley, S., and Farese, R.V. (2000). Resistance to diet-induced hypercholesterolemia and gallstone formation in ACAT2-deficient mice. *Nat Med* 6, 1341-1347.
- Bulankina, A.V., Deggerich, A., Wenzel, D., Mutenda, K., Wittmann, J.G., Rudolph, M.G., Burger, K.N.J., and Honing, S. (2009). TIP47 functions in the biogenesis of lipid droplets. *J Cell Biol* 185, 641-655.
- Celniker, S.E., Dillon, L.A., Gerstein, M.B., Gunsalus, K.C., Henikoff, S., Karpen, G.H., Kellis, M., Lai, E.C., Lieb, J.D., MacAlpine, D.M., *et al.* (2009). Unlocking the secrets of the genome. *Nature* 459, 927-930.
- Cermelli, S., Guo, Y., Gross, S.P., and Welte, M.A. (2006). The lipid-droplet proteome reveals that droplets are a protein-storage depot. *Curr Biol* 16, 1783-1795.
- Choy, P.C., and Vance, D.E. (1976). Purification of Cholinephosphate Cytidylyltransferase from Rat-Liver by Affinity Chromatography. *Biochem Bioph Res Co* 72, 714-719.
- Cole, N.B., and Murphy, D.D. (2002). The cell biology of alpha-synuclein: a sticky problem? *Neuromolecular Med* 1, 95-109.

Coleman, R., and Bell, R.M. (1978). Evidence that biosynthesis of phosphatidylethanolamine, phosphatidylcholine, and triacylglycerol occurs on the cytoplasmic side of microsomal vesicles. *J Cell Biol* 76, 245-253.

Cornell, R., and Vance, D.E. (1987). Binding of CTP: phosphocholine cytidyltransferase to large unilamellar vesicles. *Biochim Biophys Acta* 919, 37-48.

Cornell, R.B., and Northwood, I.C. (2000). Regulation of CTP:phosphocholine cytidyltransferase by amphitropism and relocalization. *Trends Biochem Sci* 25, 441-447.

Cox, J., and Mann, M. (2008). MaxQuant enables high peptide identification rates, individualized p.p.b.-range mass accuracies and proteome-wide protein quantification. *Nat Biotechnol* 26, 1367-1372.

DeLong, C.J., Qin, L.Y., and Cui, Z. (2000). Nuclear localization of enzymatically active green fluorescent protein-CTP : phosphocholine cytidyltransferase alpha fusion protein is independent of cell cycle conditions and cell types. *Journal of Biological Chemistry* 275, 32325-32330.

Ducharme, N.A., and Bickel, P.E. (2008). Lipid droplets in lipogenesis and lipolysis. *Endocrinology* 149, 942-949.

Farese, R.V., and Walther, T.C. (2009). Lipid Droplets Finally Get a Little R-E-S-P-E-C-T. *Cell* 139, 855-860.

Feldman, D.A., Rounsifer, M.E., and Weinhold, P.A. (1985). The stimulation and binding of CTP: phosphorylcholine cytidyltransferase by phosphatidylcholine-oleic acid vesicles. *Biochimica Et Biophysica Acta* 833, 429-437.

Folch, J., Lees, M., and Stanley, G.H.S. (1957). A Simple Method for the Isolation and Purification of Total Lipides from Animal Tissues. *Journal of Biological Chemistry* 226, 497-509.

Foster, L.J., de Hoog, C.L., Zhang, Y.L., Zhang, Y., Xie, X.H., Mootha, V.K., and Mann, M. (2006). A mammalian organelle map by protein correlation profiling. *Cell* 125, 187-199.

Fredrikson, G., Tornqvist, H., and Befrage, P. (1986). Hormone-Sensitive Lipase and Monoacylglycerol Lipase Are Both Required for Complete Degradation of Adipocyte Triacylglycerol. *Biochimica Et Biophysica Acta* 876, 288-293.

Friesen, J.A., Campbell, H.A., and Kent, C. (1999). Enzymatic and cellular characterization of a catalytic fragment of CTP:phosphocholine cytidyltransferase alpha. *Journal of Biological Chemistry* 274, 13384-13389.

Fruhbeck, G., Gomez-Ambrosi, J., Muruzabal, F.J., and Burrell, M.A. (2001). The adipocyte: a model for integration of endocrine and metabolic signaling in energy metabolism regulation. *Am J Physiol Endocrinol Metab* 280, E827-847.

Fujimoto, T., Ohsaki, Y., Cheng, J., Suzuki, M., and Shinohara, Y. (2008). Lipid droplets: a classic organelle with new outfits. *Histochem Cell Biol* 130, 263-279.

Fujimoto, Y., Itabe, H., Kinoshita, T., Homma, K.J., Onoduka, J., Mori, M., Yamaguchi, S., Makita, M., Higashi, Y., Yamashita, A., *et al.* (2007). Involvement of ACSL in local synthesis of neutral lipids in cytoplasmic lipid droplets in human hepatocyte HuH7. *Journal of Lipid Research* 48, 1280-1292.

Gehrig, K., Cornell, R.B., and Ridgway, N.D. (2008). Expansion of the nucleoplasmic reticulum requires the coordinated activity of lamins and CTP:phosphocholine cytidyltransferase alpha. *Molecular Biology of the Cell* 19, 237-247.

Gehrig, K., Morton, C.C., and Ridgway, N.D. (2009). Nuclear export of the rate-limiting enzyme in phosphatidylcholine synthesis is mediated by its membrane binding domain. *Journal of Lipid Research* 50, 966-976.

Geilen, C.C., Wieder, T., and Reutter, W. (1992). Hexadecylphosphocholine inhibits translocation of CTP:choline-phosphate cytidyltransferase in Madin-Darby canine kidney cells. *J Biol Chem* 267, 6719-6724.

Ghosh, S., Zhao, B., Bie, J.H., and Song, J.M. (2010). Macrophage cholesteryl ester mobilization and atherosclerosis. *Vasc Pharmacol* 52, 1-10.

Gong, J.Y., Sun, Z.Q., and Li, P. (2009). CIDE proteins and metabolic disorders. *Current Opinion in Lipidology* 20, 121-126.

Granucci, F., Vizzardelli, C., Pavelka, N., Feau, S., Persico, M., Virzi, E., Rescigno, M., Moro, G., and Ricciardi-Castagnoli, P. (2001). Inducible IL-2 production by dendritic cells revealed by global gene expression analysis. *Nat Immunol* 2, 882-888.

Guo, Y., Cordes, K.R., Farese, R.V., and Walther, T.C. (2009). Lipid droplets at a glance. *J Cell Sci* 122, 749-752.

Guo, Y., Walther, T.C., Rao, M., Stuurman, N., Goshima, G., Terayama, K., Wong, J.S., Vale, R.D., Walter, P., and Farese, R.V. (2008). Functional genomic screen reveals genes involved in lipid-droplet formation and utilization. *Nature* 453, 657-661.

Helmink, B.A., and Friesen, J.A. (2004). Characterization of a lipid activated CTP: phosphocholine cytidyltransferase from *Drosophila melanogaster*. *Bba-Mol Cell Biol L* 1683, 78-88.

Hickenbottom, S.J., Kimmel, A.R., Londos, C., and Hurley, J.H. (2004). Structure of a lipid droplet protein: The PAT family member TIP47. *Structure* 12, 1199-1207.

Hicks, A.M., DeLong, C.J., Thomas, M.J., Samuel, M., and Cui, Z. (2006). Unique molecular signatures of glycerophospholipid species in different rat tissues analyzed by tandem mass spectrometry. *Bba-Mol Cell Biol L* 1761, 1022-1029.

Holthuis, J.C.M., and Levine, T.P. (2005). Lipid traffic: Floppy drives and a superhighway. *Nat Rev Mol Cell Bio* 6, 209-220.

Houweling, M., Jamil, H., Hatch, G.M., and Vance, D.E. (1994). Dephosphorylation of CTP-phosphocholine cytidyltransferase is not required for binding to membranes. *J Biol Chem* 269, 7544-7551.

Jacobs, R.L., Devlin, C., Tabas, I., and Vance, D.E. (2004). Targeted deletion of hepatic CTP : phosphocholine cytidyltransferase alpha in mice decreases plasma high density and very low density lipoproteins. *Journal of Biological Chemistry* 279, 47402-47410.

Jamil, H., Yao, Z.M., and Vance, D.E. (1990). Feedback-Regulation of Ctp-Phosphocholine Cytidyltransferase Translocation between Cytosol and Endoplasmic-Reticulum by Phosphatidylcholine. *Journal of Biological Chemistry* 265, 4332-4339.

Johnson, J.E., Xie, M.T., Singh, L.M.R., Edge, R., and Cornell, R.B. (2003). Both acidic and basic amino acids in an amphitropic enzyme, CTP : phosphocholine cytidyltransferase, dictate its selectivity for anionic membranes. *Journal of Biological Chemistry* 278, 514-522.

Jones, H.E., Harwood, J.L., Bowen, I.D., and Griffiths, G. (1992). Lipid composition of subcellular membranes from larvae and prepupae of *Drosophila melanogaster*. *Lipids* 27, 984-987.

Kabalnov, A., Tarara, T., Arlauskas, R., and Weers, J. (1996). Phospholipids as Emulsion Stabilizers. *J Colloid Interface Sci* 184, 227-235.

Kabalnov, A., and Wennerstrom, H. (1996). Macroemulsion stability: The oriented wedge theory revisited. *Langmuir* 12, 276-292.

Kennedy, E.P. (1959). The enzymic synthesis of phospholipids. *Prog Neurobiol* 4, 260-264.

Kent, C. (1997). CTP:phosphocholine cytidyltransferase. *Biochimica Et Biophysica Acta* 1348, 79-90.

Kent, C. (2005). Regulatory enzymes of phosphatidylcholine biosynthesis: a personal perspective. *Bba-Mol Cell Biol L* 1733, 53-66.

Kuerschner, L., Moessinger, C., and Thiele, C. (2008). Imaging of lipid biosynthesis: how a neutral lipid enters lipid droplets. *Traffic* 9, 338-352.

Lagace, T.A., and Ridgway, N.D. (2005). The rate-limiting enzyme in phosphatidylcholine synthesis regulates proliferation of the nucleoplasmic reticulum. *Molecular Biology of the Cell* 16, 1120-1130.

Lass, A., Zimmermann, R., Haemmerle, G., Riederer, M., Schoiswohl, G., Schweiger, M., Kienesberger, P., Strauss, J.G., Gorkiewicz, G., and Zechner, R. (2006). Adipose triglyceridolipase-mediated lipolysis of cellular fat stores is activated by CGI-58 and defective in Chanarin-Dorfman Syndrome. *Cell Metab* 3, 309-319.

Leber, R., Landl, K., Zinser, E., Ahorn, H., Spok, A., Kohlwein, S.D., Turnowsky, F., and Daum, G. (1998). Dual localization of squalene epoxidase, Erg1p, in yeast reflects a relationship between the endoplasmic reticulum and lipid particles. *Mol Biol Cell* 9, 375-386.

- Listenberger, L.L., Han, X., Lewis, S.E., Cases, S., Farese, R.V., Jr., Ory, D.S., and Schaffer, J.E. (2003). Triglyceride accumulation protects against fatty acid-induced lipotoxicity. *Proc Natl Acad Sci U S A* 100, 3077-3082.
- MacKinnon, M.A., Curwin, A.J., Gaspard, G.J., Suraci, A.B., Fernandez-Murray, J.P., and McMaster, C.R. (2009). The Kap60-Kap95 Karyopherin Complex Directly Regulates Phosphatidylcholine Synthesis. *Journal of Biological Chemistry* 284, 7376-7384.
- Mallampalli, R.K., Salome, R.G., and Hunninghake, G.W. (1993). Lung Ctp Choline-Phosphate Cytidylyltransferase - Activation of Cytosolic Species by Unsaturated Fatty-Acid. *Am J Physiol* 265, L158-L163.
- Martin, S., Driessen, K., Nixon, S.J., Zerial, M., and Parton, R.G. (2005). Regulated localization of rab18 to lipid droplets - Effects of lipolytic stimulation and inhibition of lipid droplet catabolism. *Journal of Biological Chemistry* 280, 42325-42335.
- McCoy, D.M., Fisher, K., Robichaud, J., Ryan, A.J., and Mallampalli, R.K. (2006). Transcriptional regulation of lung cytidylyltransferase in developing transgenic mice. *Am J Resp Cell Mol* 35, 394-402.
- Miyanari, Y., Atsuzawa, K., Usuda, N., Watashi, K., Hishiki, T., Zayas, M., Bartenschlager, R., Wakita, T., Hijikata, M., and Shimotohno, K. (2007). The lipid droplet is an important organelle for hepatitis C virus production. *Nat Cell Biol* 9, 1089-U1074.
- Murphy, S., Martin, S., and Parton, R.G. (2009). Lipid droplet-organelle interactions; sharing the fats. *Bba-Mol Cell Biol L* 1791, 441-447.
- Nanjee, M.N., and Miller, N.E. (1996). Sequential microenzymatic assay of cholesterol, triglycerides, and phospholipids in a single aliquot. *Clin Chem* 42, 915-926.
- Nishino, N., Tamori, Y., Tateya, S., Kawaguchi, T., Shibakusa, T., Mizunoya, W., Inoue, K., Kitazawa, R., Kitazawa, S., Matsuki, Y., *et al.* (2008). FSP27 contributes to efficient energy storage in murine white adipocytes by promoting the formation of unilocular lipid droplets. *Journal of Clinical Investigation* 118, 2808-2821.
- Northwood, I.C., Tong, A.H.Y., Crawford, B., Drobnies, A.E., and Cornell, B.B. (1999). Shuttling of CTP : phosphocholine cytidylyltransferase between the nucleus and endoplasmic reticulum accompanies the wave of phosphatidylcholine synthesis during the G(0) -> G(1) transition. *Journal of Biological Chemistry* 274, 26240-26248.
- Ohsaki, Y., Maeda, T., Maeda, M., Tauchi-Sato, K., and Fujimoto, T. (2006). Recruitment of TIP47 to lipid droplets is controlled by the putative hydrophobic cleft. *Biochem Bioph Res Co* 347, 279-287.
- Olsen, J.V., Blagoev, B., Gnäd, F., Macek, B., Kumar, C., Mortensen, P., and Mann, M. (2006). Global, in vivo, and site-specific phosphorylation dynamics in signaling networks. *Cell* 127, 635-648.
- Park, S.H., and Blackstone, C. (2010). Further assembly required: construction and dynamics of the endoplasmic reticulum network. *Embo Rep* 11, 515-521.

Peitz, M., Jager, R., Patsch, C., Jager, A., Egert, A., Schorle, H., and Edenhofer, F. (2007). Enhanced purification of cell-permeant Cre and germline transmission after transduction into mouse embryonic stem cells. *Genesis* 45, 508-517.

Pelech, S.L., Pritchard, P.H., and Vance, D.E. (1981). cAMP analogues inhibit phosphatidylcholine biosynthesis in cultured rat hepatocytes. *J Biol Chem* 256, 8283-8286.

Ploegh, H.L. (2007). A lipid-based model for the creation of an escape hatch from the endoplasmic reticulum. *Nature* 448, 435-438.

Prieur, X., Roszer, T., and Ricote, M. (2010). Lipotoxicity in macrophages: evidence from diseases associated with the metabolic syndrome. *Bba-Mol Cell Biol L* 1801, 327-337.

Rafelski, S.M., and Marshall, W.F. (2008). Building the cell: design principles of cellular architecture. *Nat Rev Mol Cell Biol* 9, 593-602.

Rappsilber, J., Ishihama, Y., and Mann, M. (2003). Stop and go extraction tips for matrix-assisted laser desorption/ionization, nanoelectrospray, and LC/MS sample pretreatment in proteomics. *Anal Chem* 75, 663-670.

Rappsilber, J., Mann, M., and Ishihama, Y. (2007). Protocol for micro-purification, enrichment, pre-fractionation and storage of peptides for proteomics using StageTips. *Nat Protoc* 2, 1896-1906.

Robenek, H., Hofnagel, O., Buers, I., Robenek, M.J., Troyer, D., and Severs, N.J. (2006). Adipophilin-enriched domains in the ER membrane are sites of lipid droplet biogenesis. *J Cell Sci* 119, 4215-4224.

Robenek, H., Robenek, M.J., and Troyer, D. (2005). PAT family proteins pervade lipid droplet cores. *Journal of Lipid Research* 46, 1331-1338.

Robenek, M.J., Severs, N.J., Schlattmann, K., Plenz, G., Zimmer, K.P., Troyer, D., and Robenek, H. (2004). Lipids partition caveolin-1 from ER membranes into lipid droplets: updating the model of lipid droplet biogenesis. *Faseb J* 18, 866-+.

Saito, H., Kawagishi, A., Tanaka, M., Tanimoto, T., Okada, S., Komatsu, H., and Handa, T. (1999). Coalescence of Lipid Emulsions in Floating and Freeze-Thawing Processes: Examination of the Coalescence Transition State Theory. *J Colloid Interface Sci* 219, 129-134.

Savage, D.B., Petersen, K.F., and Shulman, G.I. (2007). Disordered lipid metabolism and the pathogenesis of insulin resistance. *Physiol Rev* 87, 507-520.

Shockey, J.M., Gidda, S.K., Chapital, D.C., Kuan, J.C., Dhanoa, P.K., Bland, J.M., Rothstein, S.J., Mullen, R.T., and Dyer, J.M. (2006). Tung tree DGAT1 and DGAT2 have nonredundant functions in triacylglycerol biosynthesis and are localized to different subdomains of the endoplasmic reticulum. *Plant Cell* 18, 2294-2313.

Siloto, R.M.P., Findlay, K., Lopez-Villalobos, A., Yeung, E.C., Nykiforuk, C.L., and Moloney, M.M. (2006). The accumulation of oleosins determines the size of seed oilbodies in *Arabidopsis*. *Plant Cell* 18, 1961-1974.

Singh, R., Kaushik, S., Wang, Y.J., Xiang, Y.Q., Novak, I., Komatsu, M., Tanaka, K., Cuervo, A.M., and Czaja, M.J. (2009). Autophagy regulates lipid metabolism. *Nature* 458, 1131-1164.

Sleight, R., and Kent, C. (1983). Regulation of Phosphatidylcholine Biosynthesis in Mammalian-Cells .3. Effects of Alterations in the Phospholipid Compositions of Chinese-Hamster Ovary and Lm Cells on the Activity and Distribution of Ctp-Phosphocholine Cytidylyltransferase. *Journal of Biological Chemistry* 258, 836-839.

Small, D.M., Wang, L.B., and Mitsche, M.A. (2009). The adsorption of biological peptides and proteins at the oil/water interface. A potentially important but largely unexplored field. *Journal of Lipid Research* 50, S329-S334.

Soni, K.G., Mardones, G.A., Sougrat, R., Smirnova, E., Jackson, C.L., and Bonifacino, J.S. (2009). Coatmer-dependent protein delivery to lipid droplets. *J Cell Sci* 122, 1834-1841.

Srinivas, S., Watanabe, T., Lin, C.S., William, C.M., Tanabe, Y., Jessell, T.M., and Costantini, F. (2001). Cre reporter strains produced by targeted insertion of EYFP and ECFP into the ROSA26 locus. *BMC Dev Biol* 1, 4.

Steinberger D., and Huttunen, J.K. (1972). Role of Cyclic Amp in Activation of Hormone-Sensitive Lipase of Adipose-Tissue. *Adv Cycl Nucl Res* 1, 47-&.

Stone, S.J., Levin, M.C., Zhou, P., Han, J.Y., Walther, T.C., and Farese, R.V. (2009). The Endoplasmic Reticulum Enzyme DGAT2 Is Found in Mitochondria-associated Membranes and Has a Mitochondrial Targeting Signal That Promotes Its Association with Mitochondria. *Journal of Biological Chemistry* 284, 5352-5361.

Sundler, R., and Akesson, B. (1975). Biosynthesis of Phosphatidylethanolamines and Phosphatidylcholines from Ethanolamine and Choline in Rat-Liver. *Biochem J* 146, 309-315.

Sztalryd, C., Xu, G.H., Dorward, H., Tansey, J.T., Contreras, J.A., Kimmel, A.R., and Londos, C. (2003). Perilipin A is essential for the translocation of hormone-sensitive lipase during lipolytic activation. *J Cell Biol* 161, 1093-1103.

Szymanski, K.M., Binns, D., Bartz, R., Grishin, N.V., Li, W.P., Agarwal, A.K., Garg, A., Anderson, R.G.W., and Goodman, J.M. (2007). The lipodystrophy protein seipin is found at endoplasmic reticulum lipid droplet junctions and is important for droplet morphology. *P Natl Acad Sci USA* 104, 20890-20895.

Taneva, S., Johnson, J.E., and Cornell, R.B. (2003). Lipid-induced conformational switch in the membrane binding domain of CTP:phosphocholine cytidylyltransferase: a circular dichroism study. *Biochemistry-Us* 42, 11768-11776.

Tansey, J.T., Sztalryd, C., Gruia-Gray, J., Roush, D.L., Zee, J.V., Gavrilova, O., Reitman, M.L., Deng, C.X., Li, C., Kimmel, A.R., *et al.* (2001). Perilipin ablation results in a lean mouse

with aberrant adipocyte lipolysis, enhanced leptin production, and resistance to diet-induced obesity. *P Natl Acad Sci USA* 98, 6494-6499.

Tauchi-Sato, K., Ozeki, S., Houjou, T., Taguchi, R., and Fujimoto, T. (2002). The surface of lipid droplets is a phospholipid monolayer with a unique Fatty Acid composition. *J Biol Chem* 277, 44507-44512.

Testet, E., Bessoule, J.J., Mongrand, S., Guillot-Salomon, T., Cantrel, C., and Cassagne, C. (1996). Occurrence of an acyl-CoA:1-acylglycerophosphorylcholine acyltransferase in plant mitochondria. *Febs Lett* 399, 87-91.

Thiele, C., and Spandl, J. (2008). Cell biology of lipid droplets. *Curr Opin Cell Biol* 20, 378-385.

Tilley, D.A., Evans, C.R., Larson, T.M., Edwards, K.A., and Friesen, J.A. (2008). Identification and Characterization of the Nuclear Isoform of *Drosophila melanogaster* CTP:Phosphocholine Cytidylyltransferase. *Biochemistry-Us* 47, 11838-11846.

Toomre, D., and Bewersdorf, J. (2010). A new wave of cellular imaging. *Annu Rev Cell Dev Biol* 26, 285-314.

Tremblay, R.G., Sikorska, M., Sandhu, J.K., Lanthier, P., Ribocco-Lutkiewicz, M., and Bani-Yaghoub, M. (2010). Differentiation of mouse Neuro 2A cells into dopamine neurons. *J Neurosci Meth* 186, 60-67.

Utal, A.K., Jamil, H., and Vance, D.E. (1991). Diacylglycerol signals the translocation of CTP:choline-phosphate cytidylyltransferase in HeLa cells treated with 12-O-tetradecanoylphorbol-13-acetate. *Journal of Biological Chemistry* 266, 24084-24091.

van Meer, G., Voelker, D.R., and Feigenson, G.W. (2008). Membrane lipids: where they are and how they behave. *Nat Rev Mol Cell Bio* 9, 112-124.

Vance, D.E., and Pelech, S.L. (1984). Enzyme Translocation in the Regulation of Phosphatidylcholine Biosynthesis. *Trends Biochem Sci* 9, 17-20.

Vance, D.E., and Vance, J.E. (2008). *Biochemistry of lipids, lipoproteins and membranes*, 5th edn (Amsterdam ; Boston, Elsevier).

Waltermann, M., Hinz, A., Robenek, H., Troyer, D., Reichelt, R., Malkus, U., Galla, H.J., Kalscheuer, R., Stoveken, T., von Landenberg, P., *et al.* (2005). Mechanism of lipid-body formation in prokaryotes: how bacteria fatten up. *Mol Microbiol* 55, 750-763.

Walther, T.C., and Farese, R.V., Jr. (2009). The life of lipid droplets. *Biochim Biophys Acta* 1791, 459-466.

Wang, Y., and Kent, C. (1995). Identification of an inhibitory domain of CTP:phosphocholine cytidylyltransferase. *J Biol Chem* 270, 18948-18952.

Wang, Y., MacDonald, J.I., and Kent, C. (1993a). Regulation of CTP:phosphocholine cytidyltransferase in HeLa cells. Effect of oleate on phosphorylation and intracellular localization. *J Biol Chem* 268, 5512-5518.

Wang, Y.L., Sweitzer, T.D., Weinhold, P.A., and Kent, C. (1993b). Nuclear-Localization of Soluble Ctp-Phosphocholine Cytidyltransferase. *Journal of Biological Chemistry* 268, 5899-5904.

Weinhold, P.A., Charles, L., and Feldman, D.A. (1994). Regulation of CTP: phosphocholine cytidyltransferase in HepG2 cells: effect of choline depletion on phosphorylation, translocation and phosphatidylcholine levels. *Biochim Biophys Acta* 1210, 335-347.

Wieprecht, M., Wieder, T., Paul, C., Geilen, C.C., and Orfanos, C.E. (1996). Evidence for phosphorylation of CTP:phosphocholine cytidyltransferase by multiple proline-directed protein kinases. *J Biol Chem* 271, 9955-9961.

Wilgram, G.F., and Kennedy, E.P. (1963). Intracellular Distribution of Some Enzymes Catalyzing Reactions in the Biosynthesis of Complex Lipids. *J Biol Chem* 238, 2615-2619.

Wolins, N.E., Brasaemle, D.L., and Bickel, P.E. (2006). A proposed model of fat packaging by exchangeable lipid droplet proteins. *Febs Lett* 580, 5484-5491.

Yao, Z.M., Jamil, H., and Vance, D.E. (1990). Choline Deficiency Causes Translocation of Ctp-Phosphocholine Cytidyltransferase from Cytosol to Endoplasmic-Reticulum in Rat-Liver. *Journal of Biological Chemistry* 265, 4326-4331.

Yen, C.L.E., Stone, S.J., Koliwad, S., Harris, C., and Farese, R.V. (2008). DGAT enzymes and triacylglycerol biosynthesis. *Journal of Lipid Research* 49, 2283-2301.

Zborowski, J., Dygas, A., and Wojtczak, L. (1983). Phosphatidylserine Decarboxylase Is Located on the External Side of the Inner Mitochondrial-Membrane. *Febs Lett* 157, 179-182.

Zechner, R., Strauss, J.G., Haemmerle, G., Lass, A., and Zimmermann, R. (2005). Lipolysis: pathway under construction. *Curr Opin Lipidol* 16, 333-340.

Zhang, D., Tang, W., Yao, P.M., Yang, C., Xie, B., Jackowski, S., and Tabas, I. (2000). Macrophages deficient in CTP:Phosphocholine cytidyltransferase-alpha are viable under normal culture conditions but are highly susceptible to free cholesterol-induced death. Molecular genetic evidence that the induction of phosphatidylcholine biosynthesis in free cholesterol-loaded macrophages is an adaptive response. *J Biol Chem* 275, 35368-35376.

Zimmermann, R., Lass, A., Haemmerle, G., and Zechner, R. (2009). Fate of fat: The role of adipose triglyceride lipase in lipolysis. *Bba-Mol Cell Biol L* 1791, 494-500.

CG	Protein Names	Pfam Descriptions	Ratio H/L FR9	Ratio H/L FR8	Ratio H/L FR7	Ratio H/L FR6	Ratio H/L FR5	Ratio H/L FR4	Ratio H/L FR3	Ratio H/L FR2	Ratio H/L FR1
CG8732	Lethal 44DEa	AMP-binding enzyme	0.11329	0.091427	0.099142	0.0081568	0.0018178	0.0198834	0.25128	0.25658	0.46588
CG8735	Lunapark	Predicted integral membrane metal-binding protein (DUF2296)	0.10026	0.070491	0.086954	0.044533	0.034017	0.038671	0.12879	0.21462	0.53957
CG1882	Gli-58	Alpha/beta hydrolase fold	0.089325	0.046073	0.12138	0.019631	0.017039	0.041537	0.42967	0.34505	0.57997
CG2146	Myosin V	IQ calmodulin-binding motif:Myosin head (motor domain)	0.19345	0.11053	0.95466	0.028368	0.038249	0.057249	0.33117	0.5201	2.0071
CG33146	Multiple C2 domain and transmembrane region protein	C2 domain	0.11891	0.11863	0.11598	0.045336	0.041907	0.031565	0.11522	0.17682	0.5158
CG17494	CG17494	FHA domain	0.22101	0.24836	0.24477	0.046295	0.025243	0.06824	0.45341	0.24337	0.60629
CG8331	CG8331	TB2/Dpl, HVA22 family	0.15402	0.12533	0.15492	0.016813	0.013397	0.03082	0.15474	0.19947	0.66095
CG8839	CG8839	Amidase	0.078284	0.043569	0.059047	0.0069286	0.010132	0.017271	0.16726	0.20576	0.61918
CG5112	CG5112	Amidase	0.043817	0.021057	0.033736	0.0094009	0.011117	0.015078	0.086145	0.12232	0.42095
CG3209	CG3209	Acytransferase	0.35003	0.37409	0.29309	0.022774	0.027077	0.06183	0.28795	0.42187	0.9688
CG11055	Hormone-sensitive lipase (HSL)	Alpha/beta hydrolase fold	0.041163	0.020453	0.059705	0.033238	0.022292	0.02885	0.13673	0.1709	0.40082
CG2185	CG2185	EF hand	0.39313	0.39892	0.34723	0.039304	0.01958	0.041415	0.30761	0.33877	0.94306
CG2604	CG2604	Saccharopine dehydrogenase	0.10568	0.077962	0.088665	0.017411	0.024535	0.031574	0.16129	0.19235	0.49045
CG10372	Fas-associated factor	UBX domain	0.18875	0.14405	0.15125	0.040811	0.090266	0.066485	0.329	0.37014	0.56512
CG10373	CG10373	PRA1 family protein	0.25532	0.23834	0.23058	0.0096829	0.0090985	0.01923	0.17255	0.18544	0.66747
CG18012	CG18012	Glycosyl transferases group 1	0.06248	0.041078	0.046017	0.028785	0.025394	0.028511	0.10025	0.13424	0.38665
CG13887	CG13887	B-cell receptor-associated protein 31-like	0.14978	0.13889	0.1298	0.0068348	0.0082528	0.017527	0.12197	0.20302	0.61646
CG9186	CG9186	Uncharacterised conserved lipase1 (DUF2305)	0.067661	0.042127	0.055583	0.0089324	0.014364	0.017342	0.11073	0.1607	0.50481
CG13848	Prolonged depolarization afterpotential (PDA) is not apparent	GRAL/TRIO domain	0.056468	0.036453	0.088914	0.039878	0.034145	0.03024	0.2106	0.26339	0.47333
CG6668	Atlasin	Guanylate-binding protein, N-terminal domain	0.20397	0.22537	0.22335	0.014292	0.030917	0.037319	0.20222	0.27294	0.67214
CG5295	Brunner	Patatin-like phospholipase	0.050332	0.049326	0.056386	0.04162	0.055266	0.035638	0.088409	0.13966	0.4545
CG14883	CG14883		0.15326	0.16799	0.17432	0.052571	0.061867	0.070284	0.13702	0.21956	0.56362
CG12576	CG12576		0.13018	0.1082	0.1081	0.0066756	0.0083899	0.025973	0.11349	0.16195	0.40366
CG4775	Tangol4	Transport and golgi organization	0.26206	0.20871	0.17162	0.17747	0.029744	0.21001	0.25827	0.332	0.65462
CG5167	CG5167	Saccharopine dehydrogenase	0.21065	0.13547	0.10069	0.015377	0.016705	0.02665	0.20079	0.21318	0.53396
CG33113	Rhl1	Reticulon	0.20209	0.21691	0.23804	0.017507	0.021866	0.047677	0.1994	0.24567	0.63129
CG2747	CG2747	HEAT repeat	0.27415	0.27415	0.60831	1.0701	1.2976	2.0141	1.2495	1.4804	2.7155
CG10068	CG10068	ELMO/CEP-12 family	0.14636	0.12096	0.13587	0.068815	0.093263	0.03804	0.056896	0.3204	0.56681
CG32803	CG32803	Oligosaccharide biosynthesis protein Alg14 like	0.049818	0.033433	0.10785	0.042869	0.016923	0.11426	0.12508	0.085702	1.1497
CG6308	CG6308	Reticulon	0.079599	0.050593	0.042869	0.043137	0.051212	0.089425	0.12508	0.1573	0.46178
CG10326	ARL-6-interacting protein 1 homolog	Putative adipose-regulatory protein Seipin	0.085442	0.082969	0.061545	0.068815	0.093263	0.03804	0.10741	0.13528	0.42682
CG9904	CG9904	Reticulon	0.1042	0.082969	0.14778	0.20778	0.034242	0.089425	0.10741	0.20063	0.67263
CG14512	CG14512	Glycosyltransferase family 28 C-terminal domain	0.06179	0.076717	0.076717	0.013706	0.007291	0.11976	0.14632	0.47304	0.47304
CG10778	CG10778	Putative undecaprenyl diphosphate synthase	0.23351	0.20989	0.17716	0.78606	0.78606	0.25689	0.31415	0.78312	0.78312
CG9526	CG9526	MBOAT family	0.23761	0.28267	0.22861	0.015536	0.022972	0.25267	0.25267	0.25267	0.25267
CG6746	CG6746	Protein tyrosine phosphatase-like protein, PTPA	1.0501	1.2644	0.71675	0.077489	0.076975	0.076975	0.3897	1.0984	3.2846
CG7127	Exocyst complex component 7	Exo70 exocyst complex subunit	0.35498	0.3414	0.29147	1.0987	0.092442	0.20603	0.27132	0.33665	1.5941
CG4287	CG4287	Alcohol dehydrogenase transcription factor Myb/SANT-like	0.15086	0.09344	0.12697	0.05048	0.092442	0.20603	0.24375	0.24434	0.45635
CG11100	Mes2	Yos1-like	0.24779	0.16381	0.60839	2.2301	0.45642	0.47593	2.5403	2.7391	0.87854
CG32069	CG32069	Yos1-like	0.24779	0.16381	0.60839	2.2301	0.45642	0.47593	2.5403	2.7391	0.87854
CG13852	Mps one binder kinase activator-like 1	MoBI/phocein family	0.28431	0.32149	0.37586	0.06179	0.076717	0.076717	0.26354	0.22881	0.84703
CG15611	CG15611	RhogeF domain	0.20337	0.065555					0.18835	0.15304	0.56926
CG30190	CG30193	TB2/Dpl, HVA22 family							0.028638	0.16122	1.2603
CG8841	CG8841	High-temperature-induced dauer-formation protein							0.028638	0.16122	1.2603
CG9784	CG9784	Endonuclease/Exonuclease/phosphatase family		0.29782		0.13872			0.21592		0.67332

Supplemental Table S2. Proteins identified in LD cluster1.

Protein names, Gene names and SILAC ratio (indicating purification) are shown.

CG	Protein Names	Pfam Descriptions	Ratio H/L FR9	Ratio H/L FR8	Ratio H/L FR7	Ratio H/L FR6	Ratio H/L FR5	Ratio H/L FR4	Ratio H/L FR3	Ratio H/L FR2	Ratio H/L FR1
CG3129	Rab-related protein 4	Ras family	0.23057	0.189	0.37	0.039829	0.060584	0.1307	0.81134	0.65436	0.66662
CG8709		Lipin	0.15664	0.15115	0.37827	0.06234	0.064428	0.13894	0.70327	0.6723	0.66924
CG15117	CG15117	Glycosyl hydrolases family 2	0.45925	0.1224	0.32823	0.079637	0.17668	0.15341	1.0762	0.89372	0.9579
CG10371	Protein-tyrosine phosphatase mitochondrial 1-like protein	Dual specificity phosphatase	0.32194	0.15008	0.24559	0.041065	0.03122	0.059169	0.69978	0.45407	0.5229
CG5175	Kugelkern		0.1956	0.039871	0.19682	0.020186	0.027604	0.070809	0.43048	0.35585	0.42069
CG1112	Alpha esterase7	Carboxylesterase	0.10399	0.077602	0.24454	0.012161	0.01477	0.053982	0.65693	0.48671	0.63542
CG17292	CG17292	Uncharacterized lipase2	0.1087	0.056214	0.23235	0.019015	0.022356	0.049108	0.64295	0.53098	0.63082
CG8042	CG8042	UBX domain	0.32347	0.34551	0.54853	0.048452	0.033131	0.090443	0.87746	0.86192	0.80155
CG1049, CG18330	CTP:phosphocholine cytidyltransferase 1, 2	Cytidylyltransferase	0.29397	0.071095	0.20371	0.026295	0.029615	0.081037	0.65408	0.45369	0.70855
CG4877	CG4877	MVND finger	0.44331	0.10447	1.1244	0.077899	0.096935	0.18649	2.2308	2.6198	1.735
CG13812:CG32223	CG32223		0.10079	0.055465	0.27113	0.048573			0.51447	0.57798	0.62871
CG32069	CG32069	Yos1-like	0.24779	0.16381	0.60839						0.87854

Supplemental Table S3. Proteins identified in LD cluster 2.

Protein names, Gene names and SILAC ratio (indicating purification) are shown.

CG	Protein Names	PFam Descriptions	Ratio H/L FR9	Ratio H/L FR8	Ratio H/L FR7	Ratio H/L FR6	Ratio H/L FR5	Ratio H/L FR4	Ratio H/L FR3	Ratio H/L FR2	Ratio H/L FR1
CG5887	Desat1, Fatty acid desaturase	Fatty acid desaturase	0.65647	0.65471	0.59164	0.03333	0.040714	0.24106	0.31037	0.39861	0.96306
CG12800	Probable cytochrome P450 6d4	Cytochrome P450	0.50867	0.63472	0.48107	0.032263	0.12541	0.051333	0.29647	0.39854	0.81645
CG6643	CG6643	C2 domain	0.7897	0.7589	0.63538	0.066488	0.062312	0.09961	0.69868	0.59383	1.1199
CG7601	Dehydrogenase/reductase SDR family protein 7-like	Short chain dehydrogenase	0.52371	0.59291	0.40257	0.056762	0.030348	0.048017	0.24242	0.30351	0.73145
CG10007	Thioredoxin-related transmembrane protein 2 homolog	Thioredoxin	0.61832	0.68421	0.57678	0.323	0.072748	0.52249	0.2573	0.34247	0.77017
CG10241	Probable cytochrome P450 6a17	Cytochrome P450	1.2127	1.4781	1.0959	0.085906	0.25017	0.12302	0.7044	0.85871	1.6655
CG1513	Oxysterol-binding protein	Oxysterol-binding protein;PH domain	1.8641	1.5311	1.2358	0.90913	1.0337	1.6479	1.59	0.72087	2.6533
CG31717	CG31717	PA2 superfamily	0.2664	0.27947	0.23305	0.031614	0.057936	0.057679	0.17993	0.21265	0.51585
CG11306	CG11306	Glycosyl transferases group 1	0.65546	0.79435	0.64997	0.053821	0.02716	0.087104	0.41057	0.42541	1.75278
CG2023	CG2023	Sec20	0.85371	0.82487	0.67762	0.28575	0.40526	0.1967	0.29903	0.43273	1.0916
CG9159	CG9159	Uncharacterised protein family (UPF0121)	0.33481	0.343	0.33535	0.014622	0.018467	0.03477	0.17919	0.24048	0.71313
CG2064	CG2064	Short chain dehydrogenase	0.74658	0.78132	0.58342	0.025765	0.034571	0.05216	0.39355	0.3929	0.89567
CG10425	CG10425	Short chain dehydrogenase	0.84574	0.99871	0.71465	0.018987	0.012929	0.032341	0.32276	0.41401	0.89918
CG8306	Putative fatty acyl-CoA reductase	Male sterility protein;Male sterility protein	0.71054	0.80232	0.5605	0.04598	0.041126	0.037759	0.27857	0.35125	0.87353
CG3887	Self-like protein	Selenoprotein T	0.66433	0.73845	0.5481	0.027108	0.021034	0.042646	0.23908	0.28158	0.7143
CG5014	Varp-33-1	MSP (Major sperm protein) domain	0.81062	0.93861	0.68096	0.01391	0.013976	0.044164	0.29434	0.39319	0.96981
CG9128	Phosphatidylinositide phosphatase SAC1	Sac1 homology domain	0.82491	0.93778	0.75374	0.026781	0.025918	0.048461	0.42245	0.39174	0.96663
CG5077	Oxysterol-binding protein	Oxysterol-binding protein;PH domain	0.56059	0.71714	0.59245	0.014466	0.027706	0.05097	0.22776	0.33282	1.1676
CG3961	CG3961	AMP-binding enzyme	0.70664	0.76056	0.57095	0.013222	0.014079	0.048242	0.48242	0.44943	0.77614
CG4729	CG4729	Acyltransferase	0.36328	0.38641	0.30986	0.031432	0.021728	0.037664	0.21733	0.25231	0.61255
CG2140	Cytochrome b5	Cytochrome b5-like Heme/Steroid binding domain	0.67879	0.73829	0.56783	0.011697	0.021125	0.05168	0.26932	0.26678	0.85813
CG32699	Lyso-PA acyltransferase	Acyltransferase	0.42045	0.47438	0.39761	0.03362	0.025212	0.085952	0.62965	0.66138	0.93579
CG11466	Probable cytochrome P450 9f2	Cytochrome P450	1.137	1.3906	1.1803	0.12267	0.042185	0.51148	0.72115	0.72115	1.326
CG11200	CG11200	Short chain dehydrogenase	0.69671	0.76523	0.61007	0.0081356	0.033864	0.38423	0.39524	0.39524	0.77645
CG2065	CG2065	Short chain dehydrogenase	0.78175	0.87677	0.65454	0.0081356	0.12698	0.3691	0.48272	0.99837	0.99837
CG10158	Circulating cathodic antigen homolog	Protein of unknown function (DUF837)	0.26104	0.31177	0.27011	0.077341	0.14791	0.18903	0.14791	0.51693	0.51693
CG10908	Derlin-1	Der1-like family	0.70303	0.60054	0.73051	0.039284	0.062086	0.56334	0.8555	0.56993	1.1404
CG10360	Refractory to sigma P	P81 domain;Zinc finger, ZZ type	0.6698	0.82256	1.353	0.37908	0.51945	0.8555	0.56993	0.56993	1.1322
CG13626	Syntaxin 18	SNARE-complex protein Syntaxin-18 N-terminus	0.6698	0.82256	1.353	0.37908	0.51945	0.8555	0.56993	0.56993	1.1322
CG4789	CG4789	Ras family	0.33427	0.45039	0.45039	0.24208	0.48584	0.26705	0.21248	0.51164	1.283
CG33087	CG33087	Low-density lipoprotein receptor domain class A; B	0.33427	0.45039	0.45039	0.24208	0.48584	0.26705	0.21248	0.51164	1.283
CG4825	CG4825	Phosphatidyl serine synthase	1.432	2.0056	1.0615	0.077341	0.14791	0.18903	0.14791	0.51693	0.51693
CG17593	CG17593	Protein of unknown function (DUF1682)	0.88492	1.2576	1.0453	0.039284	0.062086	0.56334	0.8555	0.56993	1.1322
CG2062	Cytochrome P450 4e2	Cytochrome P450	0.88492	1.2576	1.0453	0.039284	0.062086	0.56334	0.8555	0.56993	1.1322
CG3616	Cytochrome P450 9c1	Cytochrome P450	0.61779	0.80855	0.5077	0.017641	0.013624	0.036711	0.23421	0.26192	0.76533
CG9066	Steroid membrane binding protein	Cytochrome b5-like Heme	0.59888	0.69459	0.49617	0.017641	0.013624	0.036711	0.23421	0.26192	0.76533
CG9655	Transmembrane protein nesy	MBOAT family	0.59888	0.69459	0.49617	0.017641	0.013624	0.036711	0.23421	0.26192	0.76533
CG7400	Fatty acid (Long chain) transport protein	AMP-binding enzyme	0.62571	0.79008	0.5764	0.073074	0.031678	0.047666	0.37692	0.38348	0.82494

Supplemental Table S4. Proteins identified in LD cluster 3.

Protein names, Gene names and SILAC ratio (indicating purification) are shown.

CG	Protein Names	Pfam Descriptions	Ratio H/L FR9	Ratio H/L FR8	Ratio H/L FR7	Ratio H/L FR6	Ratio H/L FR5	Ratio H/L FR4	Ratio H/L FR3	Ratio H/L FR2	Ratio H/L FR1
CG4789	CG4789	Ras family		0.33427	0.45039				0.26705	0.21248	0.51164
CG4825	CG4825	PhosphatidyI serine synthase		1.2326	0.57953					0.30314	1.373
CG13626	Syntaxin 18	SNARE-complex protein Syntaxin-18	0.6698	0.82256		0.24208				0.53864	1.283
CG33087	CG33087	Low-density lipoprotein receptor repeat class B									3.1736
Pop2;CG5684;Dmel	Pop2, isoform B;Pop2, isoform C;RH51274p;RH46192p;GM143	CAF1 family ribonuclease	0.58451	0.28578	0.90681	0.93681	0.87842	1.0417	1.0221	0.96333	1.016
pes;G7228;Dmel	Peste, isoform A;Peste, isoform B;RE21078p	CD36 family		0.28516	0.74898	0.47111				0.6305	0.85462
mit(1)15;CG9900;z	SD07771p;Centromere/kinetochore protein zw10;Mitotic 15	Centromere/kinetochore Zw10								0.91026	1.1461
CG8683	Protein MON2 homolog	Domain of unknown function (DUF1981)	0.62003	0.16844	0.63467	1.1768	1.1802	1.0051	0.89919	1.1955	1.2599
Not1;CG1884	GH26494p;SD07194p	CCR4-Not complex component, Not1	0.42914	0.20114	0.77163	0.61201	0.70769	0.76568	0.78733	1.0561	0.98636
CG14213;Dmel_CG	CG14213, isoform A;GH15157p	Cell differentiation family, Rcd1-like	0.62977	0.22315	0.91663	0.67731	0.79607	0.99787	0.97219	1.1425	1.0327

Supplemental Table S5. Proteins identified in LD cluster 4.

Protein names, Gene names and SILAC ratio (indicating purification) are shown.

Protein Name	CG	Ratio H/L F9	Ratio H/L F8	Ratio H/L F7	Ratio H/L F6	Ratio H/L F5	Ratio H/L F4	Ratio H/L F3	Ratio H/L F2	Ratio H/L F1	Ratio H/L F9 norm	Ratio H/L F8 norm	Ratio H/L F7 norm	Ratio H/L F6 norm	Ratio H/L F5 norm	Ratio H/L F4 norm	Ratio H/L F3 norm	Ratio H/L F2 norm	Ratio H/L F1 norm		
ER																					
Reticulon	CG33113	0.20209	0.21691	0.23804	0.017507	0.021866	0.047677	0.1994	0.24567	0.63129	0.320122289	0.343598029	0.377069176	0.027732104	0.034637013	0.075523135	0.315861173	0.48375929	0.389155539	1	
Var-33-1	CG5014	0.81062	0.93661	0.689096	0.013191	0.013976	0.044164	0.29434	0.39319	0.96981	0.835854446	0.96782875	0.702158155	0.014343016	0.01441107	0.045538817	0.303502748	0.40542993	0.40542993	1	
LD																					
cgl-38	CG1882	0.089325	0.046073	0.12138	0.019631	0.017039	0.041537	0.42367	0.34505	0.57997	0.154016587	0.079440316	0.209386687	0.03848302	0.029379106	0.071619222	0.730503302	0.594944566	0.594944566	1	
Hormon sensitive lipase	CG11055	0.041163	0.020453	0.059705	0.033238	0.022392	0.02385	0.13673	0.1709	0.40082	0.102696971	0.051027893	0.148957138	0.0823925004	0.055865476	0.071977446	0.341125692	0.426375929	0.426375929	1	
Fas-associated factor 2	CG10372	0.18875	0.14405	0.15125	0.040811	0.090266	0.066485	0.329	0.37014	0.56512	0.333999838	0.254901614	0.267642271	0.07221652	0.159728907	0.117647579	0.582177237	0.654975934	0.654975934	1	
Undeclared conserved lipase1	CG9186	0.067661	0.042127	0.055583	0.0089324	0.014364	0.017342	0.11073	0.1607	0.50481	0.134032606	0.083451199	0.110106773	0.017694578	0.02845427	0.034353519	0.219349854	0.318837592	0.318837592	1	
Brunner	CG5295	0.05032	0.049326	0.056386	0.04162	0.055266	0.035638	0.088409	0.13986	0.4545	0.110741474	0.108528053	0.124061606	0.091573157	0.12159736	0.078411441	0.194519252	0.307722772	0.307722772	1	
LD+ER																					
Reticulon	CG10326	0.085442	0.055985	0.061545			0.089425	0.10741	0.15228	0.42682	0.200182747	0.131167705	0.144194274	0	0	0.209514549	0.25165175	0.35677803	0.35677803	1	
Lyso-PA acyltransferase	CG32699	0.42045	0.47438	0.39761	0.03562	0.025212	0.089592	0.62965	0.66198	0.93579	0.449299652	0.506929974	0.424892337	0.038064096	0.026941942	0.091849667	0.672853952	0.707402302	0.707402302	1	
Steroid binding protein	CG9066	0.59888	0.69459	0.49617	0.017641	0.013624	0.036711	0.23421	0.26192	0.76533	0.782512119	0.907569284	0.648308573	0.023050188	0.017801471	0.047967543	0.306024852	0.34231456	0.34231456	1	
Selenoprotein T	CG3887	0.66433	0.73845	0.5481	0.027108	0.021034	0.042646	0.23908	0.28158	0.7143	0.899627598	1	0.742230347	0.036709324	0.028489987	0.057750694	0.323759225	0.381312208	0.381312208	0.967296364	
Undeclared conserved lipase1	CG10778	0.23351	0.20989	0.17716	0.078606	0.022972		0.25689	0.31415	0.78312	0.299608172	0.267015241	0.225377198	0.021139428	0	0	0.32680714	0.396651426	0.396651426	0.966259827	
MBOAT family	CG9526	0.23761	0.28267	0.22861	0.015536			0.25267	0.25267	0.73493	0.323309703	0.384621665	0.311063639	0.021139428	0.031257399	0	0	0.34380145	0.396651426	0.396651426	1
Selin	CG9904	0.1042	0.082969	0.14778	0.20778	0.034242		0.20063	0.26339	0.67263	0.154914292	0.123350133	0.219704741	0.308906828	0.050907631	0	0	0.298276913	0.298276913	1	
Sec14 homolog	CG13948	0.056468	0.036453	0.088914	0.039878	0.034145	0.030024	0.2106	0.26339	0.47333	0.119299432	0.077013923	0.187847802	0.084249889	0.072137832	0.063887774	0.444992711	0.556461665	0.556461665	1	
Lunapark	CG8735	0.10026	0.070491	0.086954	0.044533	0.034017	0.038671	0.12879	0.21462	0.59957	0.18581463	0.130642919	0.161154252	0.08254424	0.069304467	0.071670034	0.238690068	0.39776118	0.39776118	1	
LD+other																					
Oxyesterol-binding protein	CG1513	1.8641	1.5311	1.2358	0.590913	1.0337	1.6479	1.59	0.72087	2.6533	0.702559077	0.577054988	0.46575962	0.342641239	0.389590321	0.621075642	0.599253759	0.271688087	0.271688087	1	
Undeclared conserved lipase2	CG17292	0.1087	0.056214	0.23225	0.019015	0.022356	0.049108	0.64295	0.53098	0.63082	0.169064468	0.087431371	0.361381134	0.029574617	0.034770978	0.076637919	1	0.8258496	0.8258496	0.981133836	
Short chain dehydrogenase	CG2064	0.74658	0.78132	0.58342	0.025765	0.034571	0.05216	0.39355	0.3929	0.89567	0.8335548604	0.8723330211	0.651378298	0.028766175	0.038397921	0.058235734	0.43939174	0.438666027	0.438666027	1	
Tangol4	CG4775	0.26206	0.20871	0.17162	0.17747	0.029744	0.21001	0.25827	0.322	0.63462	0.412940027	0.328873972	0.270429548	0.279647653	0.046868992	0.330922442	0.406967949	0.507390249	0.507390249	1	

Supplemental Table S6. PCPs of fluorescently tagged proteins.

Protein names, Gene names SILAC ratio (indicating purification) and normalized SILAC ratios are shown.

Gene	Gene ID	Forward	Reverse
CCT1	CG1049	ACA TCT ATG CTC CTC TCA AGG C	CTC TGC AGA CTC TGG TAA CTG C
CCT1-3'UTR	CG1049	ATG ACA TAC CCT ATG GAG CTG G	ATATTGGTTGGTGTCTGGTTGCG
CCT2	CG18830	ATG ACA TAC CCT ATG GAG CTG G	TGT TTT CGA CTA AGG GAT ACG C
CK	CG2201	TGG ACA CTA CGA ATG ACT CAG C	ACA TTA ATT ACG GAC CAA AGG C
CPT	CG7149	GTT CTC TTC ATC TTT TGG GG C	AAT GAG CCT CCG ACA AGT AGC
EK	CG3525	CTC GAA AGG TGG AGT TTT TGT C	AAG TAC ATA CCT TCG CTT TAT TAT GAC
ECT	CG5547	GTC TTG TTT AGT ATG TCG TCC CC	TTG GAA TTC GCA ATA TTT TTG G
EPT	CG6016	GAT GGA GTA TCT GGA CTG GTC G	GAC TGC AAC AGT TCT GTC TCC C
pBluescript		AATTCGATATCAAGCTTATCGAT	TAAATTGTAAGCGTTAATATTTTG

Supplemental Table S7: Sequences of Primers Used for RNAi Experiments.

Gene	Gene ID	Forward	Reverse
CCT1	CG1049	GGA AGC GGA CCT ACG AGA TA	GTG CCC TGA TCC TGA ACT T
CCT2	CG18830	GAT GAG ATC GTT CCG AAT GC	CAC AAA CAT TCC CTT CGC TT
CK	CG2201	CGG GAG TCA ATC AGT AGC CT	CGT GAT TTG TGT GTC TCC GT
CPT	CG7149	AAA TAT TGC ATG CCG ACT GA	TCT GAG TCG AAG ACC TGC TG
EK	CG3525	CCG GAG GAT AAA TCC AGA AA	ACC TTC AAC AGT TCC TTG GC
ECT	CG5547	GTG GGT CAC CTG GAC TTT CT	GTA GGA GTT CAC CAC GGG AT
EPT	CG6016	ATC CCA ACT GGC TGT TCT TC	CGA AAC CAA ATG AAT GGC TA
GAPDH	CG83393	ATG AAG GTG GTC TCC AAC GC	TCA TCA GAC CCT CGA CGA
CCTα	Pcyt1a, NM_001163160	TTG TGC AGA AGG TGG AAG AG	CAT GTG CTT CAG TGC TCC TT
beta actin	Actb, NM_007393	GGT CAT CAC TAT TGG CAA CG	TCC ATA CCC AAG GAA GG

Supplemental Table S8: Sequences of Primers Used for Quantitative Reverse Transcription PCR Experiments.

9 ABBREVIATIONS

ACAT	Acyl coenzyme A:cholesterol acyltransferase
ADRP	Adipose differentiation-related protein
AGPAT	Acylglycerol-3-phosphate-O-acyltransferase
Arg	Arginine
ARF1	ADP-ribosylation factor 1
ATGL	adipose triglyceride lipase
ATP	Adenosintriphospat
BMDM	Bone marrow derived macrophages
BODIPY	4,4-Difluoro-4-bora-3a,4a-diaza-s-indacene
cAMP	cyclic adenosine monophosphate
°C	Celsius
CCT	Choline cytidyltransferase
CD11b	Cluster of differentiation11b
CDP	Cytidine diphosphate
CDS	CDP-diacylglycerol synthetase
CE	Cholesterol ester
CEH	Cholesterol ester hydrolase
CERT	Ceramide transfer protein
CIDE	Cell death-inducing DFF45-like effector
CGI-58	Comparative Gene Identification-58
CK	Coline kinase
CoA	Coenzyme A
COP	Coat protein complex
CPT	Choline phosphotransferase
CTP	Cytidine triphosphate
Cre	Causes recombination, recombinase from phage PI
Da	Dalton

Dff	DNA fragmentation factor
DG	Diacylglycerol
DGAT	Diacylglycerol acyltransferase
Ds RNA	Double strand ribonucleic acid
DMEM	Dulbecco's Modified Eagle's Medium
DNA	Deoxyribonucleic acid
DTT	dithiothreitol
ECT	ethanolamine cytidylytransferase
EDTA	Ethylenediaminetetraacetic acid
EK	Ethanolamine kinase
EPT	Ethanolamine phosphotransferase
ER	Endoplasmic reticulum
ERGIC	ER-Golgi intermediate compartments
ERES	Er exit sites
EYFP	Enhanced yellow fluorescent protein
FACS	Fluorescence activated cell sorting
FAS	Fatty acid synthase
FDR	False discovery rate
FLiP	fluorescence-loss-in-photobleaching
FRAP	Fluorescence-recovery-after-photobleaching
FSP27	Fat-specific protein of 27 kDa
GAL4	Gene, encoding the yeast transcription activator protein Gal4
GAPDH	Glyceraldehyd-3-phosphat-Dehydrogenase
GFP	Green fluorescent protein
GPAT	Glycerol-3-phosphate acyltransferase
h	Hours
HCl	Hydrogen chloride
HSL	Hormon sensitive lipase

HTNC	His-Tat-NLS-Cre
ICAD	Inhibitor of caspase activated deoxyribonuclease
IQR	Inter-quartile range
KCl	Potassium chloride
KDEL	Lys-Asp-Glu-Leu
LC	liquid-chromatography
LD	lipid droplet
LTQ	Linear trap quadrupole
Lys	Lysine
M	Molar
MBOAT	Membrane bound O-acyl transferase
MCSF	Macrophage colony-stimulating factor
MgAc	Magnesium acetate
MgCl ₂	Magnesium chloride
Min	Minute
mM	Millimolar
MS/MS	Tandem mass spectrometry
m/z	Mass-to-charge ratio
N ₂	Nitrogen
NA	Numerical aperture
NaCl	Sodium chloride
nL	Nanoliter
NLS	Nuclear localization sequence
NP-40	tergitol
nM	Nanomolar
NSF	N-ethylmaleimide-sensitive-factor
NTP	Nucleoside triphosphate
PA	Phosphatidic acid

PAP	Phosphatidic acid phosphatase
PAT	Perilipin, ADRP, and TIP47
PBS	Phosphate buffered saline
PC	Phosphatidylcholine
PCP	Protein correlation profile
PCR	Polymerase chain reaction
PCTP	Phosphatidylcholine transfer protein
PE	Phosphatidylethanolamine
PEMT	Phosphatidylethanolamine methyltransferase
PI	Phosphatidylinositol
PMSF	phenylmethylsulfonylfluorid
PKA	Proteinkinase A
ppm	Parts per million
PS	Phosphatidylserine
PSD	Phosphatidylserine decarboxylase
PSS	Phosphatidylserine synthase
Rab	Ras-related in brain
RNA	Ribonucleic acid
RNAi	RNA interference
RPMI	Roswell Park Memorial Institute
RT	Room temperature
SD	Standard deviation
SE	Sterol ester
sh RNA	short hairpin RNA
SILAC	Stable isotope labeling with amino acids in cell culture
SNAP	Soluble NSF attachment protein
SNARE	N-ethylmaleimide-sensitive-factor attachment receptor
SREBP	Sterol regulatory element-binding protein

START	Steroidogenic acute regulatory
Tat	Peptide, derived from human immunodeficiency virus
TG	Triglyceride
TIP47	Tail-interacting protein of 47 kDa
TLC	Thin-layer chromatography
Tris	Trishydroxymethylaminomethane
UAS	Upstream activation sequence
UV	Ultraviolet
VAP	Vesicle-associated membrane protein
(v/v)	Volume per volume
μCi	Microcurie
μg	Microgram
μM	Micromolar

10 ACKNOWLEDGEMENT

Als erstes möchte ich mich bei Tobias Walther für all seine Unterstützung in den letzten drei Jahren bedanken. Vor allem für die großartige Betreuung, die viele Zeit und den Enthusiasmus, die er in mein Projekt investiert hat, sowie seinen stetigen Optimismus. Seine vielen kreativen und neuen Ideen haben meine Projekte immer voran gebracht und ich konnte viel von ihm lernen. Besonders in schwierigen Zeiten hat er geholfen, dass ich nicht den Spaß und den Glauben an die Wissenschaft verloren habe. Ganz herzlich möchte ich mich auch für seine große Unterstützung und Hilfe in allen möglichen Situationen und Bereichen des Lebens, auch außerhalb der Wissenschaft, bedanken.

I gratefully acknowledge Prof. Dr. Stefan Jentsch for supervising this thesis. I would also like to thank Prof. Dr. Charles David and all the other members of my thesis committee, who have given their time to read this manuscript and for their participation in the oral exam.

Furthermore, I would like to thank the “fat club” Nora Kory, Huajin Wang and especially Florian Wilfling, who was for a long time the only fellow combatant in the lipid droplet field, for all the discussions, their good ideas, their input for this thesis and for their help during the time in New Haven. I also thank Lena Karotki, Florian Fröhlich, Doris Berchtold, Michael Rehman and Romain Christiano for the good atmosphere in the lab and all the fun that we had together. All the extended beer hours, lab retreats, Glühwein evenings and Notfallschnäpse with them made the last years a great time.

Thanks also to Prof. Dr. Matthias Mann for the opportunity to perform mass spectrometry in his lab, Prof. Dr. Robert Farese for his input and ideas on my projects and my collaboration partners Yi Guo and Maximiliane Hilger.

Mein besonderer Dank gilt meinen Eltern Sabine und Christian und meiner Familie, die immer, je nach Lage für Unterstützung, Ablenkung und Verpflegung gesorgt haben.

Simon möchte ich ganz besonders für all seine Unterstützung und Geduld danken. Vor allem auch dafür, dass er mich in allen Situationen ermutigt hat meinen Weg zu gehen.

11 CURRICULUM VITAE

Personal data

Name: Natalie Kraemer
Address: Glötzleweg 28
81477 München
Germany
Email: kraemer@biochem.mpg.de
Date of birth: 10/23/1981
Place of birth: Gräfelfing, Germany
Citizenship: German

Education

10/2002 – 01/2008 **Diploma**, Biology, Technische Universität München, Germany
04/2002-09/2002 **History and Language Studies**, Ludwig-Maximilians-Universität München
10/2001-03/2002 **International Cultural and Business Studies**, Universität Passau, Germany
09/1994-06/2001 **Gymnasium Grafing**, Germany

Research experience

01/2011-03/2011 **PhD**, Yale School of Medicine, Department of Cell Biology, New Haven, USA, Prof. Dr. Tobias Walther
03/ 2008-12/2010 **PhD**, Max Planck Institute of Biochemistry, Organelle Architecture and Dynamics, Munich, Germany, Dr. Tobias Walther
09/2010-11/2010 **Research Visit**, University of California San Francisco, Gladstone Institute of Cardiovascular Disease, San Francisco USA, Prof. Dr. Robert Farese
03/2007-01/2008 **Diploma Thesis**: “Functional Characterization of the Interaction between RuBisCo and the Assembly Chaperone RbcX”, Max Planck Institute of Biochemistry, Cellular

Biochemistry, Munich, Germany, Prof. Dr. Ulrich Hartl

10/2004-03/2005

Research Visit, University of California San Francisco,
Department of Biochemistry and Biophysics, San Francisco
USA, Prof. Dr. Peter Walter